1969-1-F
Vol. I
Copy ____

Chu, Chiao-Min

THE UNIVERSITY OF MICHIGAN

COLLEGE OF ENGINEERING
DEPARTMENT OF ELECTRICAL ENGINEERING
Radiation Laboratory

Doppler Radiation Study: Phase I Report of Contract N62269-68-C-0715 Volume I.

By
CHIAO-MIN CHU, SOON K. CHO and JOSEPH E. FERRIS

December 1969

1969-1-F - Volume I

Contract With: Naval Air Development Center
Johnsville, Warminster, Pa. 18974

Administered through:
OFFICE OF RESEARCH ADMINISTRATION • ANN ARBOR

The discussion or instructions concerning commercial products herein do not constitute an endorsement by the Government, nor do they convey or imply the license or right to use such products.

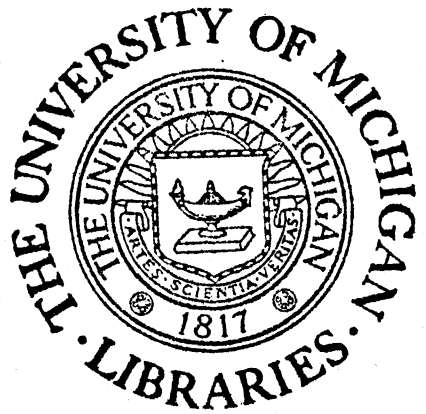

FOREWORD

This report was prepared by The University of Michigan Radiation Laboratory, Department of Electrical Engineering. This is Volume 1 of the Final Report of Phase I under Contract N62269-68-C-0715, "Doppler Radiation Study" and covers the period 1 July 1968 through 1 July 1969. The research was carried out under the direction of Professor Ralph E. Hiatt, Head of the Radiation Laboratory and the Principal Investigator was Professor Chiao-Min Chu. The sponsor of this research is the U.S. Naval Air Development Center, Johnsville, PA., and the Technical Monitor is Mr. Edward Rickner.

ABSTRACT

The radiation characteristics of a doppler velocity sensor radar have been studied. A theoretical investigation has been made of the reflection of the electromagnetic radiation from an anisotropic Gaussian surface. In particular, from the known angular spectrum of ocean surfaces, the bistatic scattering cross section is derived for an open developed sea. The results thus obtained are then applied to the study of the reflected radiation from the doppler sensor equipment on an airplane. Computer programs are set up to calculate the directional distribution of the reflected radiation for a transmitting antenna of given radiation pattern. Computed results for the AN/APN-153 antenna, showing the spatial and temporal variations of the reflected radiation, are given for a wide range of relative positions of the transmitter and receiver for a few different wind speeds. Finally, the reflected radiation from an anisotropic ocean surface of Gaussian distribution is compared with models of specularly and diffusely reflecting surfaces.

TABLE OF CONTENTS

NOMENCLATURE

A_o	A dimensionless parameter: A ratio of (scale length)^2 to mean-square height of a sea surface in x-direction.
B_o	A dimensionless parameter: A ratio of (scale length)^2 to mean-square height of a sea surface in y-direction.
C	A factor involved in the Neumann spectrum.
dB	Decibel .
E_1, E_2	Incident and reflected electric field strengths.
f	Radiation frequency.
$F(\theta, \phi)$	Normalized antenna radiation pattern.
F_2	Normalized radiation power density .
F_{2d}	Normalized radiation power density per unit solid angle for a Lambert scattering in the direction of arrival of maximum radiation intensity.
F_{2M}	Normalized radiation power density per unit solid angle for a sea surface in the direction of arrival of maximum radiation intensity.
F_{2S}	Normalized radiation power density for specular reflection.
$G(\underline{r}, \underline{r}')$	Free-space Green's function.
G_r	Gain of a receiving antenna.
G_t	Gain of a transmitting antenna.
g	Acceleration of earth's gravity.
$H(\hat{i}_x, \hat{i}_y)$	Correlation function of a random surface.
H_1, H_2	Incident and reflected magnetic field strength.
i	$\sqrt{-1}$.
J_e	Electric surface current.

$K_{\ell m}$	A function of surface slopes
k	Radiation wave number
L_m	Wavelength of the sea surface-wave with the minimum phase velocity.
ℓ_x, ℓ_y	Correlation distances of a sea surface in x- and y-directions.
N	Index of refraction.
$\hat{n}$	Unit normal vector.
p_i	Incident radiation power density.
P_r	Total received power.
p_r	Received power density.
P_t	Transmitted power.
p_{2s}	Specularly reflected radiation power density.
q_x, q_y, q_z	Parameters associated with the phase of the radiation in x-, y- and z-directions.
R_m	Hypothetical maximum range of detection.
$R_\perp$, $R_\parallel$	Reflection coefficients for perpendicular and parallel field components.
$\underline{r}$	Position vector.
$\underline{r}_a$	Position vector for a transmitting antenna.
$\underline{r}_r$	Position vector for a receiving antenna.
t	Time.
U	Wind speed.
X	Normalized x-coordinate with its origin at the transmitting antenna.
x	Rectangular x-coordinate.

x_a	Rectangular x-coordinate of a transmitting antenna.
x_o	Rectangular x-coordinate of a reflection point.
x_r	Rectangular x-coordinate of a receiving antenna.
$\hat{x}$	Unit x-vector .
Y	Normalized y-coordinate with its origin at the transmitting antenna.
y	Rectangular y-coordinate.
y_a	Rectangular y-coordinate of a transmitting antenna.
y_o	Rectangular y-coordinate of a reflection point.
y_r	Rectangular y-coordinate of a receiving antenna.
$\hat{y}$	Unit y-vector .
z	Rectangular z-coordinate.
z_a	Rectangular z-coordinate of a transmitting antenna.
z_o	Rectangular z-coordinate of a reflection point.
z_r	Rectangular z-coordinate of a receiving antenna.
$\hat{z}$	Unit z-vector.
z_x, z_y	Surface slopes in x- and y-directions.
α	A parameter defined as q_x/q_z .
β	A parameter defined as q_y/q_z .
Γ	Coefficient of surface tension/water density.
θ	Latitude angle in spherical coordinates.
θ_1, θ_2	θ-coordinates of incident and reflected radiations.
θ_o	θ-coordinate of a radiation pattern of a transmitting antenna.

θ_{2d}	θ-coordinate of maximum reflected radiation intensity for a Lambert surface.
θ_{2M}	θ-coordinate of maximum reflected radiation intensity for a sea surface.
θ_{2S}	θ-coordinate of specularly reflected radiation intensity.
κ_1, κ_2	Sea surface-wave numbers in x- and y-directions.
λ	Free-space radiation wavelength.
ξ	Normalized height variables.
$\sigma(\Omega_2, \Omega_1)$	Scattering cross section .
σ	Sea surface-wave angular frequency.
τ_x, τ_y	Correlation distances for a random surface inx- and y-directions.
ϕ	Azimuth angle in spherical coordinates.
ϕ_1, ϕ_2	ϕ-coordinates of incident and reflected radiations.
ϕ_o	ϕ-coordinate of a radiation pattern of a transmitting antenna.
ϕ_{2d}	ϕ-coordinate of a maximum reflected radiation intensity for a Lambert surface.
ϕ_{2M}	ϕ-coordinate of maximum reflected radiation intensity for a sea surface.
ϕ_{2S}	ϕ-coordinate of specularly reflected radiation intensity.
Φ	Sea Surface-wave spectrum.
ψ	Wind direction.
$\hat{\Omega}_1, \hat{\Omega}_2$	Unit vectors for the directions of incident and reflected radiations.
Ω	Solid Angle.

I

INTRODUCTION

This report summarizes the results of the continued theoretical and experimental investigation of the radiation characteristics of a doppler velocity sensor radar. In the previous work (Chu, et al, 1968) the characteristics of the direct radiation, the reflected radiation from a specularly reflecting surface, and a diffused Lambert surface were reported, along with the estimates of the detectability of such radiation. In the present investigation (Contract N62269-68-C-0715) attention is focused on the characteristics of the reflected radiation from an anisotropic Gaussian surface in the belief that such a surface poses a more realistic model for an open developed sea.

Appendix A presents theoretical formulas of the reflected radiation from a random sea surface. In deriving the bistatic cross section of an anisotropic Guassian surface, through the physical optics approach, the Neumann spectrum was adopted as an angular spectrum of an open developed sea which incorporates the effect of the wind speed. The expressions thus derived were used in the various computations pertinent to the discussion of the problem.

In chapter II we present the basic formulation of the problem in calculating the reflected radiation. Based on the radiation pattern of the transmitting antenna, reflected radiations are discussed in detail in terms of the angular distribution of reflected radiation.

In Chapter III the various computed results for the reflected radiations from an anisotropic sea surface are presented together with the effect of the wind speed on the apparent direction of arrival, and maximum intensity per unit solid angle of the reflected radiation for various geometric conditions. These results are compared with the corresponding cases of both a specularly reflecting surface and a Lambert surface.

Finally, in Appendix B, the computer programs are presented for the numerical evaluation of the reflected radiation intensity for any transmitting radiation pattern, relative geometry between the transmitter and receiver and the parameters describing the sea state.

The use of these computed results in the estimation of the detectibility of the reflected radiation are given in Volume II of the report (Classified Secret). Volume II also contains a description of laboratory and field tests and the results obtained.

II

THE MATHEMATICAL FORMULATION OF A REFLECTED RADIATION

2.1 Introduction

In order to compute the reflected radiation from an antenna observed at any point, it is necessary to know the following:

a) the radiation pattern of the antenna,

b) the reflecting properties of the ground or sea surface, and

c) the relative position of the antenna and the point of observation.

In the previous report (Chu et al, 1968), the radiation pattern of the doppler antenna AN/APN-153 and a coordinate system specifying the orientation and relative position between the antenna and the position of observation have been given. A summary of the pertinent facts that are used in the estimation of the reflected radiation is included here for completeness. The mathematical formulations for the calculation for a specularly reflecting ground, a diffusely reflecting ground (Lambert surface) and an approximate model for an ocean surface are given.

2.2 Coordinate System

Referring to Fig. 2-1, we shall choose a fixed, right-handed rectangular coordinate system with the ground as the x-y plane. The z-axis is assumed to be directed upwards, and the x-axis is chosen in the direction of the ground velocity of the airplane carrying the doppler antenna. Thus, for normal level flight, the longitudinal axis of the aircraft is parallel to the x-axis while the transverse axis is parallel to the y-axis.

The position of the aircraft is represented by:

$$\underline{r}_a : \left\{x_a, y_a, z_a\right\} ,$$

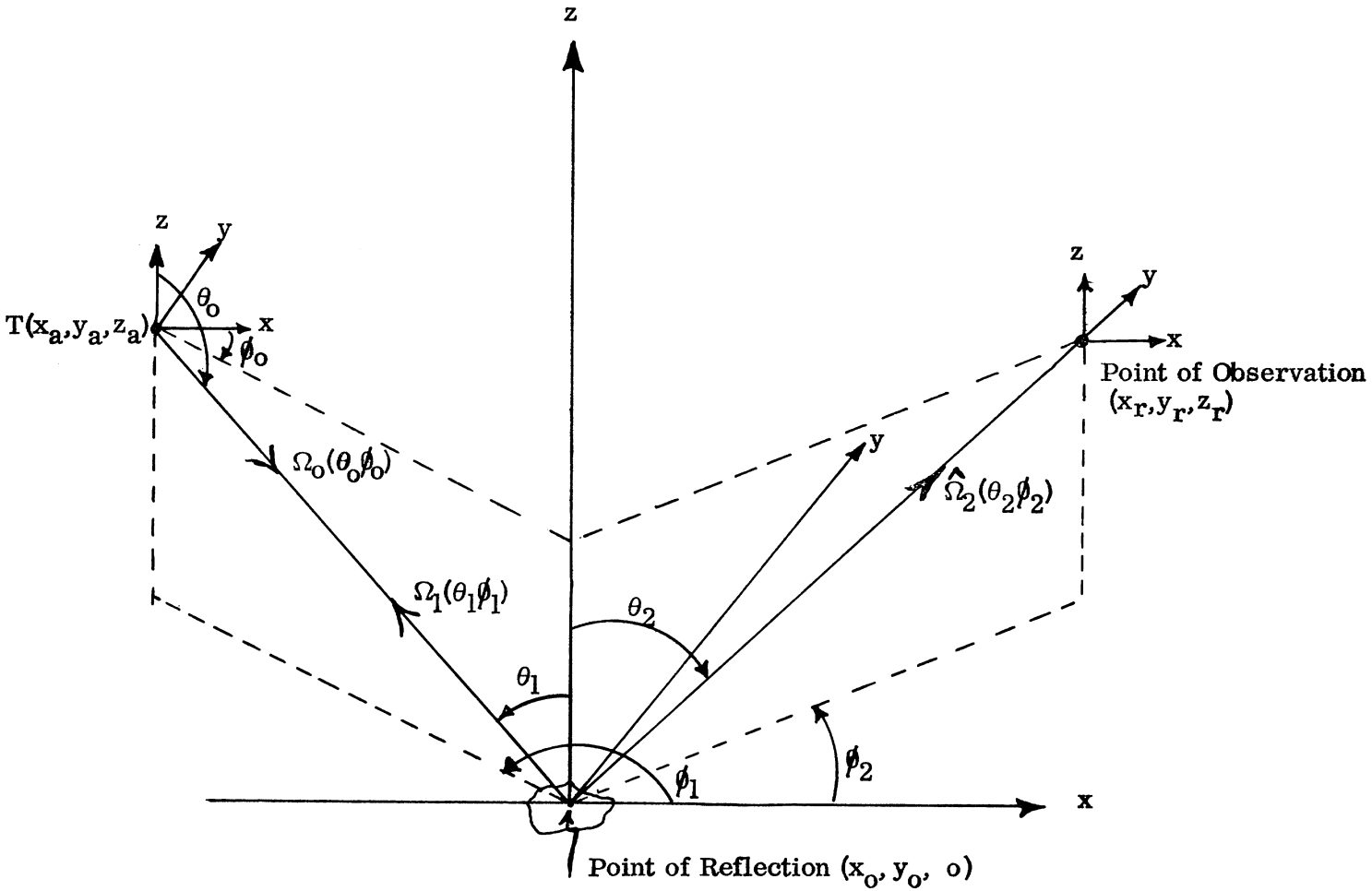

Fig. 2-1: The Coordinate System

while the point of observation is represented by

$$\underline{r}_r : \{x_r, y_r, z_r\} \ .$$

Since only the relative positions between the antenna and the point of observation are essential in computing the reflected radiation, it is convenient to introduce the normalized coordinates defined by

$$X = \frac{x_r - x_a}{z_a} \tag{2.1}$$

$$Y = \frac{y_r - y_a}{z_a} \tag{2.2}$$

and

$$\xi = \frac{z_a - z_r}{z_a + z_r} = \frac{1 - \frac{z_r}{z_a}}{1 + \frac{z_r}{z_a}} \tag{2.3}$$

The direction of the radiation from the antenna, observed at a point, or reflected from a point on the ground, is represented by a unit vector.

$$\hat{\Omega} : \{\theta, \phi\} \ ,$$

where θ, ϕ are the local latitude and the azimuth angles. In the vector notation, therefore,

$$\hat{\Omega} = \hat{x} \sin\theta \cos\phi + \hat{y} \sin\theta \sin\phi + \hat{z} \cos\theta \ , \tag{2.4}$$

where $\hat{x}$, $\hat{y}$, $\hat{z}$ are unit vectors in the x, y and z directions respectively.

The variables used in specifying the coordinates and directions used in calculation of reflected radiation are illustrated in Fig. 2-1 and explained by the following:

i) The transmitter is located at $\underline{r}_a : (x_a, y_a, z_a)$,

ii) A ray of radiation originated from the transmitter is designated by the direction $\hat{\Omega}_o : (\theta_o, \phi_o)$,

iii) The ray in the direction Ω_o would be reflected at a ground point $\underline{r}_o : \{x_o, y_o, 0\}$,

where

$$x_o = x_a + z_a \tan\theta_o \cos\phi_o \tag{2.5}$$

$$y_o = y_a + y_z \tan\theta_o \sin\phi_o \tag{2.6}$$

iv) Referring to a local coordinate system at the point of reflection, the ray of incident radiation appears to come from $-\Omega_1$ where

$$\hat{\Omega}_1 : (\theta_1, \phi_1) = -\hat{\Omega}_o \quad .$$

Evidently,

$$\theta_1 = 180^o - \theta_o \tag{2.7}$$

and

$$\phi_1 = \phi_o + 180^o \quad . \tag{2.8}$$

v) The incident radiation may be reflected diffusely from the ground. The direction of the reflected radiation is represented by

$$\hat{\Omega}_2 : (\theta_2, \phi_2) \quad .$$

vi) The reflected radiation in the direction Ω_2 is observed at a point r_r

$$\underline{r}_r : (x_r, y_r, z_r)$$

where

$$x_r = x_o + z_r \tan\theta_2 \cos\phi_2 \tag{2.9}$$

$$y_r = y_o + z_r \tan\theta_2 \sin\phi_2 \quad . \tag{2.10}$$

In general, of course, the radiation from the transmitter is distributed and specified by the radiation pattern, and the reflected radiation observed at any point may also be distributed. It appears to be coming from various directions of $\hat{\Omega}_2(\theta_2, \phi_2)$. For a fixed $\underline{r}_a$ and $\underline{r}_r$, the relation between (θ_1, ϕ_1) and (θ_2, ϕ_2) can easily be obtained by eliminating x_o, y_o from (2.5) through (2.10). The results expressed in the normalized coordinates, are given by

$$(X + \tan\theta_1 \cos\phi_1) = \frac{z_r}{z_a} \tan\theta_2 \cos\phi_2 \tag{2.11}$$

$$(Y + \tan\theta_1 \sin\phi_1) = \frac{z_r}{z_a} \tan\theta_2 \sin\phi_2 \tag{2.12}$$

2.3 Radiation Pattern

The radiation pattern of the doppler antenna of interest (AN/APN-153) has been measured and reported in the previous Final Report (Chu et al, 1968). The antenna is composed of two sets of slots alternately energized, with switching frequency 1 cps. One set of slots, energized by Feed No. 1, generates beams in the right-forward direction (Beam 1) and the left backward direction (Beam 2) while the other set, energized by Feed No. 2, generates the beams in the left-forward (Beam 3) and the right backward (Beam 4) directions. These beams are illustrated in Fig. 2-2.

The reduction of measured radiation pattern for the AN/APN-153, expressed as $F(\theta_o, \phi_o)$, has been reported by Chu et al (1968). Contour plots for Feed No. 1 are illustrated in Figs. 2-3a and b. The same information may be reduced to $F(\theta_1, \phi_1)$ by the change of variables given by Eqs. (2.7) and (2.8). The pattern of Feed No. 2 is essentially the same as Feed No. 1 except that ϕ_o is replaced by $360^o - \phi_o$.

In terms of $F(\theta_1, \phi_1)$, the power density (Poynting vector) incident at the surface z=0 from the direction $-\hat{\Omega}_1(\theta_1, \phi_1)$ is given by:

$$p_i(\hat{\Omega}_1) = p_i(\theta_1, \phi_1) = \frac{P_t G_t F(\theta_1, \phi_1)}{4\pi z_a^2 \sec^2\theta_1} \tag{2.13}$$

2.4 Reflecting Surface and Reflected Radiation

When an incident radiation impinges on a surface, the energy may be specularly reflected, or diffusely scattered, as illustrated in Fig. 2-4a, b. For secular reflection, assuming that the reflecting surface is an infinitely conducting plane, the intensity (power density) of the reflected radiation is only in the direction

$$\theta_2 = \theta_1 \tag{2.14}$$

$$\phi_2 = \phi_1 \pm 180^o \tag{2.15}$$

and the reflected power density is given by

$$p_r = p_i \quad . \tag{2.16}$$

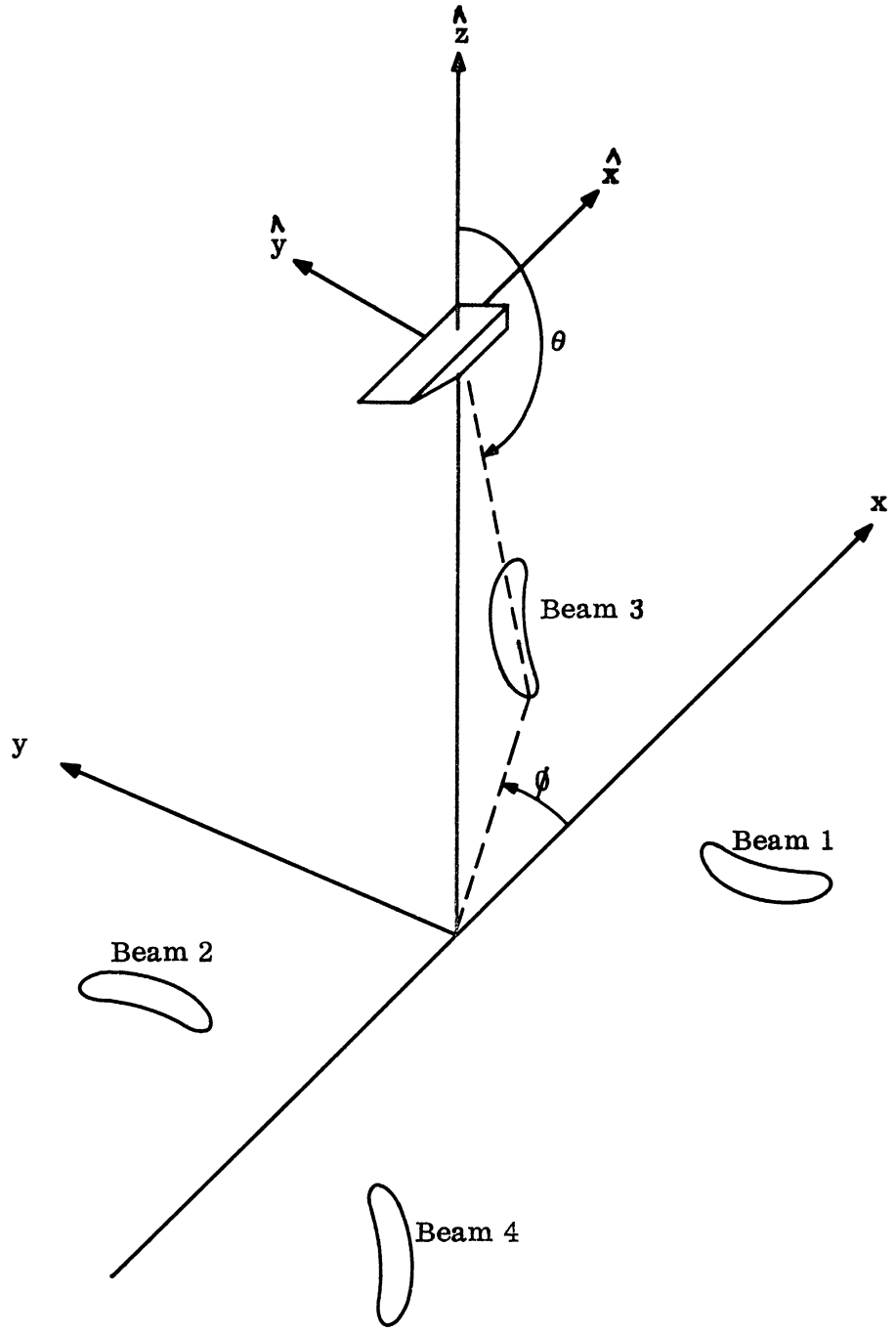

Fig. 2-2: Beams of Radiation and Ground Illumination for APN/153 Antenna System.

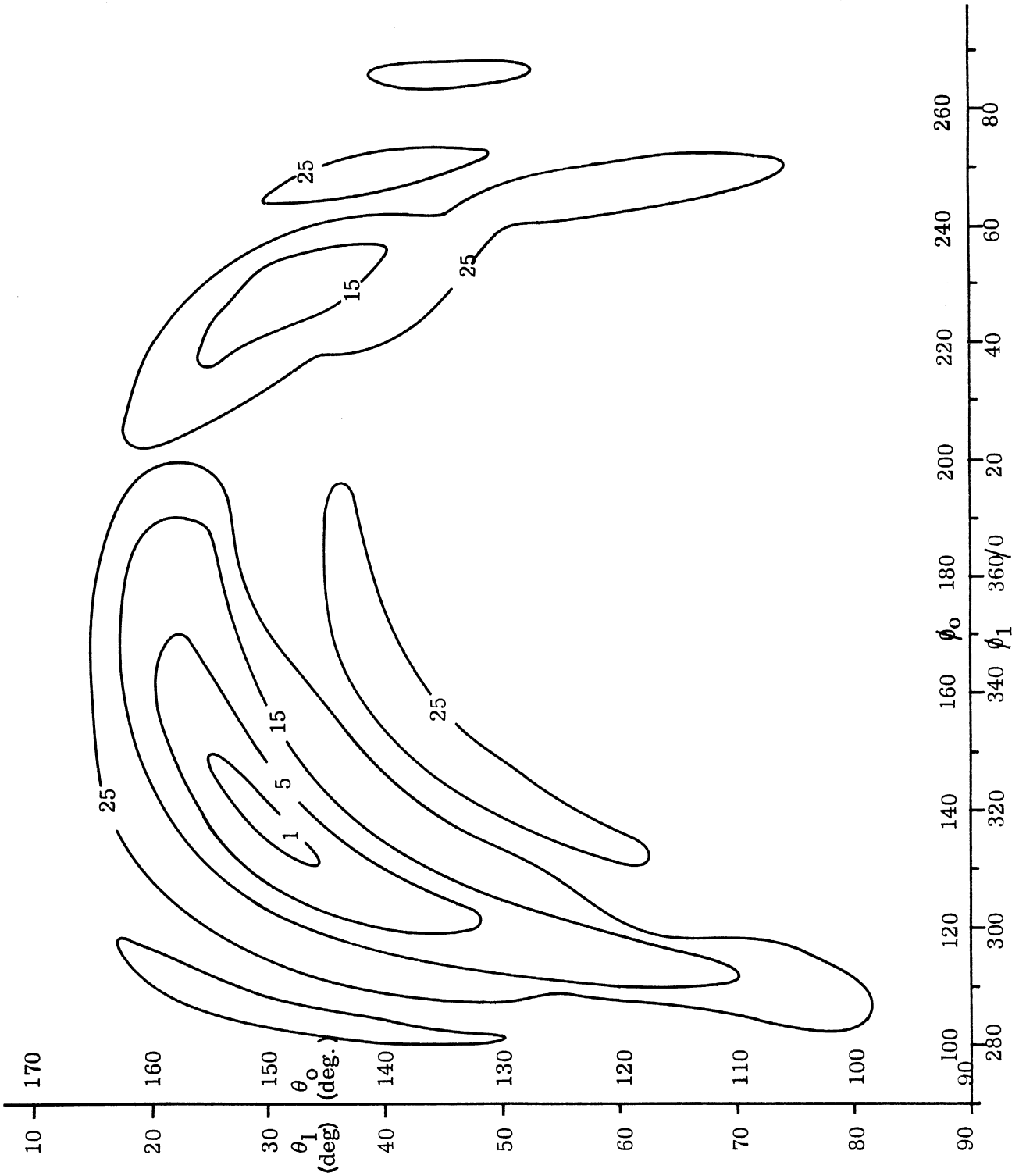

Fig. 2-3a: Radiation Pattern for Feed No. 1 of AN/APN-153 in terms of Azimuth and latitude angles θ and ϕ of Local Spherical Coordinate system. Number on each contour is power level in dB below the radiation in the direction of major lobe.

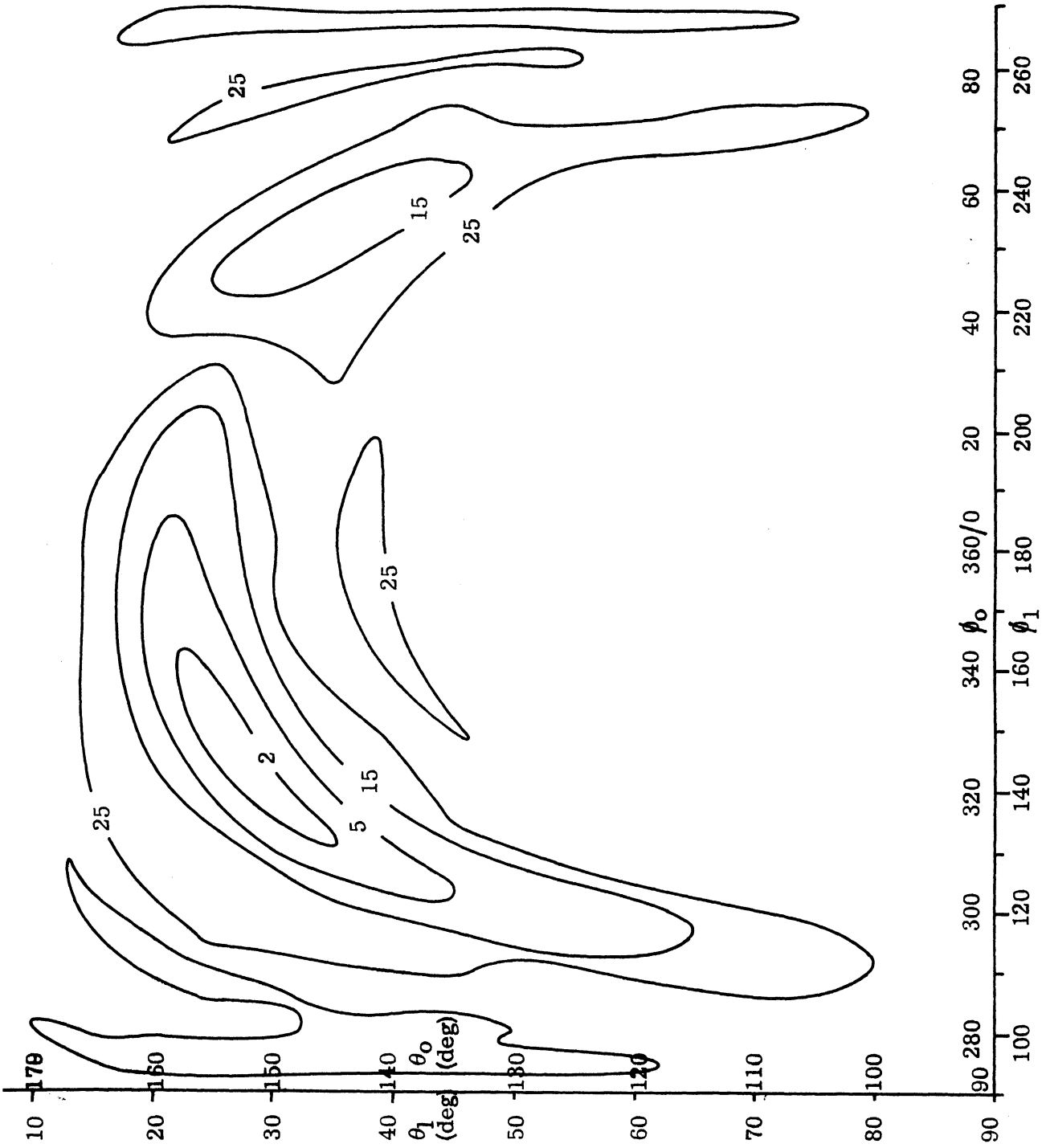

Fig. 2-3b: Radiation Pattern for Feed No. 1 of ANTENNA AN/APN-153 in Terms of Azimuth and Latitude Angles θ and ϕ of Local Spherical Coordinate System. Number on each contour is power level in dB below radiation in direction of major lobe.

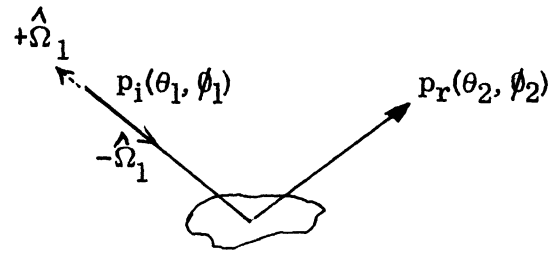

Fig. 2-4a: Specular Reflection . $\theta_2=\theta_1$, $\phi_2=\phi_1 \pm 180^o$

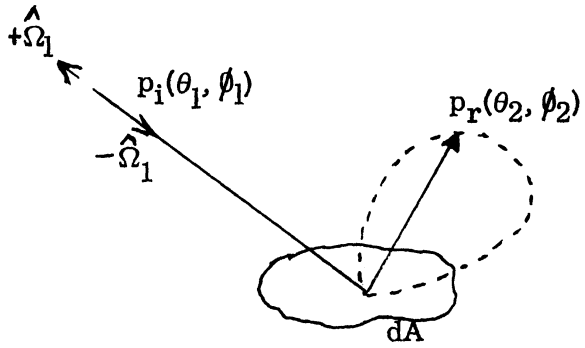

Fig. 2-4b: Diffused Reflection.

On the other hand, in the case of a diffused scattering, the scattered power is distributed over the upper hemisphere. The distribution of the scattered power may be expressed in terms of a bistatic scattering cross section (per unit area), $\sigma(\hat{\Omega}_2, \hat{\Omega}_1)$. In scattering problems, this bistatic cross section is conventionally defined as 4π times the power scattered by a unit area of the surface from an incident beam of unit intensity in the direction $\hat{\Omega}_1$, into a unit solid angle in the direction $\hat{\Omega}_2$. That is,

$$\left(\frac{dP_r}{d\Omega_2}\right) = \frac{1}{4\pi} \left(dA\right) \left(p_i\right) \sigma(\hat{\Omega}_2, \hat{\Omega}_1) \tag{2.17}$$

(scattered power per unit solid angle.) (area of scattering surface) (incident power density)

In optics work, the scattering cross section per unit area is sometimes defined in a slightly different form. That is,

$$\frac{dP_r}{d\Omega_2} = \frac{1}{4\pi} \underbrace{dA\ p_i\ \cos\theta_1}_{\text{(total power intercepted)}} \gamma(\hat{\Omega}_2, \hat{\Omega}_1) \ ,$$

with $\gamma(\hat{\Omega}_2, \hat{\Omega}_1)$ the radar cross section, related through

$$\gamma(\hat{\Omega}_2, \hat{\Omega}_1) = \frac{\sigma(\hat{\Omega}_2, \hat{\Omega}_1)}{\cos\theta_1} \ .$$

This expression was used in the first quarterly report on this contract (Chu, 1968) but to avoid confusion, the cross section $\sigma(\hat{\Omega}_2, \hat{\Omega}_1)$ as used in Eq. (2.17) will be used henceforth.

By definition, then, the scattered power density due to an area dA observed at a point at a distance r from dA and in the direction $\hat{\Omega}_2$ is given by

$$dp_r = \frac{dA\ p_i}{4\pi r^2} \sigma(\hat{\Omega}_2, \hat{\Omega}_1) \tag{2.18}$$

Now, if we sample the scattered power from the extended ground reflector at a fixed point, the scattered power appears to be coming from various directions (different $\hat{\Omega}_2$). This fact is illustrated in Fig. 2-5. The directional properties of this observed radiation may be expressed in terms of the scattered power intercepted by a unit surface per unit solid angle of the beamwidth: i.e.

$$\frac{dp_r}{d\Omega_2} = \frac{p_i(\hat{\Omega}_1)}{4\pi \cos\theta_2} \sigma(\hat{\Omega}_2, \hat{\Omega}_1) \quad . \tag{2.19}$$

For a narrow beam receiver of an effective aperture area A with beamwidth $d\Omega_2$ staradians, the scattered power received is then

$$P_r = A \frac{p_i(\hat{\Omega}_1)}{4\pi \cos\theta_2} \sigma(\hat{\Omega}_2, \hat{\Omega}_1)\, d\Omega_2 \quad . \tag{2.20}$$

On the other hand, for an omnidirectional receiver of an effective aperture A, the scattered power received is

$$P_r = A \int_0^{\pi/2} \frac{\sin\theta_2}{\cos\theta_2} d\theta_2 \int_0^{2\pi} d\phi_2 \frac{p_i(\hat{\Omega}_1)}{4\pi} \sigma(\hat{\Omega}_2, \hat{\Omega}_1) \quad . \tag{2.21}$$

Other modifications of Eq. (2.18) incorporating the radiation pattern of the receiving antenna can also be deduced. However, in the absence of the detailed information on the characteristics of the receiving systems, perhaps our estimation of detectability has to be based on one or both of the above limiting cases.

The evaluation of the observed scattered radiation, even with the knowledge of $\sigma(\hat{\Omega}_2, \hat{\Omega}_1)$, has to be resorted to the numerical computation, due to the numerical function $p_i(\hat{\Omega}_1)$ as given by Eq. (2.13), and the involved relations between $\hat{\Omega}_1$ and $\hat{\Omega}_2$ depending on the relative position of the transmitter and the receiver, as given by (2.11) and (2.12). In the work reported by Chu et al (1968), a simple model of $\sigma(\hat{\Omega}_2, \hat{\Omega}_1)$ (Lambert's law of scattering) was chosen. For this simple model,

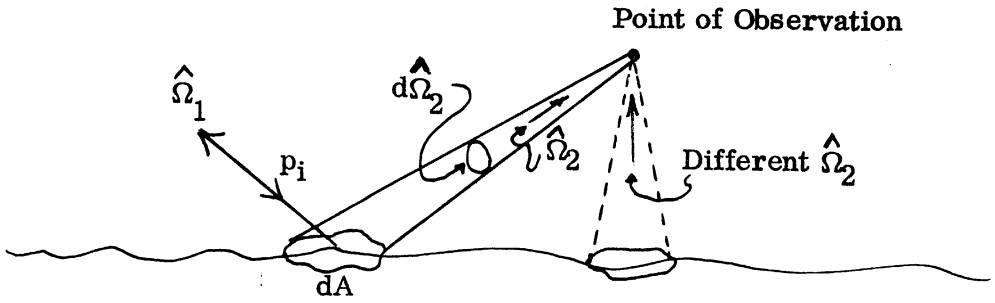

Fig. 2-5: Scattering Geometry.

$$\sigma(\hat{\Omega}_2, \hat{\Omega}_1) = 4 \cos\theta_1 \cos\theta_2 \tag{2.22}$$

and the evaluation of P_r for this case has been reported therein (Chu et al, 1968).

In the current work, a more realistic model for the bistatic cross section $\sigma(\hat{\Omega}_2, \hat{\Omega}_1)$ is considered. Due to the lack of information of this bistatic cross section for rough ground or sea surface, both theoretical and some limited experimental work has been carried out to gain some knowledge of the bistatic scattering cross section.

The theoretical bistatic scattering cross section for an open developed sea (cf. Eq. A. 117) is given by

$$\sigma(\hat{\Omega}_2, \hat{\Omega}_1) = \frac{\ell_x \ell_y}{q_z^4 H(0,0)} \left[1 - \hat{\Omega}_2 \cdot \hat{\Omega}_1\right]^2 \exp\left\{ - \frac{(q_x \cos\psi + q_y \sin\psi)^2 \ell_x^2 + (q_y \cos\psi - q_x \sin\psi)^2 \ell_y^2}{4 q_z^2 H(0,0)} \right\}, \tag{2.23}$$

where

$H(0,0)$ is the mean square height of the sea surface;

ℓ_x, ℓ_y are the correlation distances of the surface height parallel and transverse to the direction of the surface wind, respectively;

ψ is the angle between the direction of the surface wind and the x axis;

$q_z = \cos\theta_1 + \cos\theta_2$,

$q_x = \sin\theta_1 \cos\phi_1 + \sin\theta_2 \cos\phi_2$,

and

$q_y = \sin\theta_1 \sin\phi + \sin\theta_2 \sin\phi_2$.

A detailed derivation of Eq. (2.23) and the approximations involved in the derivation are given in Appendix A. From the reported ocean spectrum, the dependence of $H(0,0)$, ℓ_x and ℓ_y on the surface wind velocity U are estimated and the results presented in Figs. A-4 and A-5, respectively.

In order to gain some insight into the scattering model given by Eq. (2.23), such as the effect of the wind and aspect variations, let us introduce the following parameters:

i) The parameters of the sea surface defined by $A_o \triangleq \ell_x^2/4H(0,0)$ and $B_o \triangleq \ell_y^2/4H(0,0)$

ii) The directional variables

$$\alpha \triangleq \frac{q_x}{q_z} = \frac{\sin\theta_1 \cos\phi_1 + \sin\theta_2 \cos\phi_2}{\cos\theta_1 + \cos\theta_2}$$

and

$$\beta \triangleq \frac{q_y}{q_z} = \frac{\sin\theta_1 \sin\phi_1 + \sin\theta_2 \sin\phi_2}{\cos\theta_1 + \cos\theta_2} \ .$$

In terms of these normalized parameters, (2.23) may be reduced to

$$\sigma(\hat{\Omega}_2, \hat{\Omega}_1) = \sqrt{A_o B_o}\ (1+\alpha^2+\beta^2) \exp\left[-A_o(\alpha\cos\psi + \beta\sin\psi)^2 - B_o(\beta\cos\psi - \alpha\sin\psi)^2\right] \tag{2.24}$$

In particular, when $\psi = 0$, i.e. the incident radiation is in the direction of the wind,

$$\sigma(\hat{\Omega}_2, \hat{\Omega}_1) = \sqrt{A_o B_o}\ (1+\alpha^2+\beta^2)^2 \exp\left[-A_o\alpha^2 - B_o\beta^2\right] . \tag{2.25}$$

In Fig. 2-6, the normalized quantities A_o, B_o and $\sqrt{A_o B_o}$ for the model of sea chosen in the present study is presented. Due to the large value of A_o and B_o obtained for this model it is evident that σ is maximum at $\alpha = 0$, $\beta = 0$ (forward direction) and has a maximum value of $\sqrt{A_o B_o}$. The cross section, however, decreases very rapidly away from this forward direction. For a rough estimate of the decreasing of σ from the maximum, the beamwidth of the scattered power may be approximated by

$$\Delta\theta = \Delta\phi \cong \frac{2}{\sqrt{A_o}} \ .$$

For U = 1.5 m/sec, the beamwidth is approximately 10^{o} and for U = 4 m/sec, it is approximately 15^{o}.

To discuss the effect of the direction of the wind on the scattering cross section, let us assume that the direction of incident wave and the direction of reflected wave (i.e. $\hat{\Omega}_1$ and $\hat{\Omega}_2$) are fixed and compare the ratio of $\sigma(\hat{\Omega}_2, \hat{\Omega}_1)$ for $\psi \neq 0$ with that for $\psi = 0$. Straightforward algebraic manipulation then yields

$$\frac{\sigma(\psi \neq 0)}{\sigma(\psi = 0)} = \exp\left\{ - \frac{(B_o - A_o)}{2} \left[(\alpha^2-\beta^2) - (\alpha^2-\beta^2)\cos 2\psi - 2\alpha\beta \sin 2\psi \right] \right\} .$$

Thus, as the wind direction represented by ψ changes, this ratio varies between the limits

$$\exp\left[-(B_o - A_o)\alpha^2\right]$$

and

$$\exp\left[(B_o - A_o)\beta^2\right] ,$$

corresponding to the variation of ψ which satisfies the relation

$$\tan 2\psi = \frac{2\alpha\beta}{\alpha^2-\beta^2}$$

For those directions of incident and reflected radiations for which α and β are not small, the effect of the wind direction would be pronounced. This feature is not present in all isotropic models of the rough surface scattering, for which $A_o = B_o$.

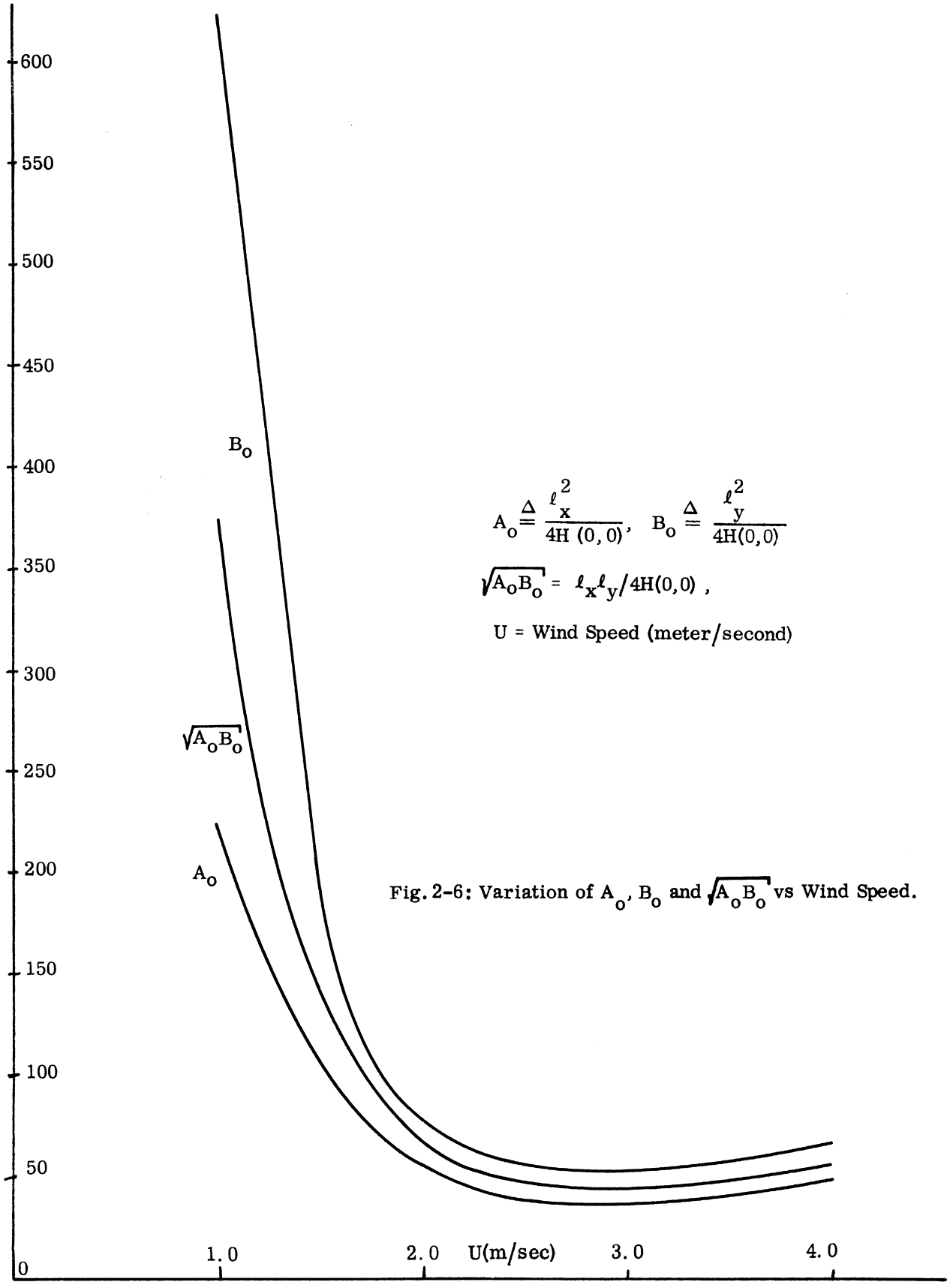

$$A_o \triangleq \frac{\ell_x^2}{4H(0,0)}, \quad B_o \triangleq \frac{\ell_y^2}{4H(0,0)}$$

$$\sqrt{A_oB_o} = \ell_x\ell_y/4H(0,0),$$

U = Wind Speed (meter/second)

Fig. 2-6: Variation of A_o, B_o and $\sqrt{A_oB_o}$ vs Wind Speed.

III

CALCULATION OF REFLECTED RADIATION

3.1 Introduction

In estimating the detectability of the reflected radiation from a doppler antenna such as the AN/APN-153 by a receiver of various beamwidths, the knowledge of the angular distribution of the reflected radiation at different points of observation, relative to the transmitting antenna, appears to be of prime importance. From the general theory of the surface reflection and the radiation pattern of the antenna AN/APN-153 given in Ch. II, the computation of the reflected radiation and its distribution may be carried out. In this Chapter, the basic formulas are presented together with the numerical schemes employed and some typical results of such calculations.

3.2 Mathematical Formulas

In this section we summarize the mathematical formulas and numerical schemes used in calculating the reflected radiation of the AN/APN-153 antenna for three types of the reflecting surfaces discussed in the preceding chapter.

3.2.1 Specular Reflecting Surface

For a specularly reflecting surface, the reflected radiation appears to come from a single direction, solely depending on the relative position between the transmitter and the receiver. From Eqs. (2.11) and (2.12), it is obvious that the direction of arrival of the reflected radiation is related to the relative position

$$\left(X,\ Y,\ \frac{z_r}{z_a}\right)$$

by

$$X = \left(1 + \frac{z_r}{z_a}\right) \tan\theta_{2s} \cos\phi_{2s} \tag{3.1}$$

$$Y = \left(1 + \frac{z_r}{z_a}\right) \tan\theta_{2s} \sin\phi_{2s}\ , \tag{3.2}$$

where $\hat{\Omega}_{2s} : \{\theta_{2s}, \phi_{2s}\}$ is the direction of arrival of the reflected radiation. This radiation originates from the antenna located in a direction (θ_1, ϕ_1), where

$$\theta_1 = \theta_{2s} \tag{3.3}$$

and

$$\phi_1 = \phi_{2s} + 180^o \ . \tag{3.4}$$

The intensity of the reflected radiation (power/unit area) can be calculated by the method of images. The result is

$$p_{2s} = \frac{P_t G_t}{4\pi z_a^2} \ F_o(\theta_1, \phi_1) \ \frac{\cos^2 \theta_1}{(1+ \frac{z_r}{z_a})^2} \ . \tag{3.5}$$

The calculation of p_{2s} as a function of X, Y and z_r/z_a was given in Chu et al (1968). However, the directional characteristics of the reflected radiation was not considered there. For the calculation of the angles θ_{2s} and ϕ_{2s} for any given X, Y and z_r/z_a, the following relations may be used:

$$\tan \phi_{2s} = \frac{Y}{X} \tag{3.6}$$

$$\tan \theta_{2s} = \frac{\sqrt{X^2 + Y^2}}{1 + \frac{z_r}{z_a}} \ . \tag{3.7}$$

For the estimation of the reflected power intensities and for the convenience of their comparison for three types of reflecting surfaces, we define the normalized power density as the following:

$$F_{2s}(X, Y, \frac{z_r}{z_a}) \triangleq \frac{p_{2s}}{\frac{P_t G_t}{z_a^2}} = 4\pi \ F_o(\theta_1, \phi_1) \ \frac{\cos^2 \theta_1}{(1+ \frac{z_r}{z_a})^2} \ . \tag{3.8}$$

3.2.2 Diffusely Reflecting Surface

For the surface whose reflecting properties are defined by a scattering cross section $\sigma(\hat{\Omega}_2, \hat{\Omega}_1)$, the reflected radiation observed at a point appears to be coming from various directions. The radiation which originates from an antenna located in the direction (θ_1, ϕ_1) relative to the reflecting point will be distributed. To an observer stationed at a relative position X, Y and z_r/z_a, the reflected power of the radiation originally in the direction (θ_1, ϕ_1) appears to be coming from the direction (θ_2, ϕ_2), where

$$\frac{z_r}{z_a} \tan\theta_2 \cos\phi_2 = X + \tan\theta_1 \cos\phi_1 , \tag{3.9}$$

$$\frac{z_r}{z_a} \tan\theta_2 \sin\phi_2 = Y + \tan\theta_1 \sin\phi_1 . \tag{3.10}$$

The intensity of the reflected radiation, by the definition of the scattering cross section, may be expressed by

$$\frac{dp_r}{d\Omega_2} = \frac{P_t G_t}{4\pi z_a^2} \cos^2\theta_1 \frac{F_o(\theta_1, \phi_1)}{\cos\theta_2} \sigma(\hat{\Omega}_2, \hat{\Omega}_1) \tag{3.11}$$

Physically, of course, this may be interpreted as the power that is intercepted by a receiver of unit aperture per unit solid angle. For the purpose of comparing the direction and magnitude, we shall define the normalized quantity,

$$F_{2M}(X, Y, \frac{z_r}{z_a}, \hat{\Omega}_2) \triangleq \frac{dp_r}{d\Omega_2} \Big/ \frac{G_t P_t}{z_a^2}$$

$$= \frac{\cos^2\theta_1}{4\pi \cos\theta_2} F_o(\theta_1, \phi_1) \sigma(\hat{\Omega}_2, \hat{\Omega}_1) \tag{3.12}$$

In the case of the Lambert surface,

$$\sigma = 4 \cos\theta_1 \cos\theta_2 . \tag{3.13}$$

Whence,

$$F_{2d} = \frac{F_o(\theta_1, \phi_1)}{\pi} \cos^3 \theta_1 \quad , \tag{3.14}$$

F_{2d} denoting the case for completely diffused scattering (Lambert scattering).

3.2.3 A Moderately Rough Sea Surface

For this model, the scattering cross section is given by (2.23). Consequently, we have

$$F_{2M} = \frac{1}{4\pi} \frac{\cos^2 \theta_1}{\cos \theta_2} F_o(\theta_1, \phi_1)(1+\alpha^2+\beta^2)^2 \sqrt{A_o B_o}$$

$$\cdot \exp\left[-A_o(\alpha \cos\psi + \beta \sin\psi)^2 - B_o(\beta \cos\psi - \alpha \sin\psi)^2\right] , \tag{3.15}$$

where

$$\alpha \triangleq \frac{\sin\theta_1 \cos\phi_1 + \sin\theta_2 \cos\phi_2}{\cos\theta_1 + \cos\theta_2} \equiv \frac{q_x}{q_x} \tag{3.16}$$

and

$$\beta \triangleq \frac{\sin\theta_1 \sin\phi_1 + \sin\theta_2 \sin\phi_2}{\cos\theta_1 + \cos\theta_2} \equiv \frac{q_y}{q_z} \tag{3.17}$$

A computer program for evaluation of the normalized quantity F_{2M} corresponding to (3.15) is included in Appendix B. Starting from the given θ_o, ϕ_o, X, Y, we first calculate z_r/z_a and θ_z, ϕ_z by the transformation equations (3.9) and (3.10). Then, for a given wind speed U(m/sec) and the direction ψ, the values of F_{2M} are calculated for each set of (θ_1, ϕ_1) or (θ_o, ϕ_o). F_{2d} and F_{2s} can be calculated relatively easily by using (3.14) and (3.8), respectively.

3.3 Power Level and Directional Variation of Reflected Radiation

Before presenting the computed numerical results for the angular distribution of the reflected radiation, it may prove fruitful to look at the physical situation which partially explains angular variations of the reflected radiation. Let us refer to Figs. 2-3a and b, the radiation patterns of the antenna AN/APN-153, where contours of constant $F_o(\theta_1, \phi_1)$ are shown. Each ray originating from the antenna in the direction, say, (θ_1, ϕ_1), would reach an observer, after diffused

reflection, from the direction (θ_2, ϕ_2). The relation between (θ_1, ϕ_1) and (θ_2, ϕ_2), of course, depends on the geometry between the transmitter and the receiver. For a receiver fixed at (X, Y, z_r/z_a), the direction of a set of (θ_1, ϕ_1) along a given contour of F_o will appear to reach the receiver from different directions. This geometric effect is illustrated in Figs. 3-1a - 3-1d. The contours shown in Figs. 3-1a and 3-1b are the contours of F_o seen by a receiver at (X=0, Y=0.5, z_r/z_a = 0.5); the Figs. 3-1c and 3-1d at (X=0, Y=0.5, z_r/z_a = 0.1). As seen from these illustrations, the receiver at different locations will see different shapes of the radiation patterns, depending, of course, on its relative coordinates. Thus, as shown in Figs. 3-1a and 3-1b, the receiver at (0, 0.5, 0.5) will see the portion of the major lobe of the Beam No. 1 much more elongated, and the minor lobe somewhat contracted, while the receiver will witness the major lobe of the Beam No. 2 greatly contracted and its minor lobe very much elongated. The same antenna pattern viewed at the same X, Y coordinates, but different relative height (z_r/z_a = 0.1) is illustrated in Figs. 3-1c and 3-1d. Thus, it is evident that the deformation of the beam shape, after reflection, is critically dependent on the position of the observation.

It should be noted that the contours illustrated in Figs. 3-1a through 3-1d are not the contours of equally reflected power, due to the angular dependence of the reflecting property of the surface. For example, the normalized reflected power densities (F_{2M}) are different even on the same contour. In Figs. 3-2a and 3-2b, on each contour of constant F_o, several points are selected and indicated by the dots. The normalized reflected power density, F_{2M}, corresponding to these points (directions of reflected radiation), are tabulated in Table 3.1 for the down wind speed of 1.5 m/sec. It is seen that the direction in which F_{2M} is maximum is shifted from the direction of the peak of the corresponding transmitting antenna radiation pattern. Moreover, the shape of the contour of the constant F_{2M}, after reflection, is drastically modified. In Figs. 3-3a and 3-3b and Table 3-2, similar plots and values are given for a Lambert surface for comparison. Here the modification of the contours of the constant power (F_{2d}) is seen less drastic. In fact, the direction in which F_{2d} is maximum appears to correspond to that of the antenna radiation pattern.

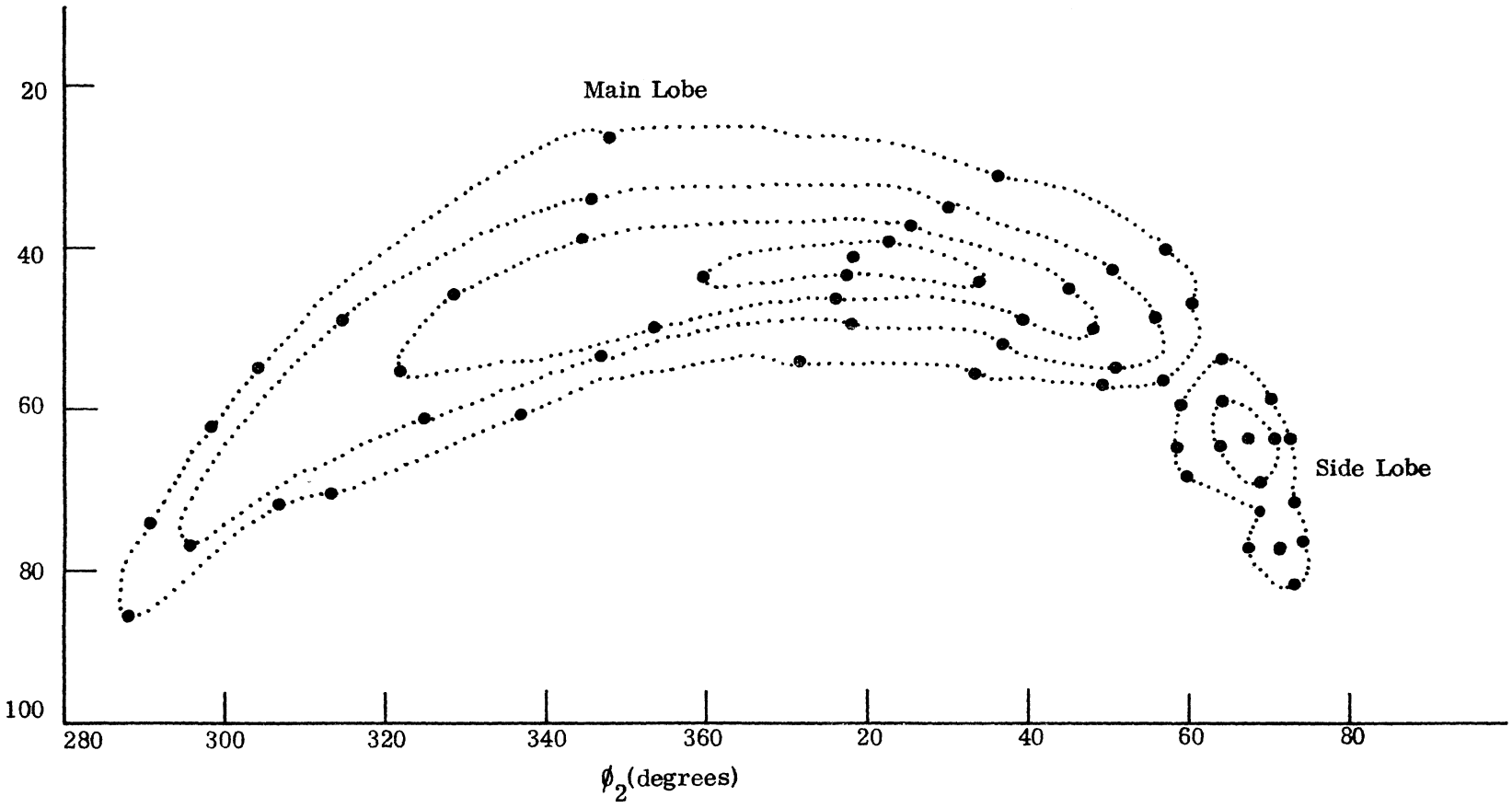

Fig. 3-1a: Contour of Radiation Pattern of Beam No. 1 viewed at x=0, y=0, z_r/z_a=0.5.

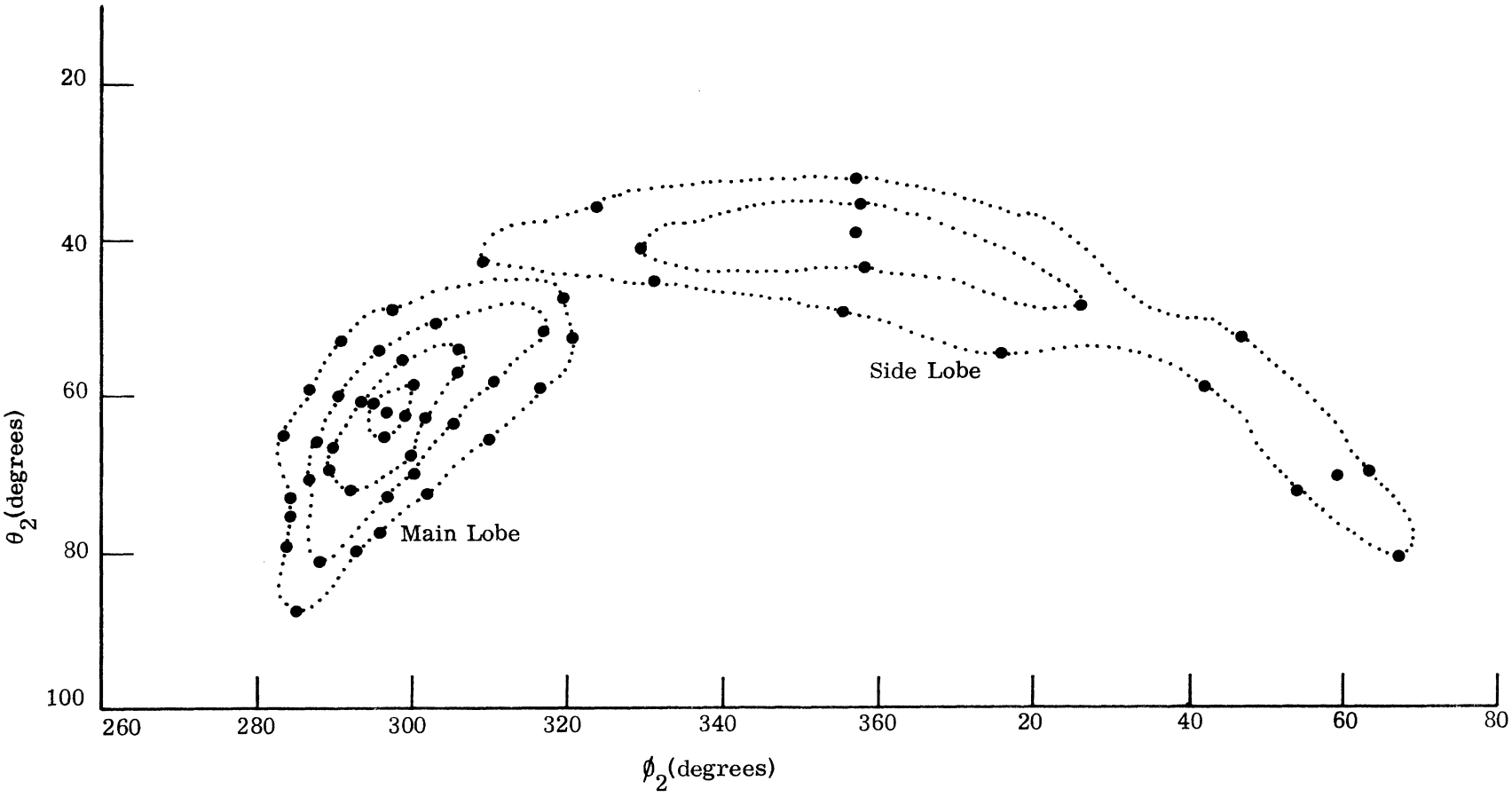

Fig. 3-1b: Contour of Radiation Pattern of Beam No. 2 viewed at x=0, y=0.5, z_r/z_a=0.5.

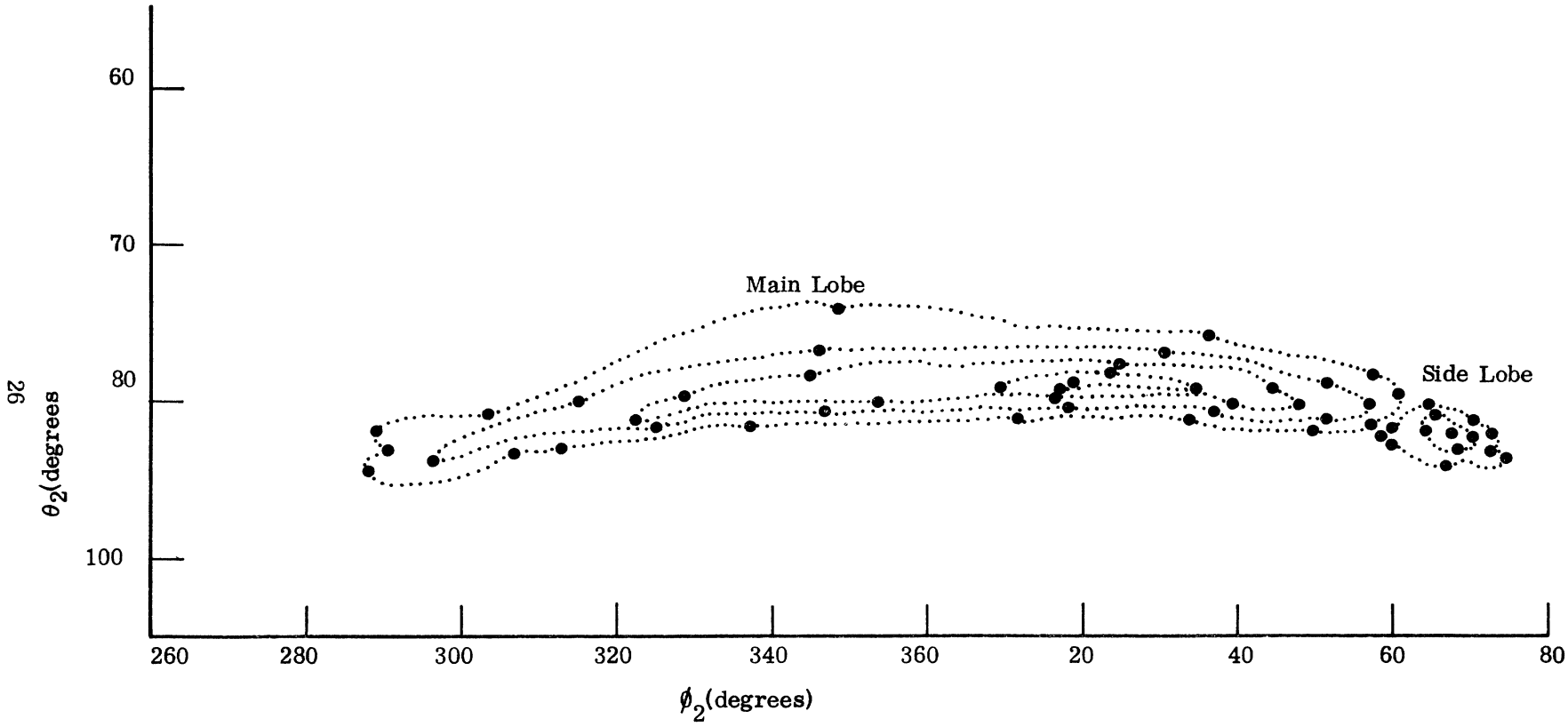

Fig. 3-1c: Contour of Radiation Pattern of Beam No. 1 viewed at x=0, y=0.5, z_r/z_a=0.1.

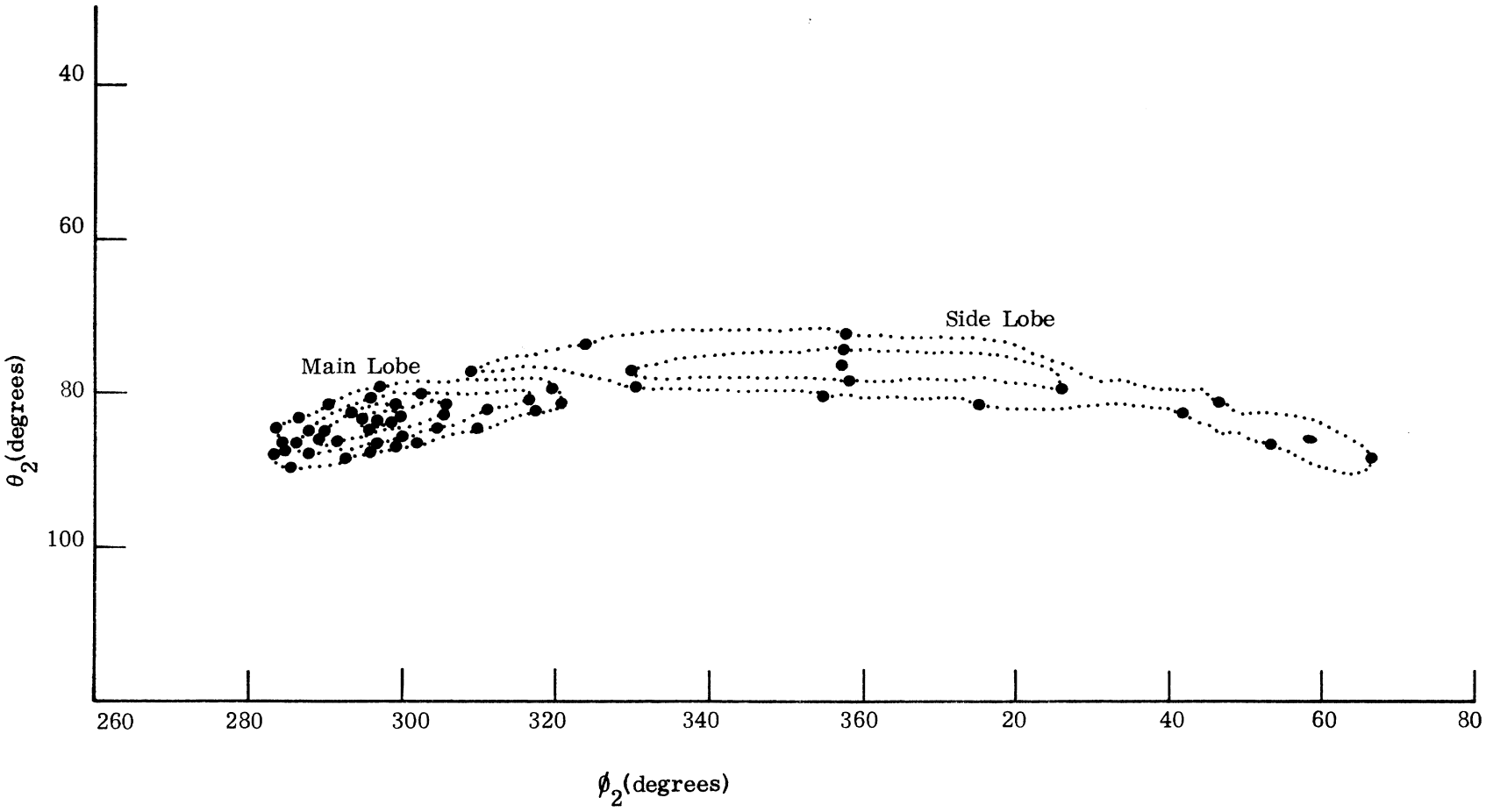

Fig. 3-1d: Contour of Radiation Pattern of Beam No. 2 viewed at x=0, y=0.5, z_r/z_a=0.1 .

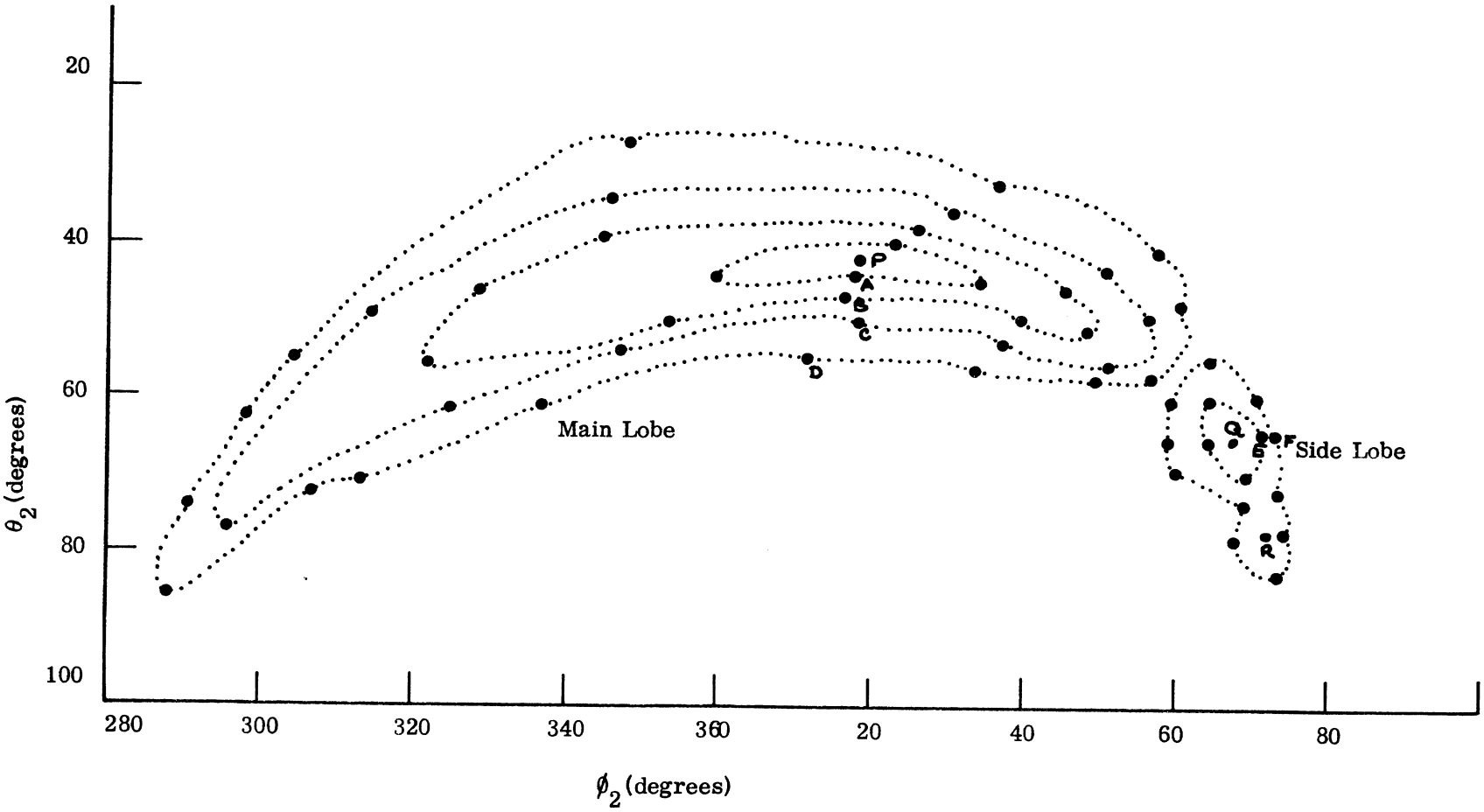

Fig. 3-2a: Contour of Radiation Pattern of Beam No. 1 viewed at x=0, y=0.5, z_r/z_a=0.5 .
Consult the Table 3.1 for db F_{2M} at the wind speed U=1.5 m/sec , the wind direction ψ=0 .

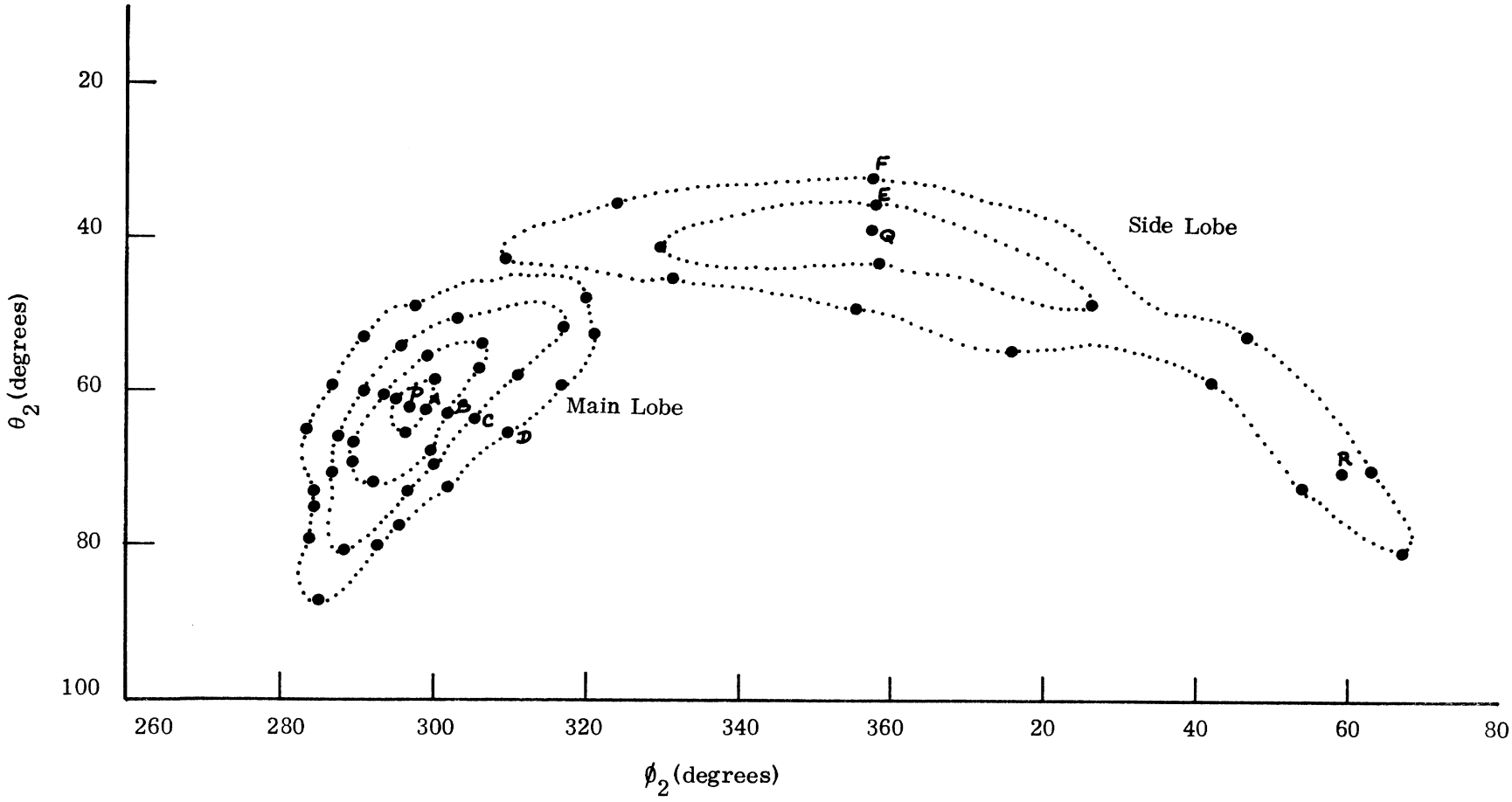

Fig. 3-2b: Contour of Radiation Pattern of Beam No. 2 viewed at x=0, y=0.5, z_r/z_a=0.5 .
Consult the Table 3-1 for db F_{2M} at the wind speed U=1.5 m/sec , the wind direction ψ=0 .

TABLE 3-1: Normalized Reflected Radiation Density, F_2M, for Different Directions of Incidence, received at X = 0, Y = 0.5, Z_r/Z_a = 0.5. The Wind Speed U = 1.5 m/Sec, its Direction ψ = 0.

	Points and Power Levels of F_0	dB F_2M of Beam No. 1 (Fig. 3-2a)	dB F_2M of Beam No. 2 (Fig. 3-2b)
Main Lobe	p: peak of F_0	-161.3	-678.2
	-1dB contour: read counter-clockwise, starting from A	-185.3, -155.8, -130.6, -273.6	-698, -477, -620, -620
	-5dB contour: read counter clock-wise, starting from B	-243.7, -214.4, -219.6, -146.7, -114.6, -289.7, -556.3, -554.3, -469.1	-750, -402, -303, -360, -605, -607, -607, -605, -616
	-15dB contour: read counter clockwise, starting from C	-292.6, -291.0, -361.2, -214.1, -131.0, - 95.0, -235.0, -246.7, -233.9, -235.2, -558.4	-760, -450, -266, -232, -329, -572, -576, -588, -576, -542, -572
	-25dB contour: read counter clockwise, starting from D	-448, -402.7, -423.2, -418.7, -189.8, -113.2, - 72.3, -163.7, -158.2, -161.8, -159.2, -161.2, -145.3, -159.4, -152.3	-580, -526, -295, -206, -232, -317, -560, -555, -559, -557, -543, -557, -550
Side Lobe	Q: peak of side lobe	-141.4	-199.5
	-15dB contour: read counter clockwise starting from E	-140.8, -542.8, -542.7, -548.7	-168.0, -138.9, -263.7, -567.8
	-25dB contour: read counter clockwise, starting from F	-544.2, -518.3, -335.6, -567.4, -560.1, -561.1, -564.7, -572.0, -564.7, -554.7, -555.7	-146.1, - 90.3, -144.8, -207.7, -348.6, -679.7, -683.6, -690.1, -682.0, -673.0, -675
	R: a point in -25dB range	-557	-675.4

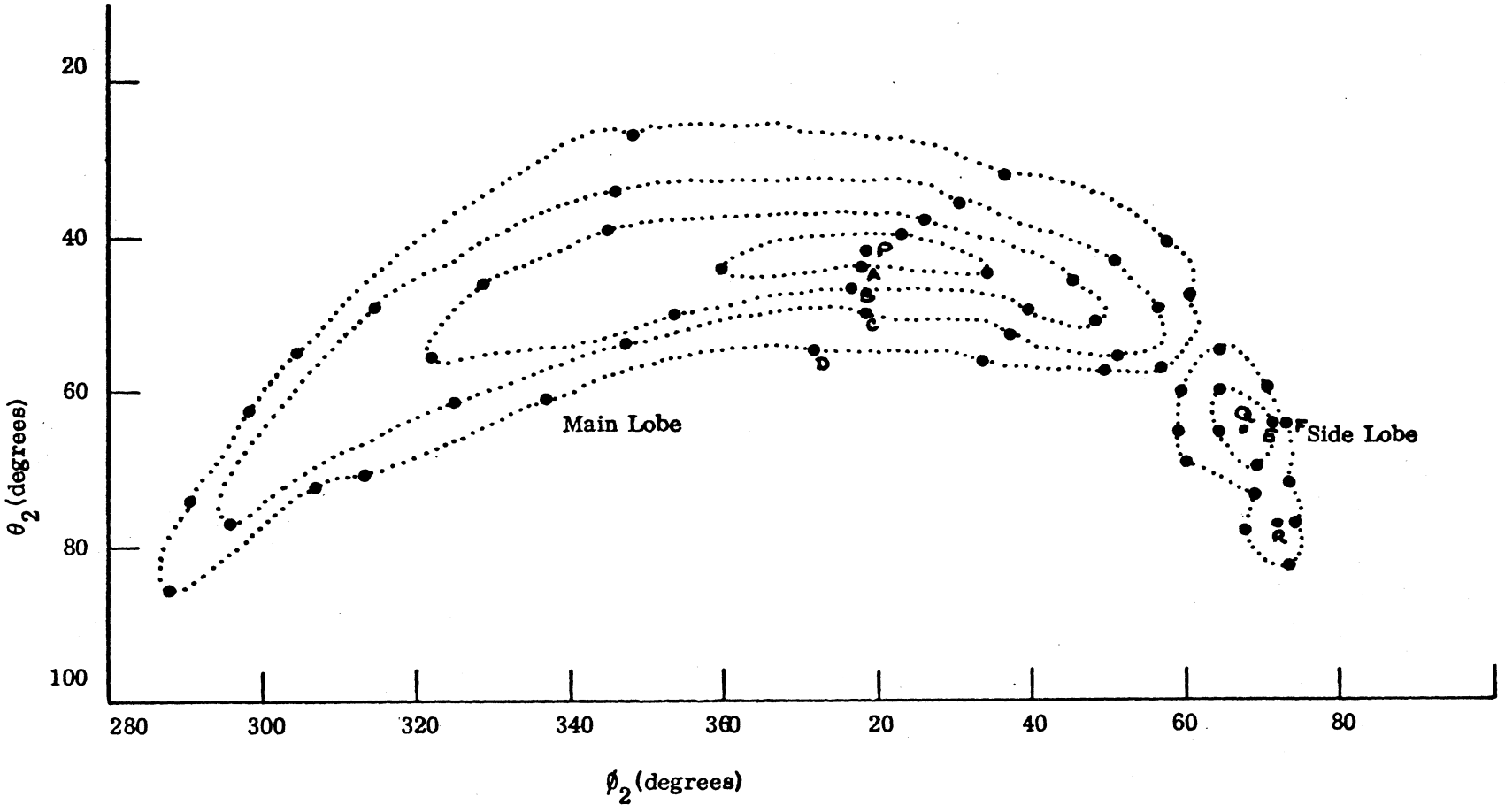

Fig. 3-3a: Contour of Radiation Pattern of Beam No. 1 viewed at x=0, y=0.5, z_r/z_a=0.5 .
Consult the Table 3.2 for db F_{2M} at the wind speed U=1.5 m/sec , the wind direction ψ=0 .

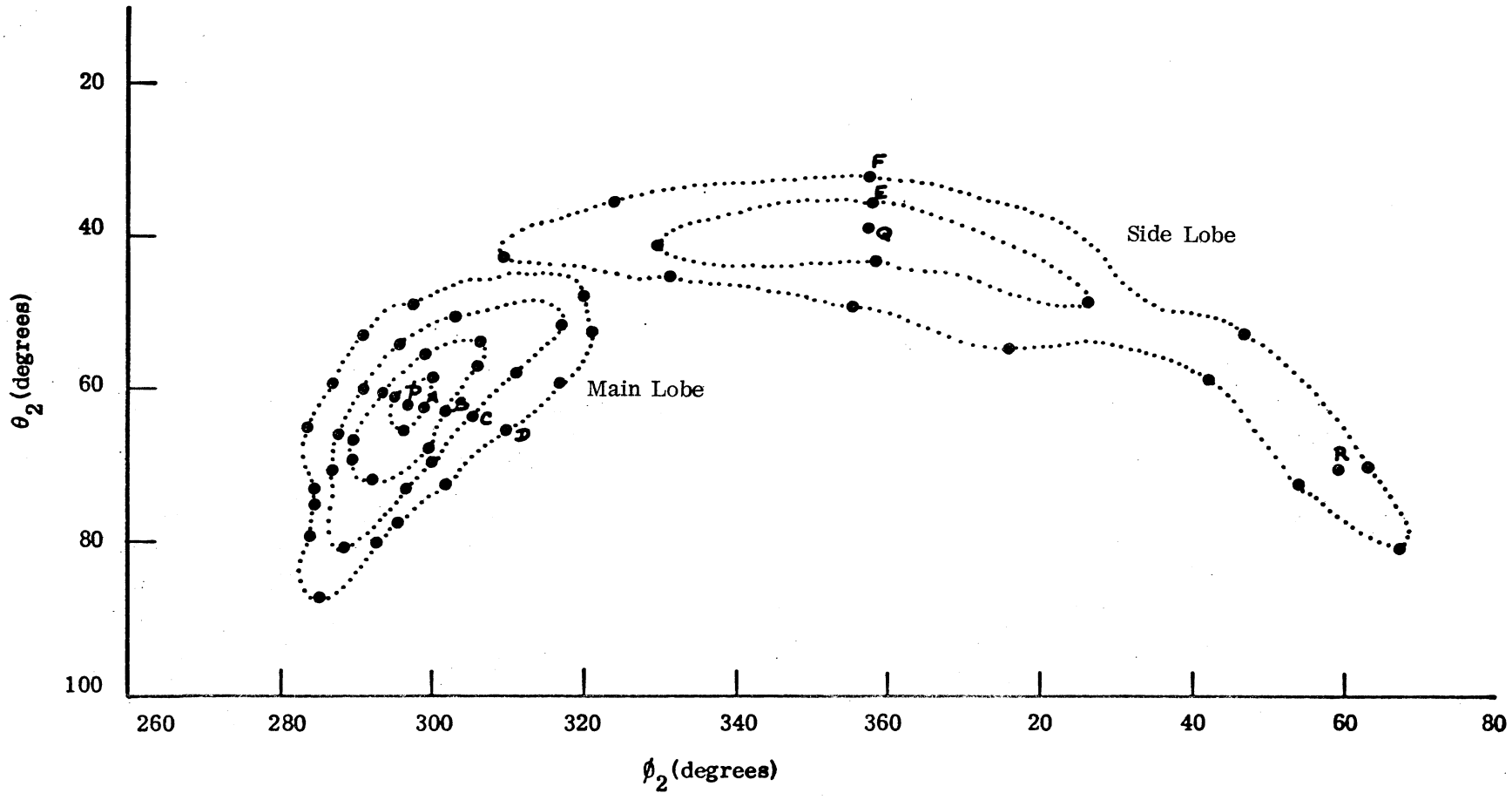

Fig. 3-3b: Contour of Radiation Pattern of Beam No. 2 viewed at x=0, y=0.5, z_r/z_a=0.5 .
Consult the Table 3.2 for db F_{2M} at the wind speed U=1.5 m/sec , the wind direction ψ=0 .

TABLE 3-2: Normalized Reflected Radiation Density, F_2d, for Different Directions of Incidences, received at X = 0, Y = 0.5, Z_r/Z_a = 0.5.

	Points and Power Levels of F_0	dB F_2d of Beam No. 1 (Fig. 3-3a)	dB F_2d of Beam No. 2 (Fig. 3-3b)
Main Lobe	p: peak of F_0	-7.3	-7.3
	-1dB contour: read counter clockwise, starting from A	- 7.5, - 7.4, - 8.7, - 9	- 7.5, - 7.4, - 8.7, - 9
	-5dB contour: read counter clockwise, starting from B	-13, -10.5, -11.0, -10.3, -11.5, -14.0, -14.7, -15.2, -24.3	-13, -10.5, -11.0, -10.3, -11.5, -14.0, -14.7, -15.2, -24.3
	-15dB contour: read counter clockwise, starting from C	-24.1, -22.7, -20.6, -19, -21.5, -21.1, -26.6, -40, -35.1, -30.4, -23.7	-24.1, -22.7, -20.6, -19, -21.5, -21.1, -26.6, -40, -35.1, -30.4, -23.7
	-25dB contour: read counter clockwise, starting from D	-31, -32, -31.2, -28.2, -33.8, -32.8, -30, -40, -37.3, -42.3, -41.6, -53.6, -28.5, -42.3, -32.0	-31, -32, -31.2, -28.2, -33.8, -32.8, -30, -40, -37.3, -42.3, -41.6, -53.6, -28.5, -42.3, -32.0
Side Lobe	Q: peak of side lobe	-20.2	-20.2
	-15dB contour: read counter clockwise, starting from E	-20, -22, -23.1, -30.3	-20, -22, -23.1, -30.3
	-25dB contour: read counter clockwise, starting from F	-24.2, -28.2, -31.7, -39, -33.4, -35.6, -40.4, -50.8, -47.8, -33.8, -30.8	-24.2, -28.2, -31.7, -39, -33.4, -35.6, -40.4, -50.8, -47.8, -33.8, -30.8
	R: A point in -25dB	-35.6	-35.6

3.4 Direction of Maximum Intensity of Reflected Radiation

The apparent direction of arrival of the reflected radiation received at any position is taken as the direction toward which a narrow beam receiving antenna would intercept the maximum amount of radiation intensity. For a specularly reflecting surface, this apparent direction of arrival, denoted by (θ_{2s}, ϕ_{2s}), may be calculated by Eqs. (3.6) and (3.7). For a diffusely reflecting surface, such as a random sea surface, this apparent direction of arrival, denoted by (θ_{2M}, ϕ_{2M}), is to be obtained by searching for the direction in which $F_2(\theta_2, \phi_2)$ is maximum. Discussions on the directions of arrival are given in this section. These are illustrated in Figs. 3-4a through 3-15b inclusive. In Figs. 3-4a and 3-4b the apparent direction of arrival for an observer located at $Y = 0.5$, $z_r/z_a = 0.5$, at the downwind speed of 1.5 m/sec is plotted against X to show the change in the apparent direction of arrival with the relative receiving position. In these curves are inserted the direction of arrival for a specularly reflecting surface for ready comparison. In Figs. 3-5a and b, similar curves are shown for the case of the cross-wind. In Figs. 3-6a and b and 3-7a and b, similar curves are shown for the receiver positioned at the relative height of 0.1. Figs. 3-8a through 3-11b show the corresponding cases at the wind speed of 4m/sec. The effects of the wind speed on the direction of arrival are shown in Figs. 3-12a and and b at $Y = 0.5$, $z_r/z_a = 0.1$ for the down-wind case; Figs. 3-13a and b show the similar curves for the cross-wind case. It is seen from these curves that the wind speed has little effect on the direction of arrival in the down-wind, but in the cross-wind case, the direction of arrival is sensitive to the wind speed in the range $|x| \leqslant 1$. Figs. 3-14a and b show the effect of the wind direction on the direction of arrival at the wind speed of 1.5m/sec at $Y = 0.5$, $z_r/z_a = 0.1$; Figs. 3-15a and b show the similar curves at the wind speed of 4m/sec. It is observed from these curves that the direction of arrival is slightly more sensitive to the change in the wind direction for the lower wind speed than in the higher wind speed, the significant effect being confined, again, more or less within the range $|x| \leqslant 1$.

For completeness, the approximate direction of arrival for the case of a Lambert surface, denoted by (θ_{2d}, ϕ_{2d}), are presented in Figs. 3-16a, b and Figs. 3-17a, b. In this case, based on the argument given in the last section, the maximum direction of arrival corresponds to the peak of each major lobe, and hence appears to be multi-valued. However, it should be noted that only one of the directions of arrival, corresponding to the reflecting point which is the closest to the point of observation, should have the dominant effect on the total reflected power received.

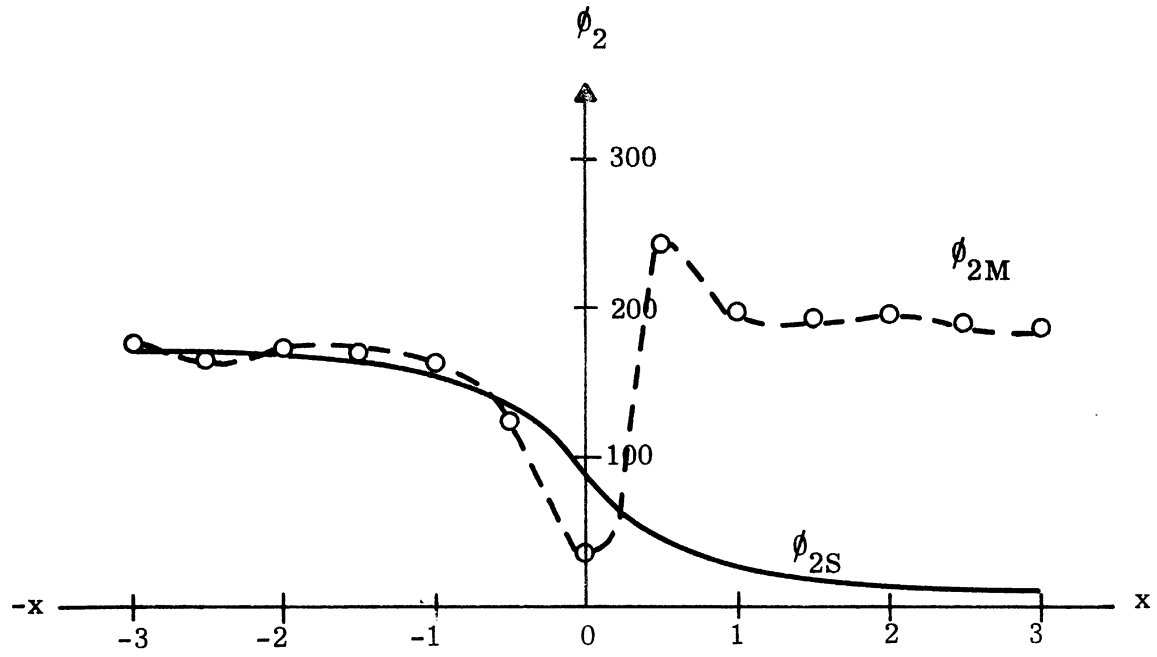

Fig. 3-4a: Comparison of the Maximum Directions of Arrival (Azimuth) for the random ocean and Specular Surfaces at down-wind speed of 1.5 m/sec. The relative Receiver Height is 0.5, Y = 0.5.

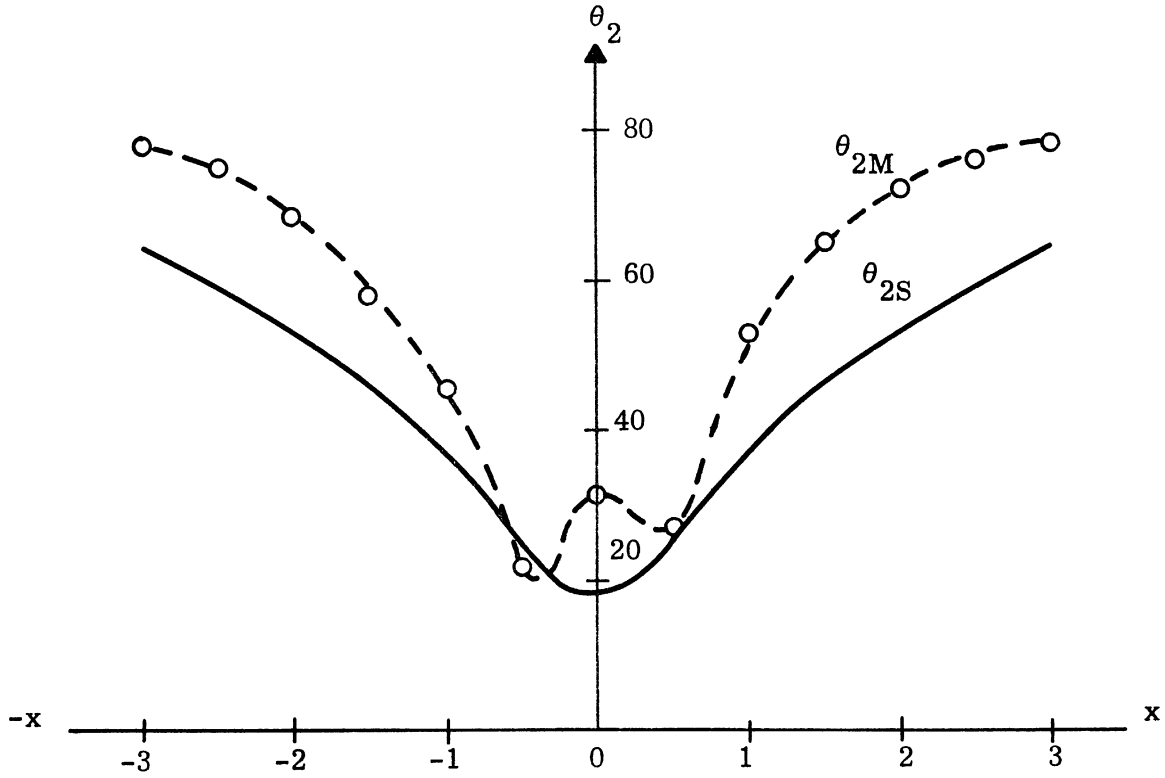

Fig. 3-4b: Comparison of the Maximum Directions of Arrival (latitude) for the random and Specular Surfaces at down-wind speed of 1.5 m/sec. The relative Receiver Height is 0.5, Y = 0.5.

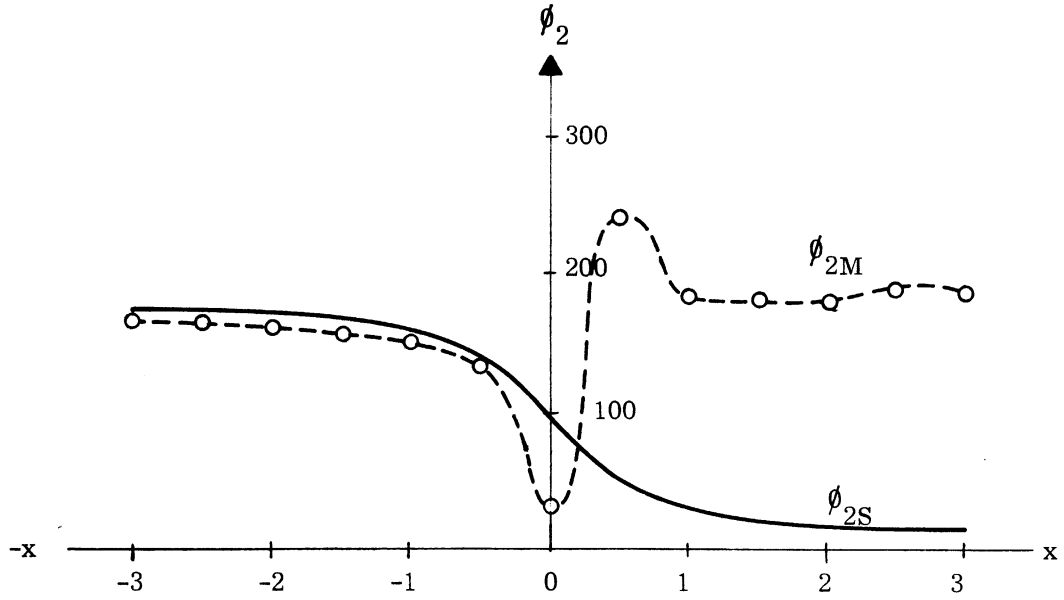

Fig. 3-5a: Comparison of the Maximum Direction of Arrival (Azimuth) for the random ocean and Specular Surfaces at the cross-wind speed of 1.5 m/sec. The Relative Receiver Height $\frac{z_r}{z_a} = 0.5$, Y=0.5.

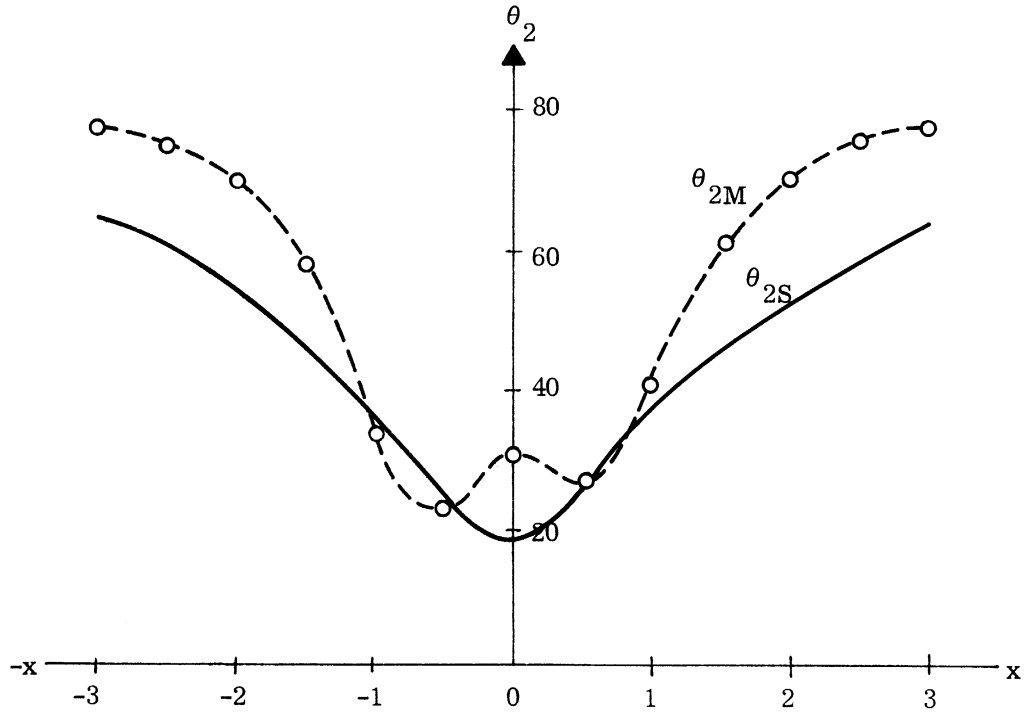

Fig. 3-5b: Comparison of the Maximum Direction of Arrival (Latitude) for the Random Ocean and Specular Surfaces at the cross-wind speed of 1.5 m/sec. The relative Receiver Height $\frac{z_r}{z_a} = 0.5$, Y = 0.5.

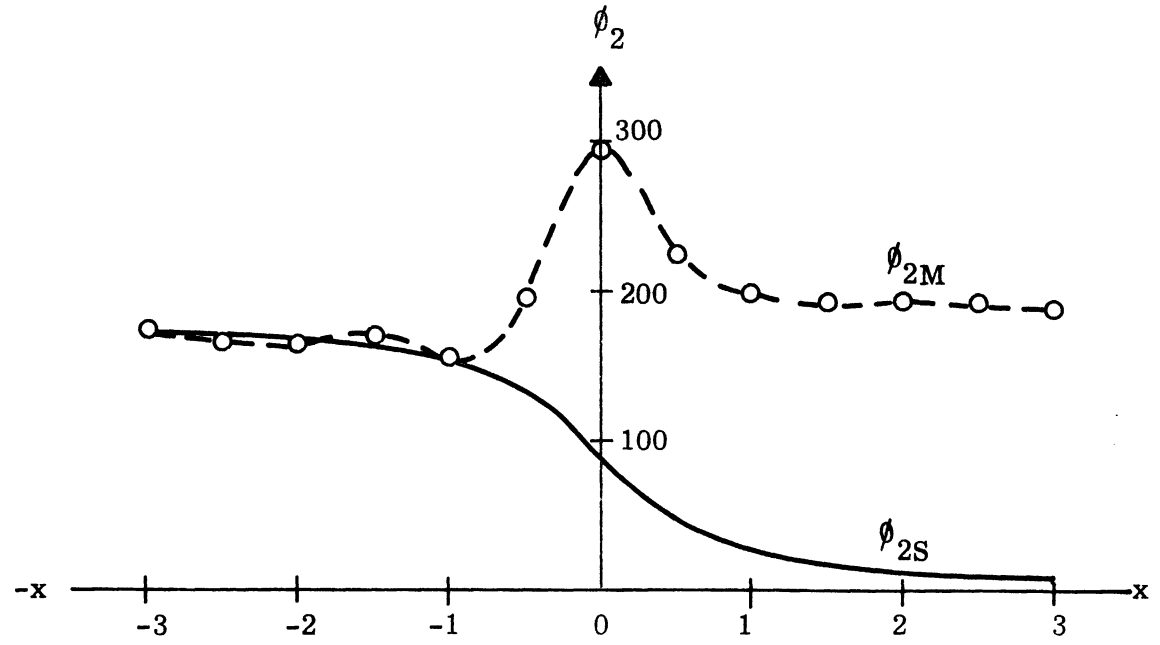

Fig. 3-6a: Comparison of the Maximum Directions of Arrival (Azimuth) for the Random and Specular Surfaces at down-wind speed of 1.5 m/sec. The relative Receiver Height is 0.1, Y = 0.5.

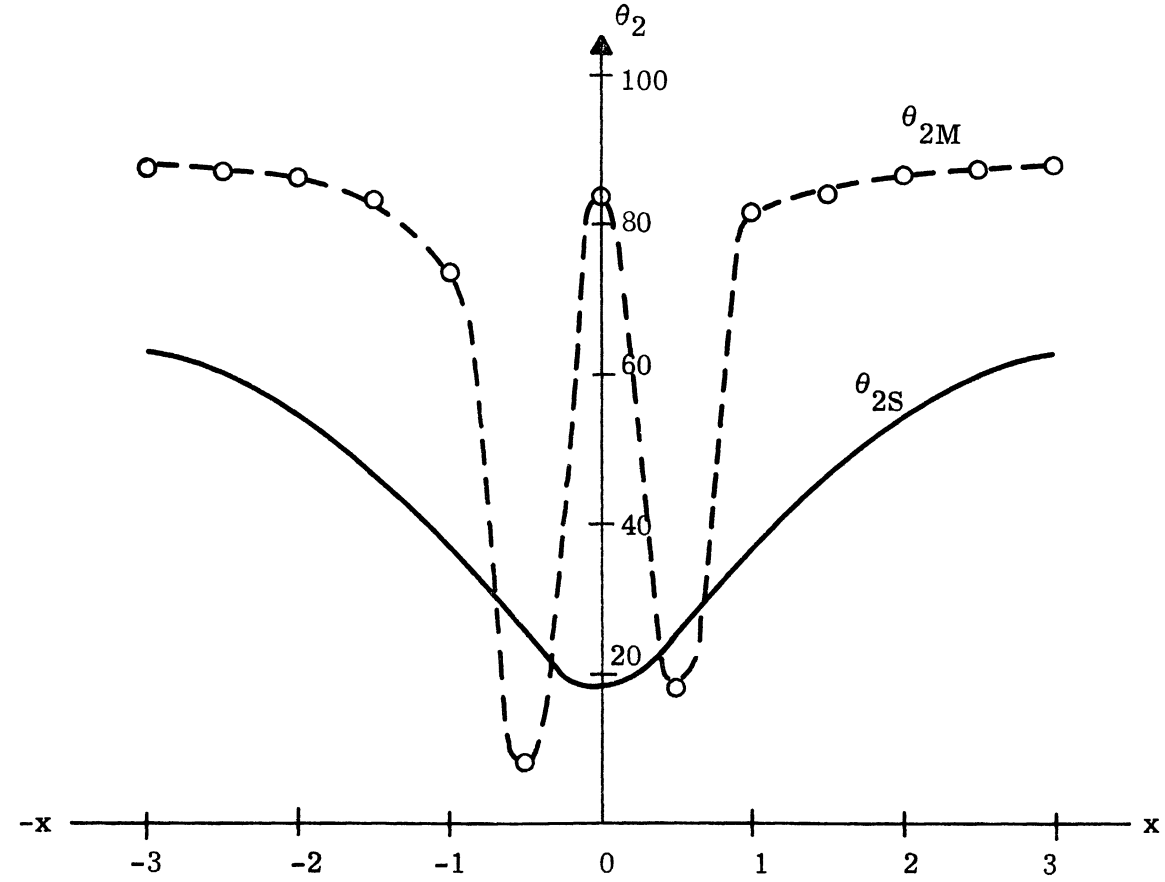

Fig. 3-6b: Comparison of the Maximum Directions of Arrival (latitude) for the Random and Specular Surfaces at down-wind speed of 1.5 m/sec. The Relative Receiver Height is 0.1, Y = 0.5.

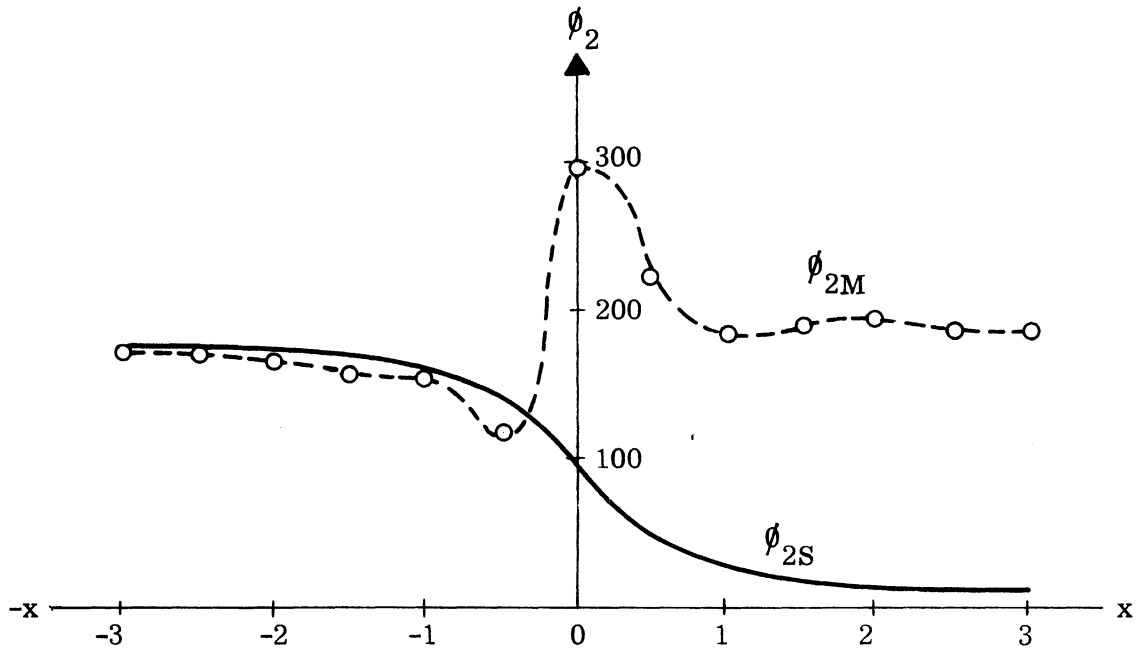

Fig. 3-7a: Comparison of the Maximum Direction of Arrival (Azimuth) for the Random Ocean and Specular Surfaces at the cross-wind speed of 1.5 m/sec. The Relative Receiver Height $\frac{z_r}{z_a} = 0.1$, Y = 0.5.

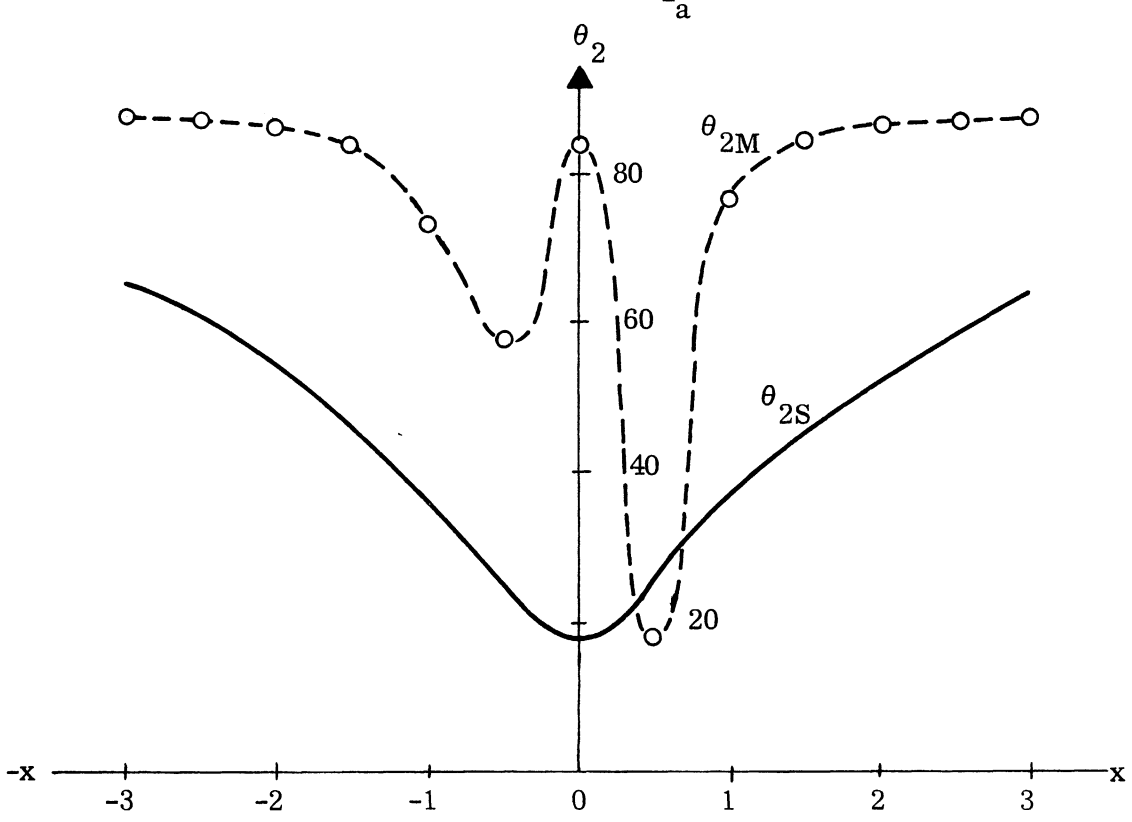

Fig. 3-7b: Comparison of the Maximum Direction of Arrival (Latitude) for the Random Ocean and Specular Surfaces at the cross-wind speed of 1.5 m/sec. The Relative Receiver Height $\frac{z_r}{z_a} = 0.1$, Y = 0.5.

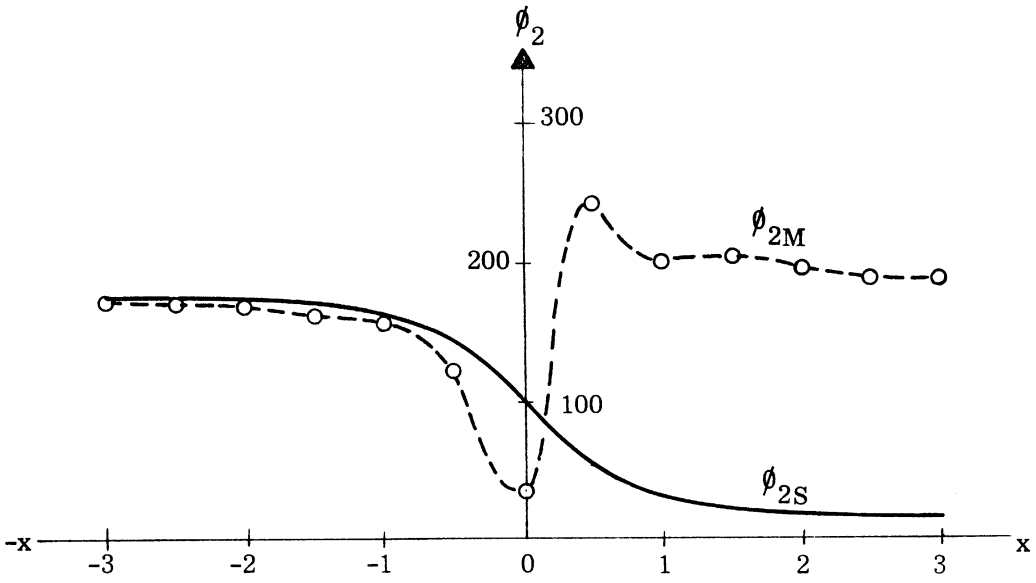

Fig. 3-8a: Comparison of the Maximum Direction of Arrival (Azimuth) for the Random Ocean and Specular Surfaces at the down-wind speed of 4 m/sec. The Relative Receiver Height $z_r/z_a = 0.5$, $Y = 0.5$.

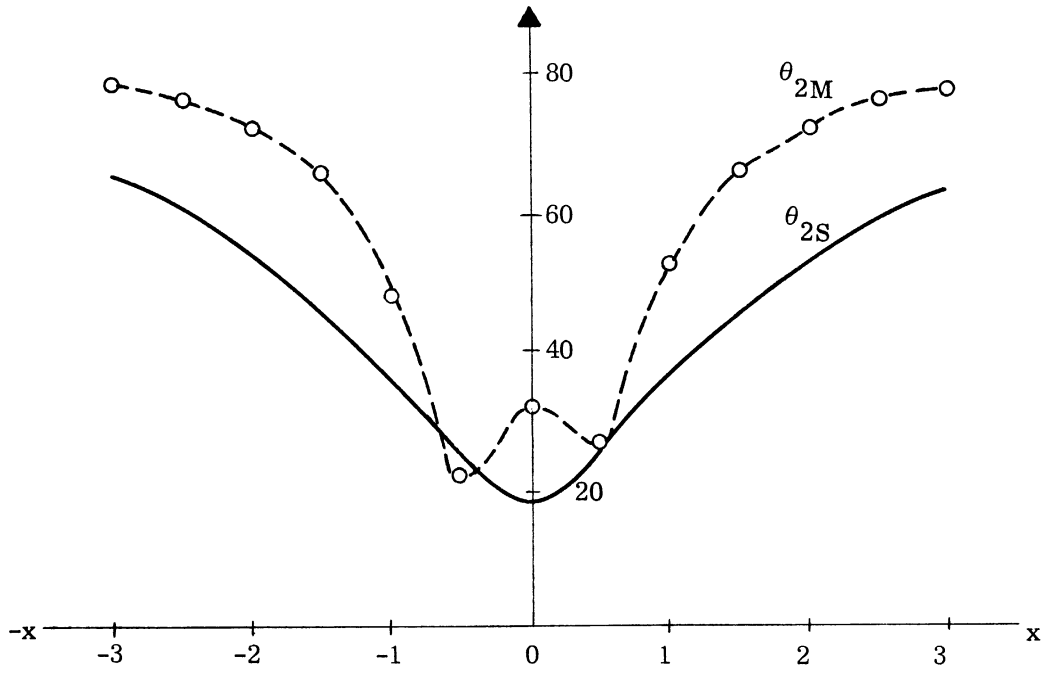

Fig. 3-8b: Comparison of the Maximum Direction of Arrival (Latitude) for the Random Ocean and Specular Surfaces at the down-wind speed of 4 m/sec. The Relative Receiver Height $z_r/z_a = 0.5$, $Y = 0.5$.

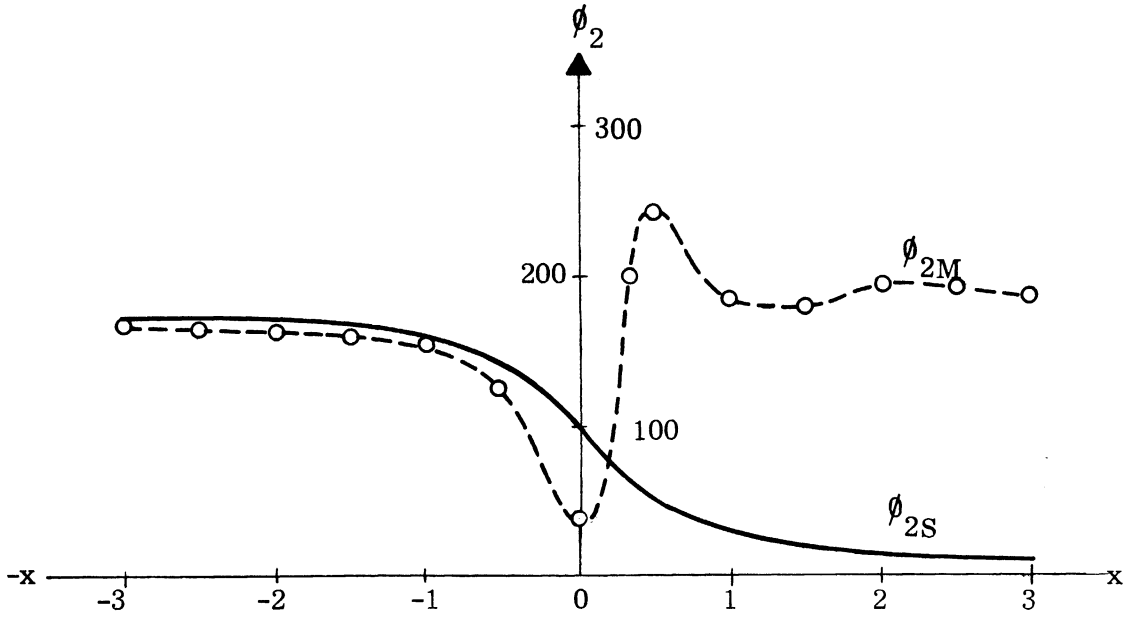

Fig. 3-9a: Comparison of the Maximum Direction of Arrival (Azimuth) for the Random Ocean and Specular Surfaces at the cross-wind speed of 4 m/sec. The Relative Receiver Height z_r/z_a = 0.5, Y = 0.5.

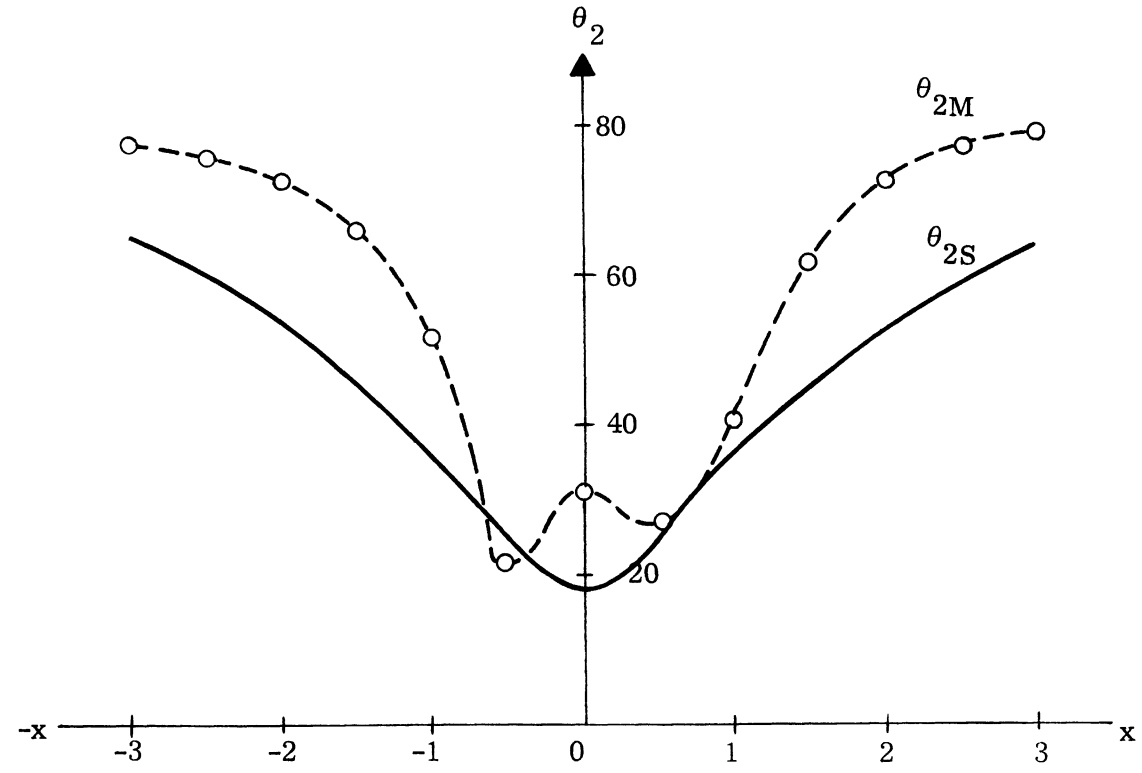

Fig. 3-9b: Comparison of the Maximum Direction of Arrival (Latitude) for the Random Ocean and Specular Surfaces at the cross-wind speed of 4 m/sec. The Relative Reciever Height z_r/z_a = 0.5, Y = 0.5.

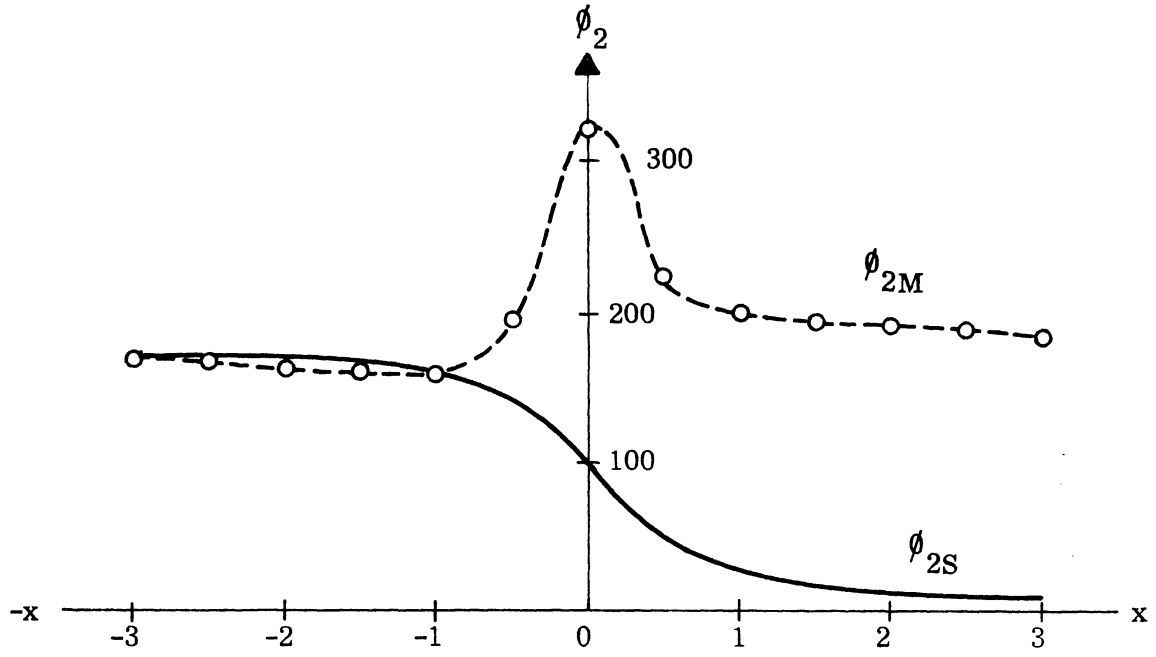

Fig. 3-10a: Comparison of the Maximum Direction of Arrival (Azimuth) for the Random Ocean and Specular Surfaces at the down-wind speed of 4 m/sec. The Relative Receiver Height $z_r/z_a = 0.1$, $Y = 0.5$.

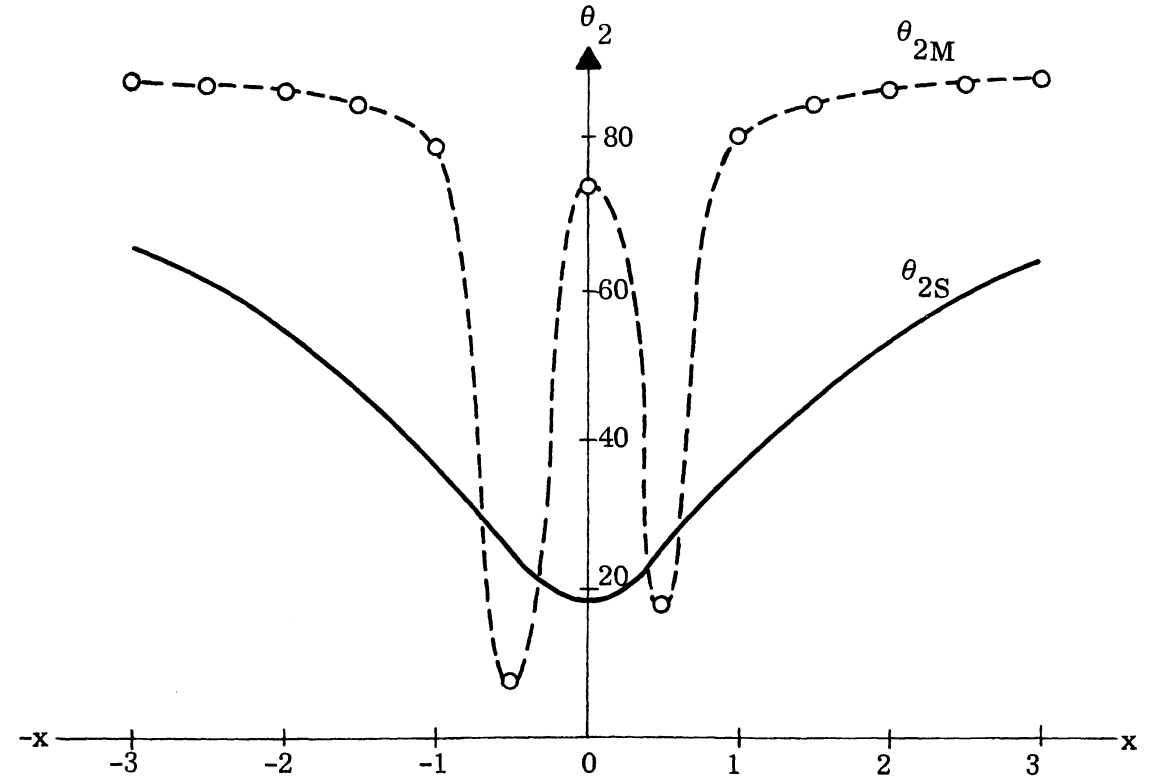

Fig. 3-10b: Comparison of the Maximum Direction of Arrival (Latitude) for the Random Ocean and Specular Surfaces at the down-wind speed of 4 m/sec. The Relative Receiver Height $z_r/z_a = 0.1$, $Y = 0.5$.

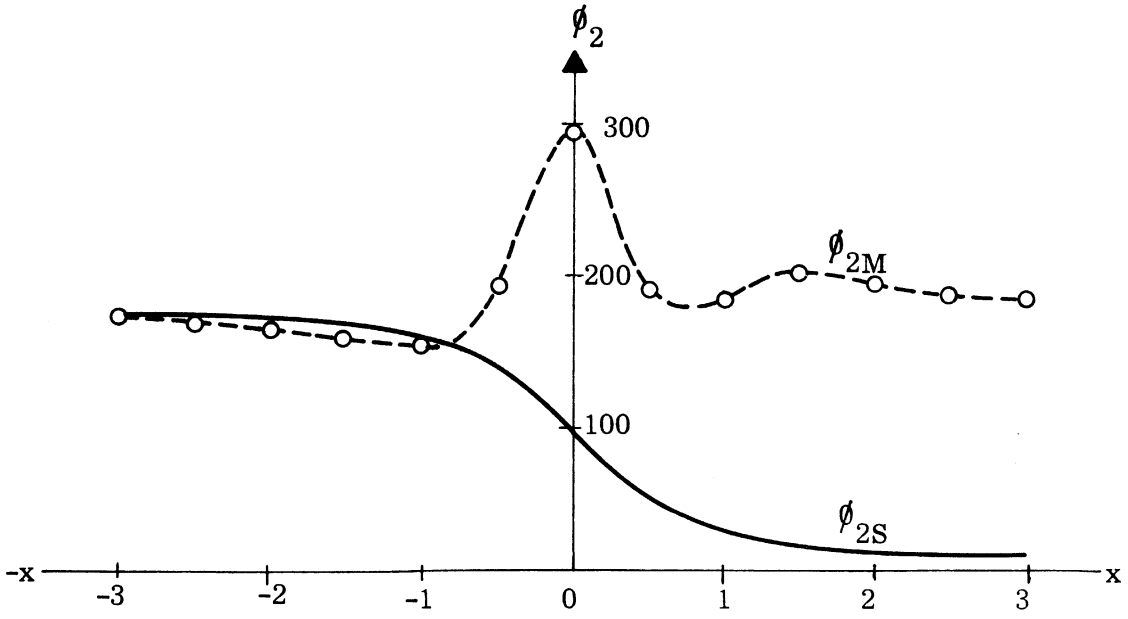

Fig. 3-11a: Comparison of the Maximum Direction of Arrival (Azimuth) for the Random Ocean and Specular Surfaces at the cross-wind speed of 4 m/sec. The Relative Receiver Height $z_r/z_a = 0.1$, $Y = 0.5$.

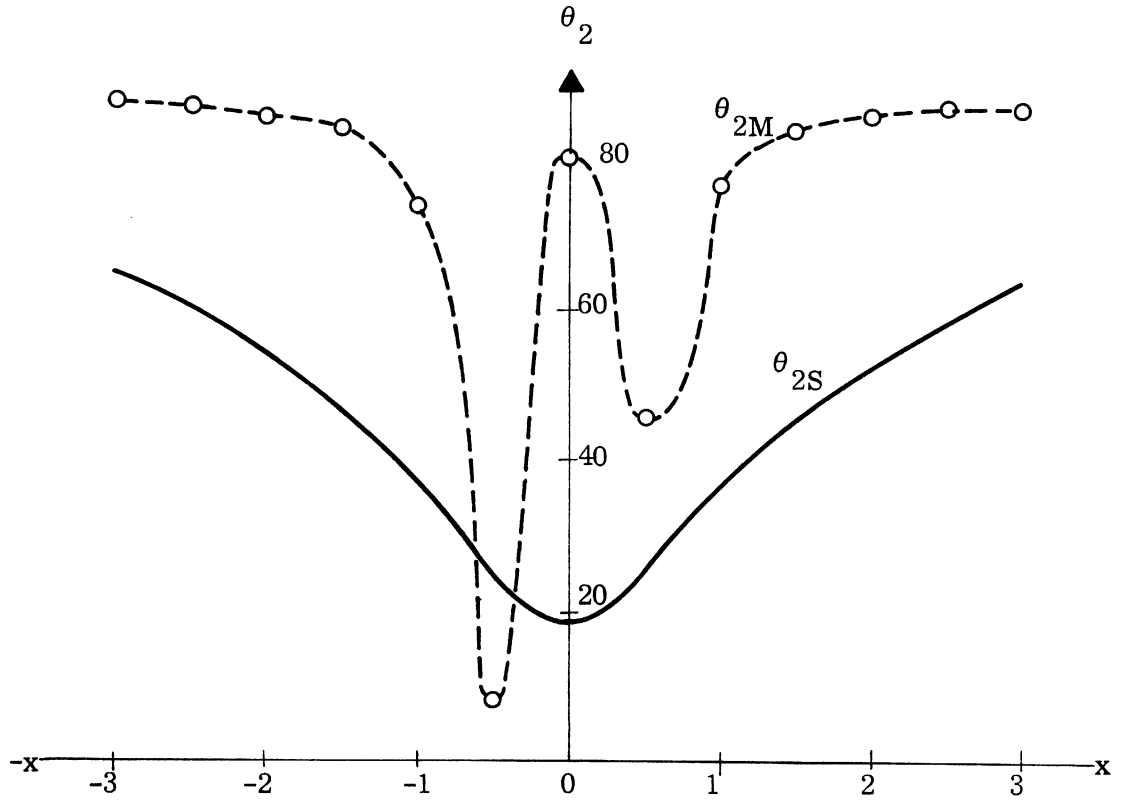

Fig. 3-11b: Comparison of the Maximum Direction of Arrival (Latitude) for the Random Ocean and Specular Surfaces at the Cross-wind speed of 4 m/sec. The Relative Receiver Height $z_r/z_a = 0.1$, $Y = 0.5$.

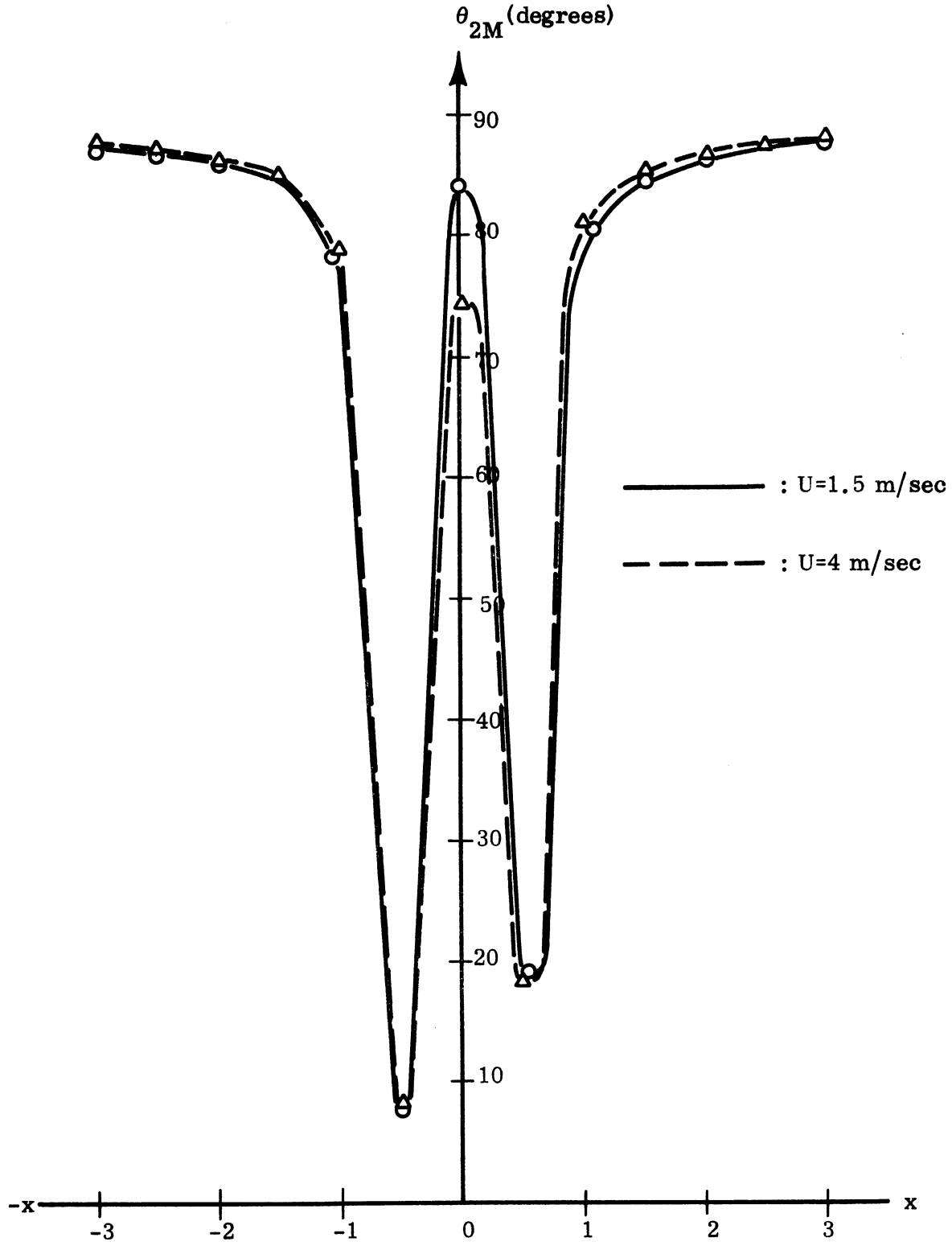

Fig. 3-12a: The Effect of the Wind Speeds (U=1.5, 4 m/sec) on the Directions of the Maximum Reflected Radiation Intensities (Latitude) for the Down-wind Case. The Relative Receiver Height is 0.1, y=0.5 .

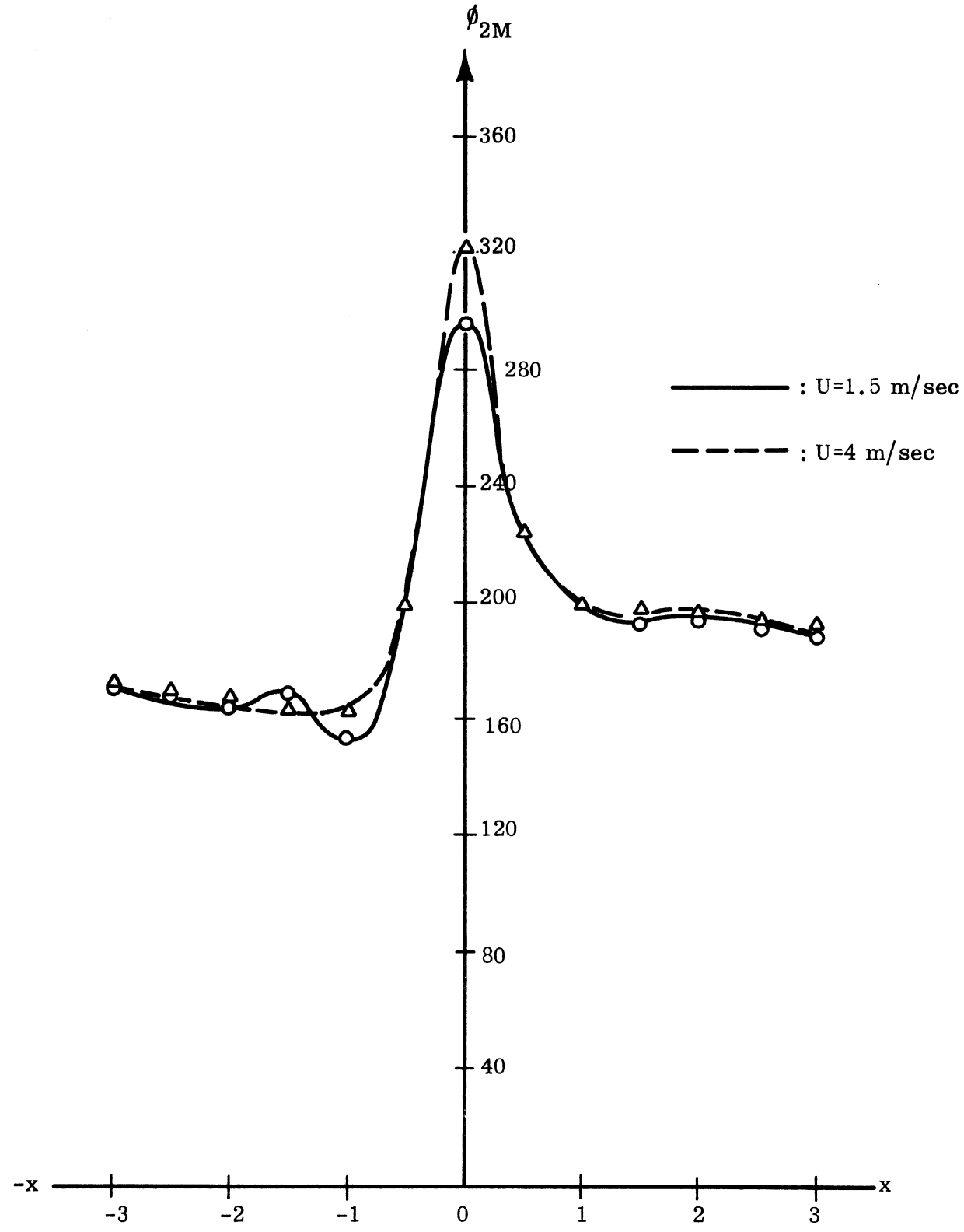

Fig.3-12b: The Effect of the Wind Speeds (U=1.5, 4 m/sec) on the Directions of the Maximum Reflected Radiation Intensities (Azimuth) for the Down-wind Case.
The Relative Receiver Height is 0.1 , y=0.5 .

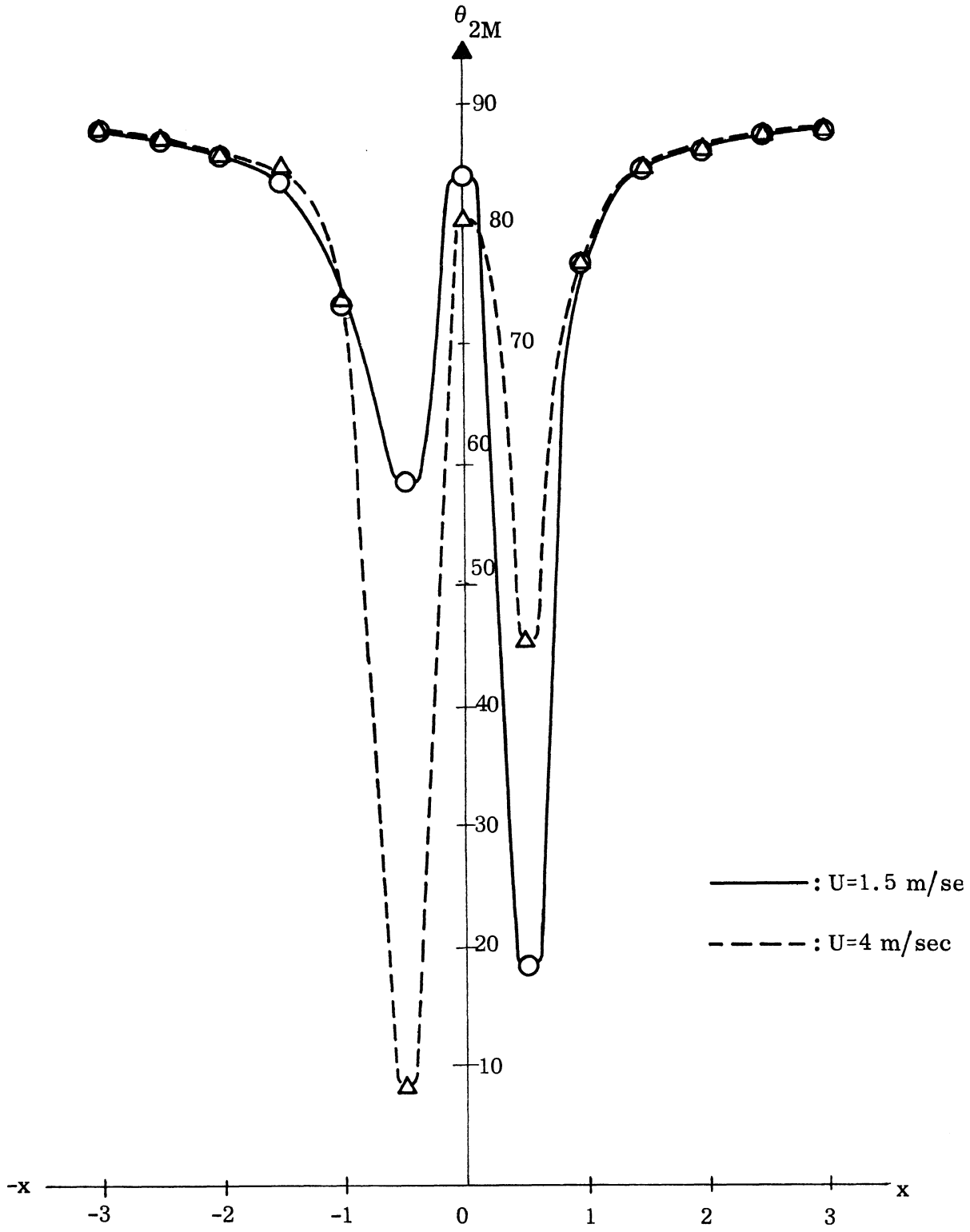

Fig. 3-13a: The Effect of the Wind Speed (U = 1.5, 4 m/sec) on the Direction of the Maximum Reflected Radiation Intensities (Latitude) for the Cross-Wind Case. The Relative Receiver Height z_r/z_a = 0.1, Y = 0.5.

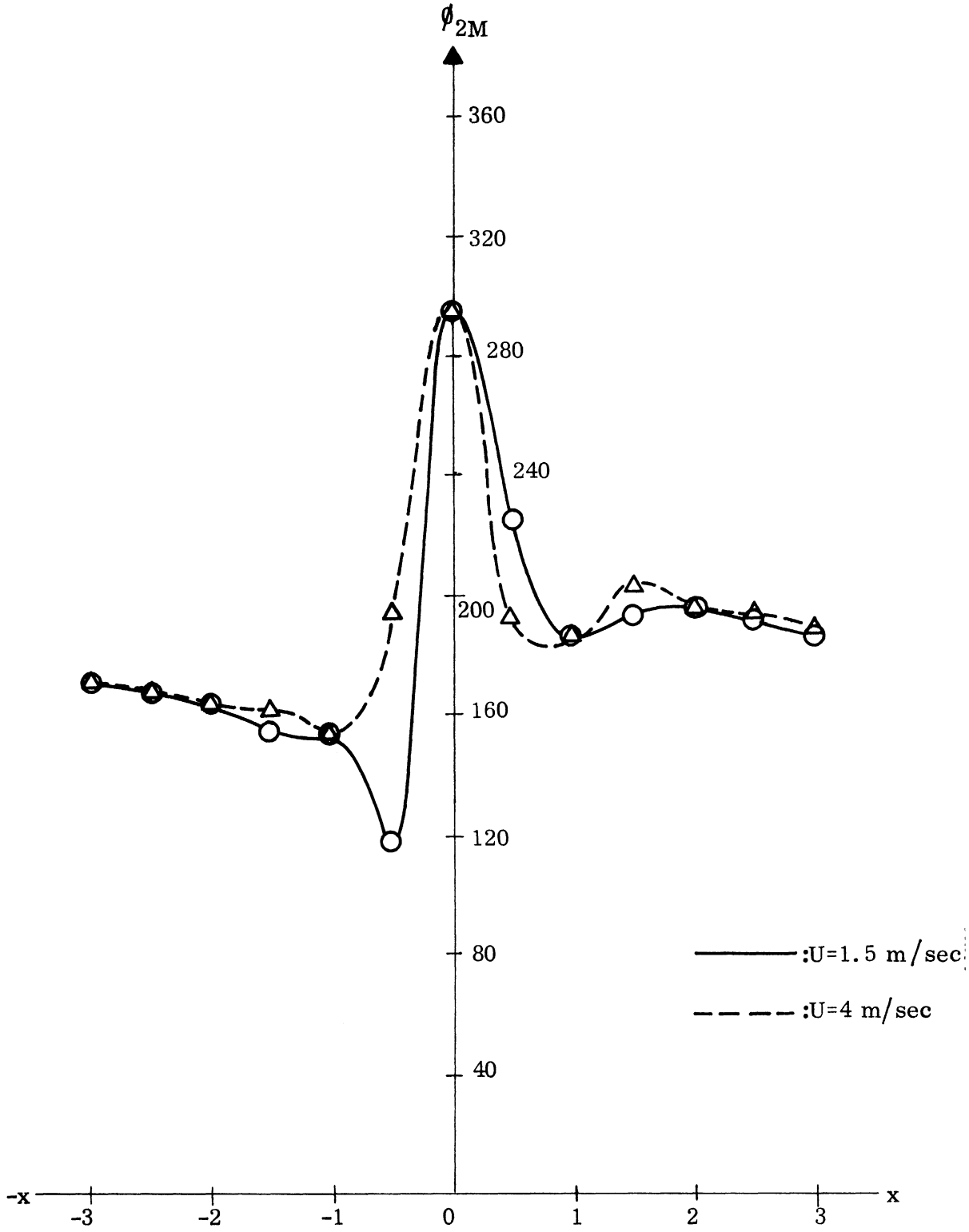

Fig. 3-13b: Effect of the Wind Speeds (U = 1.5, 4 m/sec) on the Directions of the Maximum Reflected Radiation Intensities (Azimuth) for the Cross-Wind Case. The Relative Receiver Height z_r/z_a = 0.1, Y = 0.5.

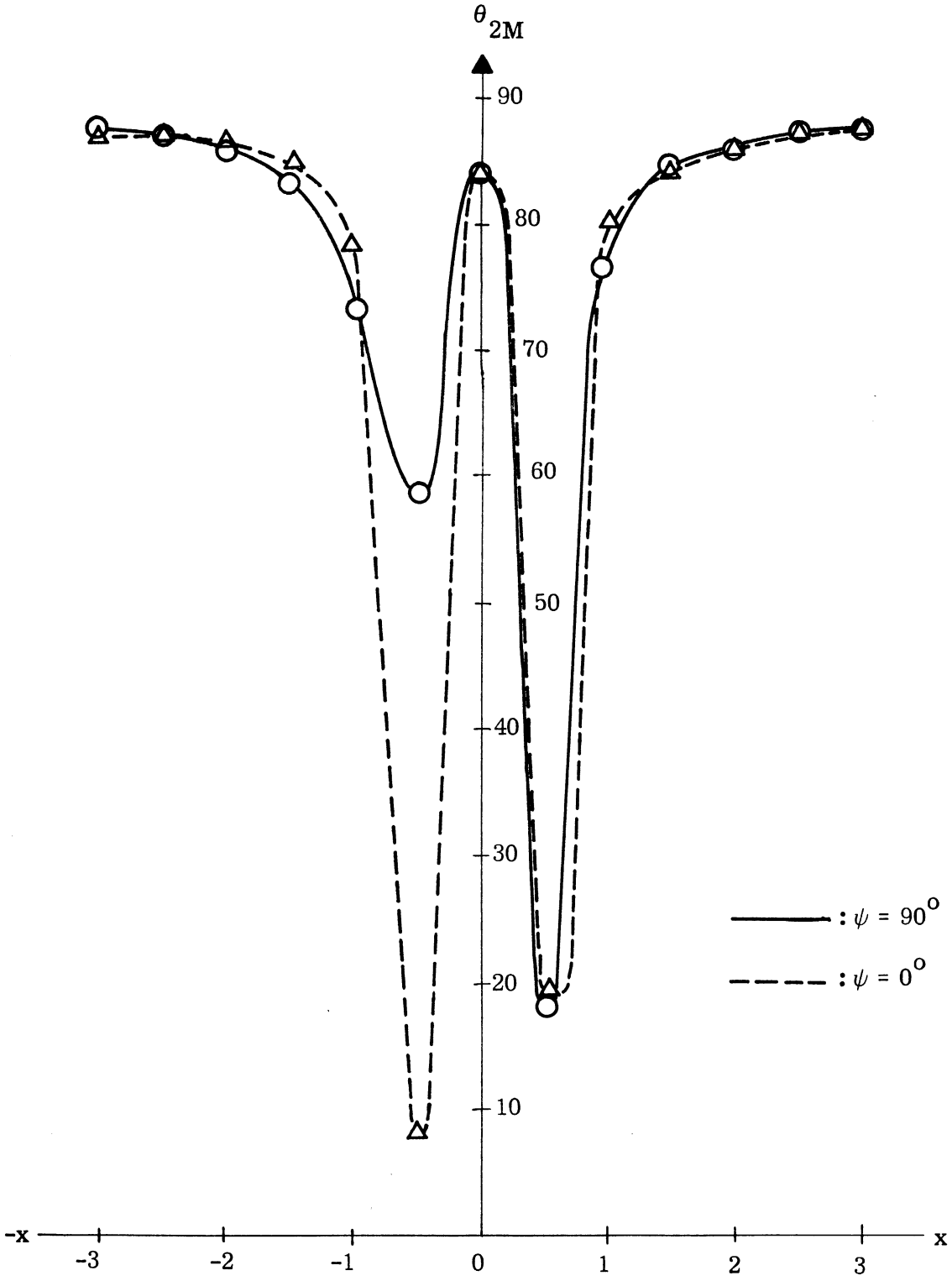

Fig. 3-14a: Effect of the Wind Directions on the Direction of Maximum Radiation Intensity (Latitude) at Y = 0.5, z_r/z_a = 0.1 for the Wind Speed of 1.5 m/sec.

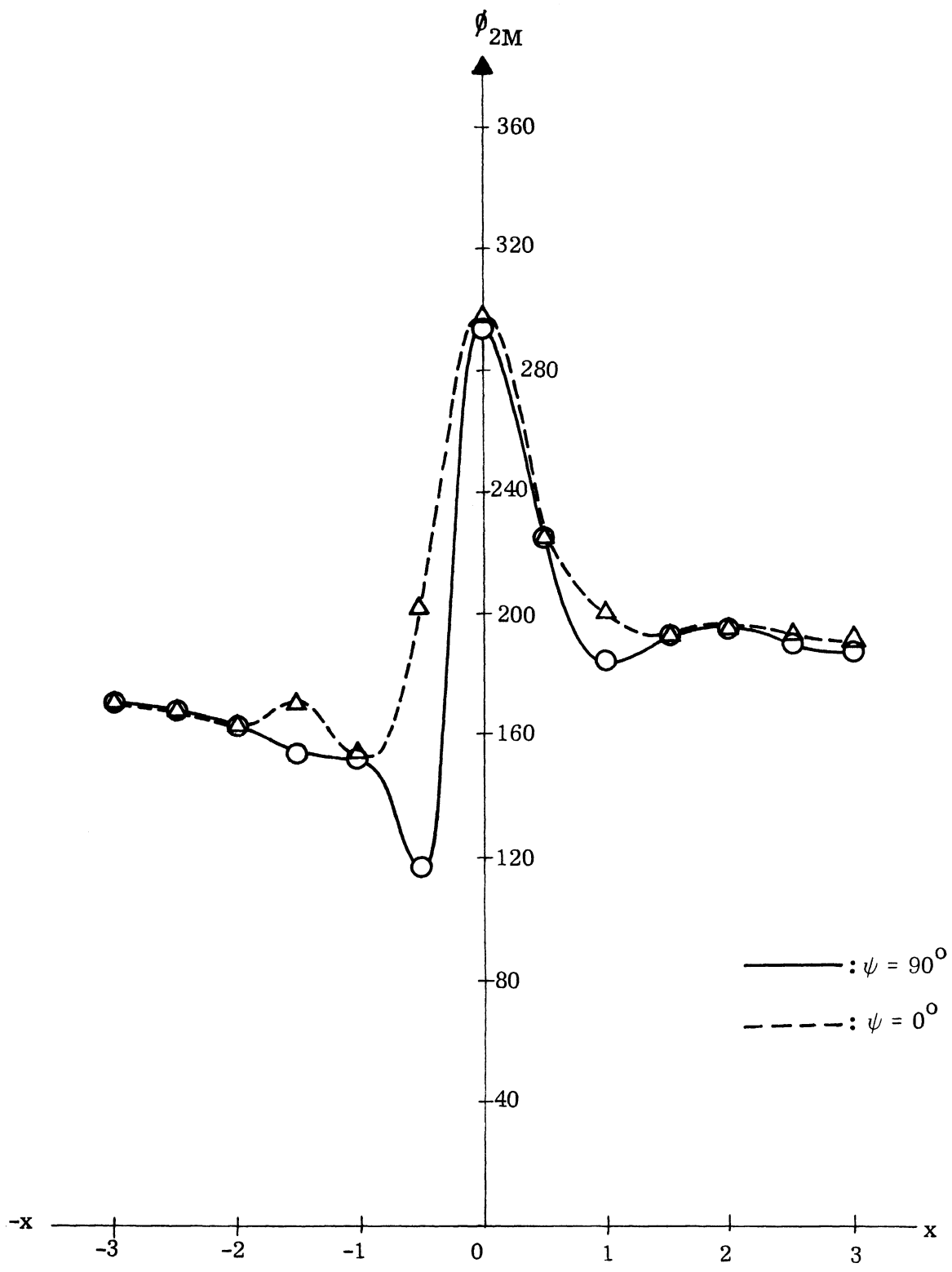

Fig. 3-14b: Effect of the Wind Direction on the Direction of Maximum Radiation Intensity (Azimuth) at Y = 0.5, z_r/z_a = 0.1, for the Wind Speed of 1.5 m/sec.

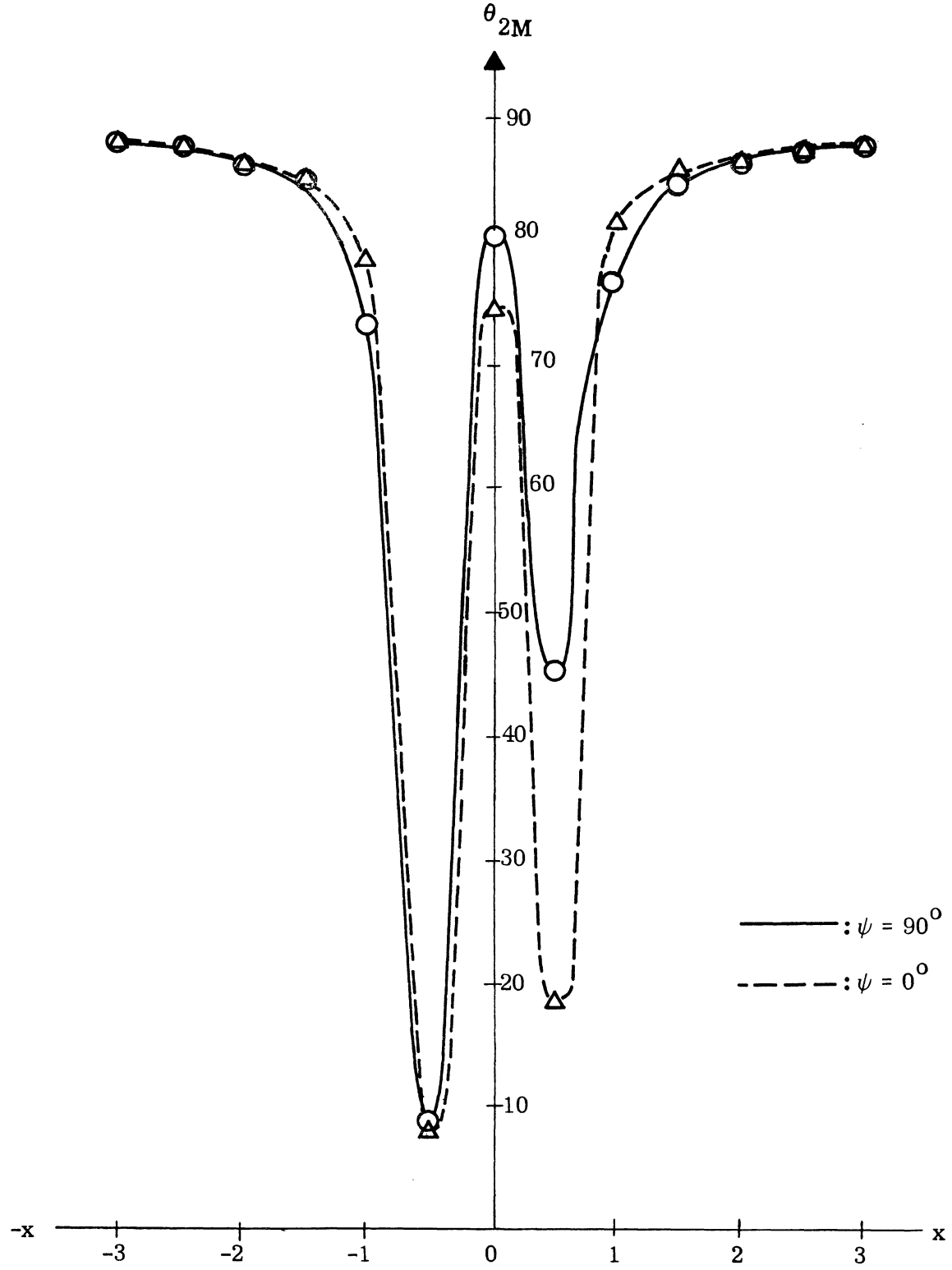

Fig. 3-15a: Effect of the Wind Direction on the Direction of the Maximum Radiation Intensity (Latitude) at Y = 0.5, z_r/z_a = 0.1 for the Wind Speed of 4 m/sec.

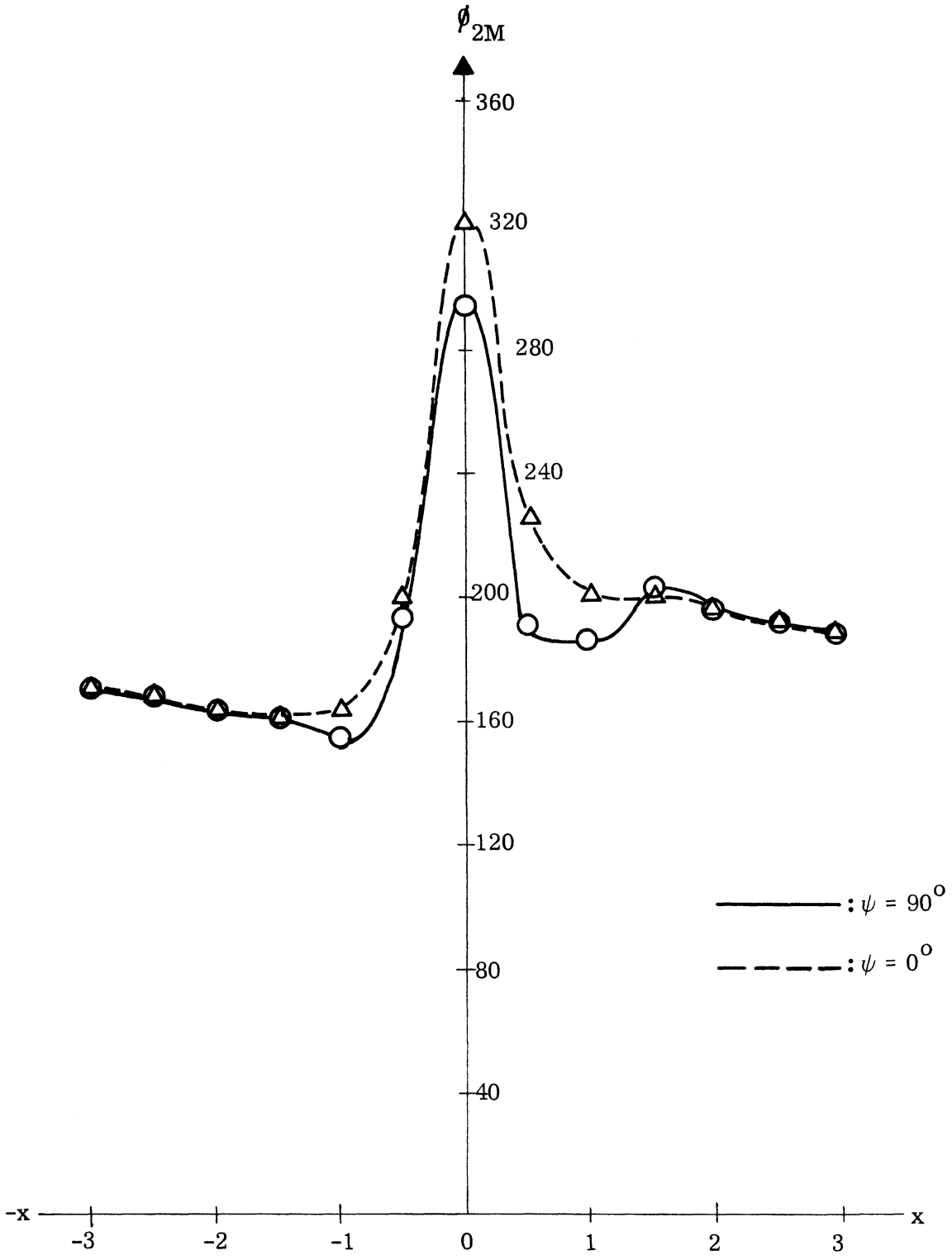

Fig. 3-15b: Effect of the Wind Direction on the Direction of the Maximum Radiation Intensity (Azimuth) at Y = 0.5, z_r/z_a = 0.1 for the Wind Speed of 4 m/sec.

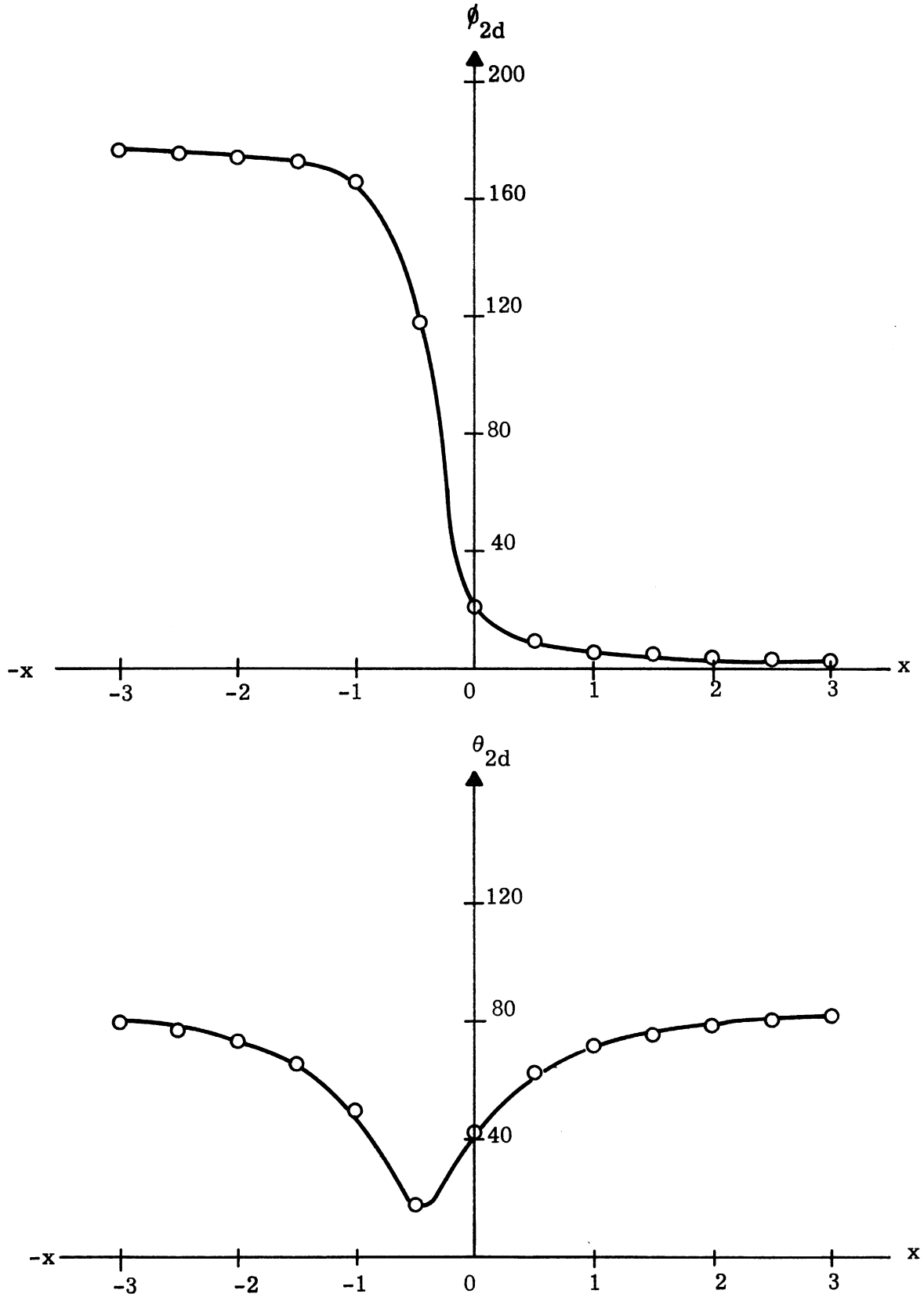

Fig. 3-16a: Directions of Arrival for a Lambert Surface at y=0.5, z_r/z_a=0.5 for Beam No. 1 .

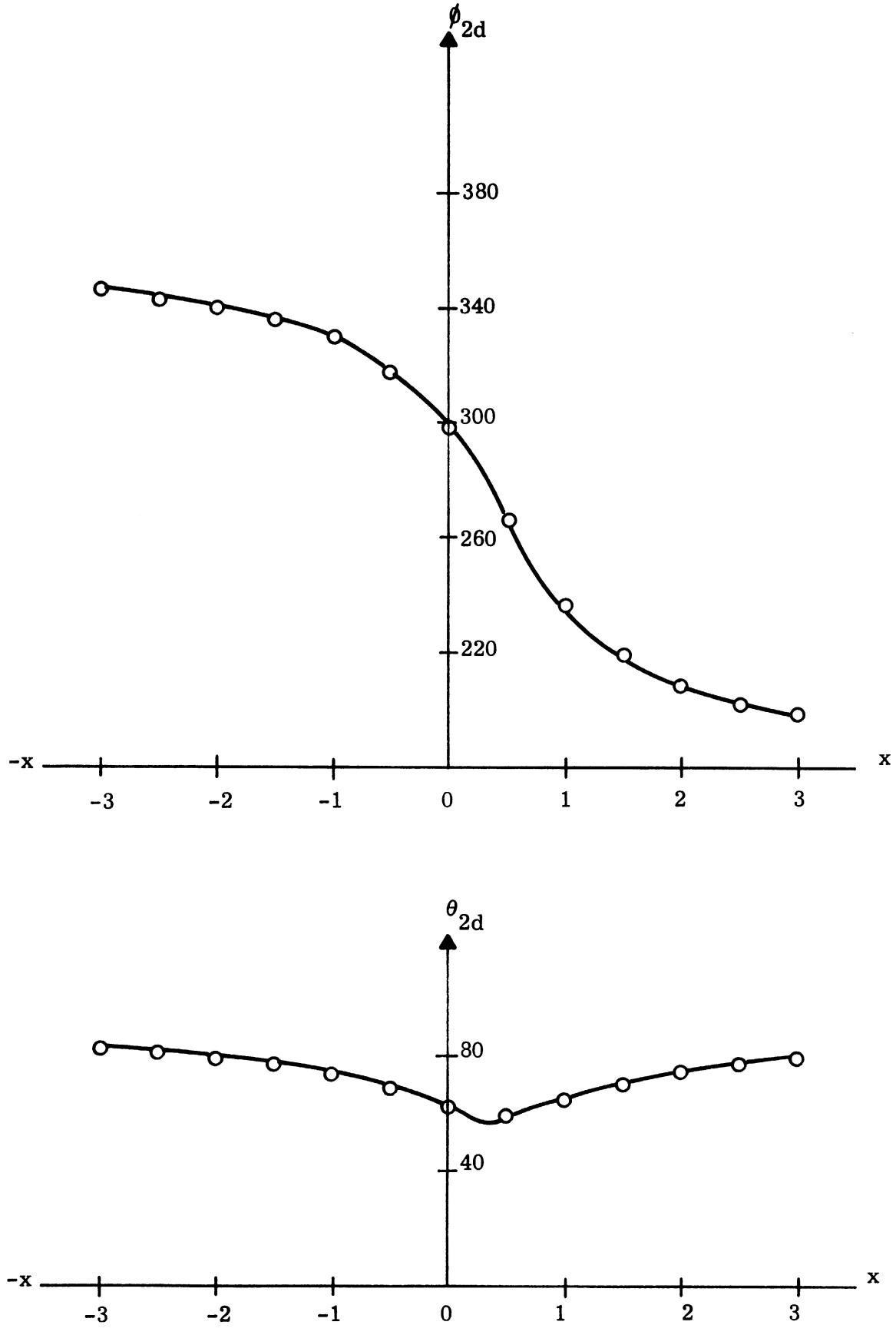

Fig. 3-16b: Directions of Arrival for a Lambert Surface at y=0.5, z_r/z_a=0.5, for Beam No. 2 .

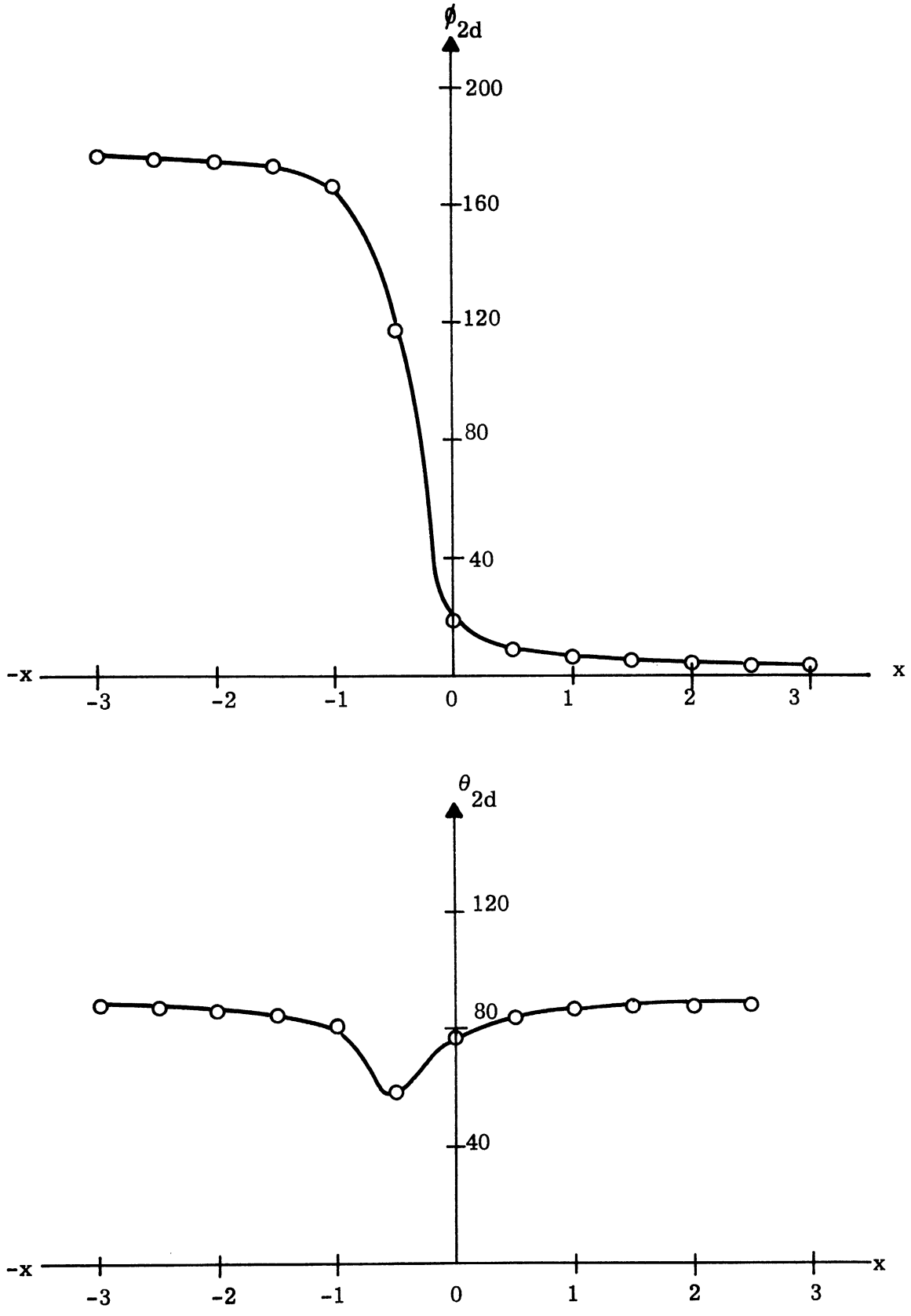

Fig. 3-17a: Directions of Arrival for a Lambert Surface at y=0.5, z_r/z_a=0.1 for Beam No. 1 .

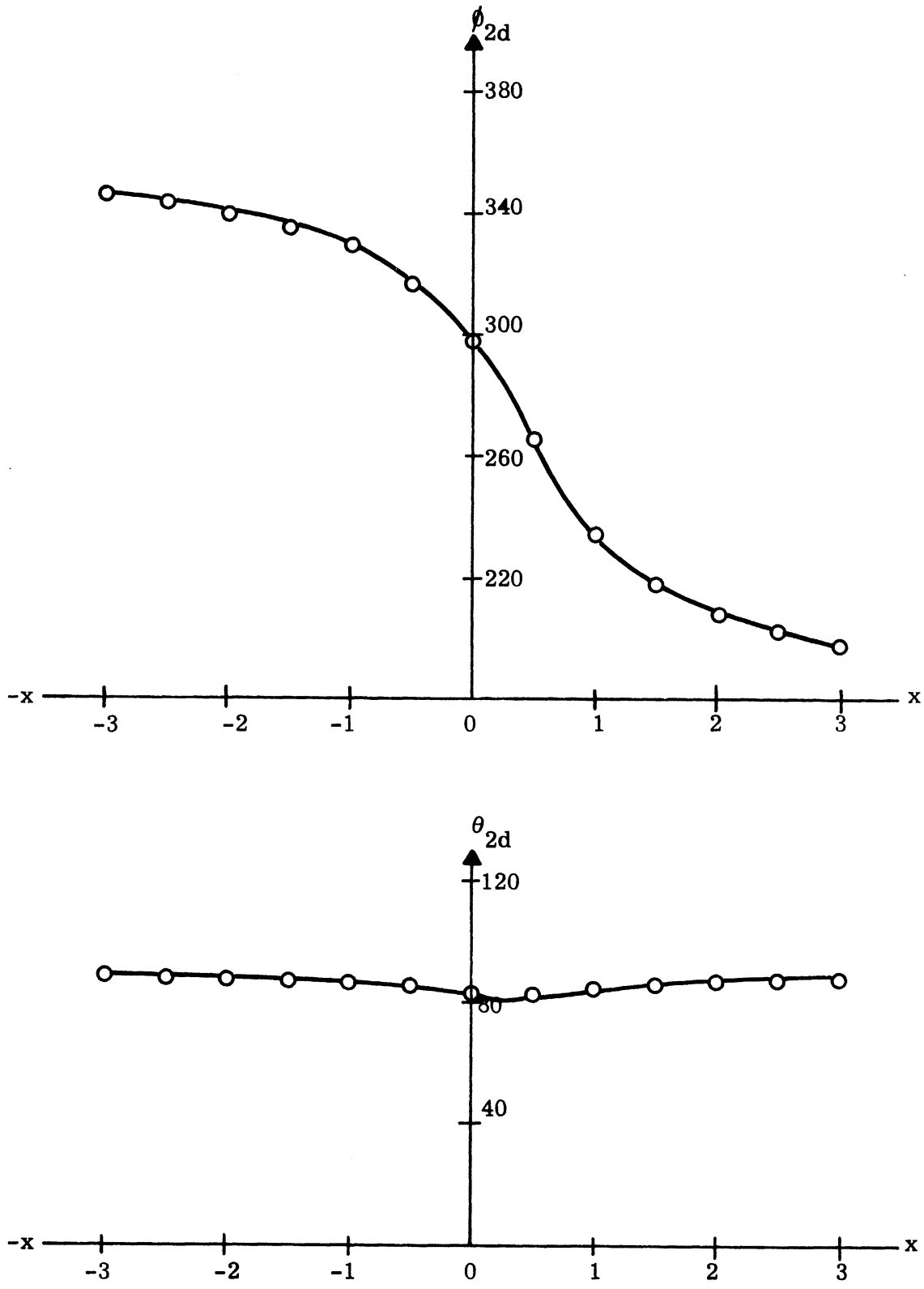

Fig. 3-17b: Directions of Arrival for a Lambert Surface at y=0.5, z_r/z_a=0.1 for Beam No. 2 .

3.5 Magnitude of Maximum Reflected Radiation

Due to the distributed nature of the reflected radiation from a diffused surface, we shall compare principally the intensity of radiation in the apparent direction of arrival, along which the intensity is maximum. For the case of the specularly reflecting surface, the reflected radiation observed at any point appears to come only from one direction, the magnitude of which may be represented by a normalized power density, F_{2s}, given by Eq. (3.8). In terms of F_{2s}, the observed power density at any point is obtained by

$$P_{2s} \underset{(\text{watts/m}^2)}{} = \frac{P_t G_t}{z_a^2} F_{2s} \quad .$$

For the case of the diffusely reflecting surface, the normalized intensity, F_{2M} and F_{2d} are given by (3.12) and (3.14), respectively. In terms of these normalized quantities, the power density per unit solid angle is expressed by

$$\frac{dp_{2r}}{d\Omega_2} = \frac{P_t G_t}{z_a^2} F_{2M} \text{ (or } F_{2d}) \quad .$$

$$(\text{watts/m}^2/\text{steradian})$$

In this section, the variations of F_{2s}, F_{2d} and F_{2M} with relative receiving points are discussed. It should be recognized, however, that the direct comparison of F_{2s} with F_{2M} (or F_{2d}) is meaningless unless the radiation pattern of the receiving antenna is taken into account. For the case of the narrow-beam antenna, the relative magnitude of F_{2s} and F_{2M} times the angular beamwidth of the receiving antenna (in steradians) probably could be taken for an approximate comparison of the reflected power observed.

In Fig. 3-18a, we show the variation of F_{2M} (in the apparent direction of arrival) at the relative receiver height fixed at 0.1 and at different Y for the down-wind speed of 1.5 m/sec; in Fig. 3-18b, similar curves at the relative receiver height fixed at 0.5 are shown. Similar curves are presented in Figs. 3-19a and b for the down-wind speed of 4m/sec. Figs. 3-20a through 3-21b deal with the corresponding cases for the cross-wind. In Figs. 3-22a and b, we show

the effect of the wind speed on the variation of Maximum Reflected Radiation Intensity for the down-wind case at ($Y = 0.5$, $z_r/z_a = 0.1$) and ($Y = 0.5$, $z_r/z_a = 0.5$), respectively. Similar curves shown in Figs. 3-23a and b deal with the cross-wind case. It is noticed that the overall level of dbF_{2M} is slightly higher in the down-wind case than in the corresponding cross-wind case, the difference being more pronounced at the lower receiver height. Figs. 3-24a and b present the effect of the wind direction at the wind speed of 1.5m/sec at two different relative receiver heights of 0.1 and 0.5, respectively. Similar curves shown in Figs. 3-25a and b deal with the wind speed of 4m/sec. It is seen that, in general, the change in the wind direction has a rather minor effect on the dbF_{2M} variation, even though the effect appears to be more significant at points at the lower receiver height. Finally, the variation of F_{2M} for the down-wind case is compared with those of F_{2d} and F_{2s} in Fig. 3-26a at the relative receiver height fixed at 0.1 and $Y = 0.5$. In Fig. 3-26b a similar comparison is made at the relative receiver height fixed at 0.5. Similar comparisons are presented in Figs. 3-27a and b for the cross-wind case. The use of this information and its relation to the problem of estimating the detectability is discussed in Vol. II of this report.

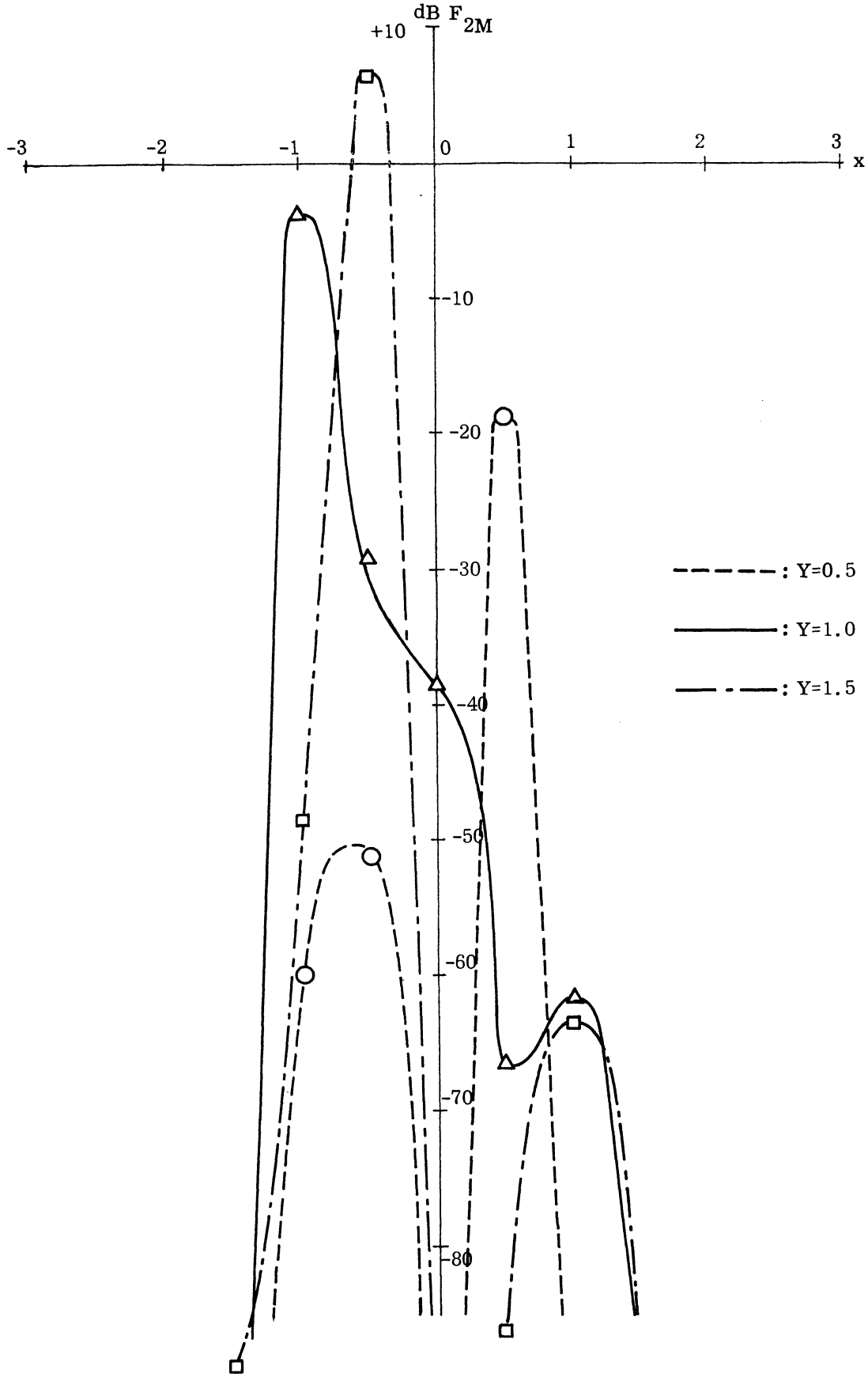

Fig. 3-18a: dBF_{2M} for Down-Wind Speed of 1.5 m/sec at $z_r/z_a = 0.1$.

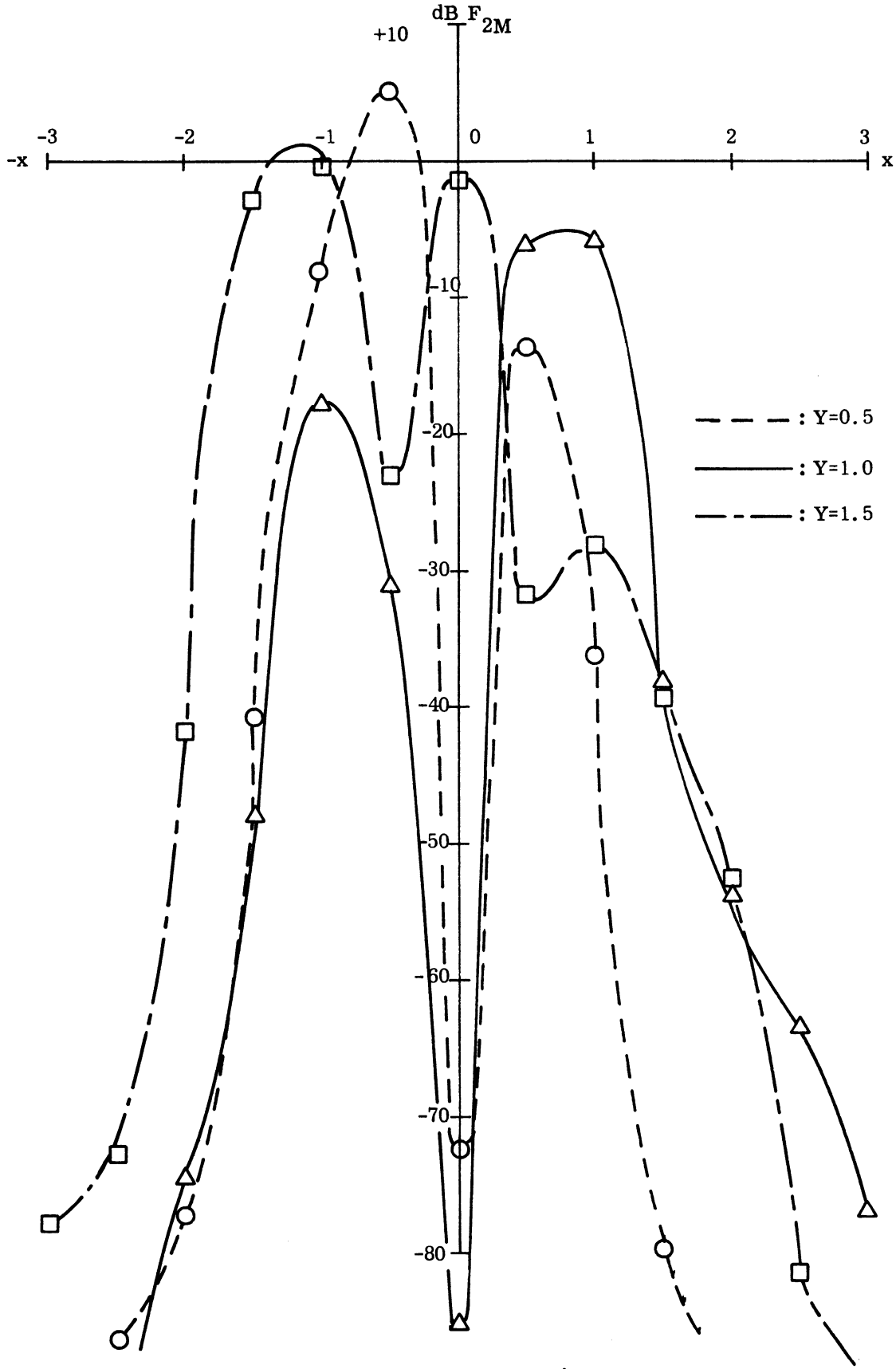

Fig. 3-18b: dBF_{2M} for Down Wind Speed of 1.5 m/sec at $z_r/z_a = 0.5$.

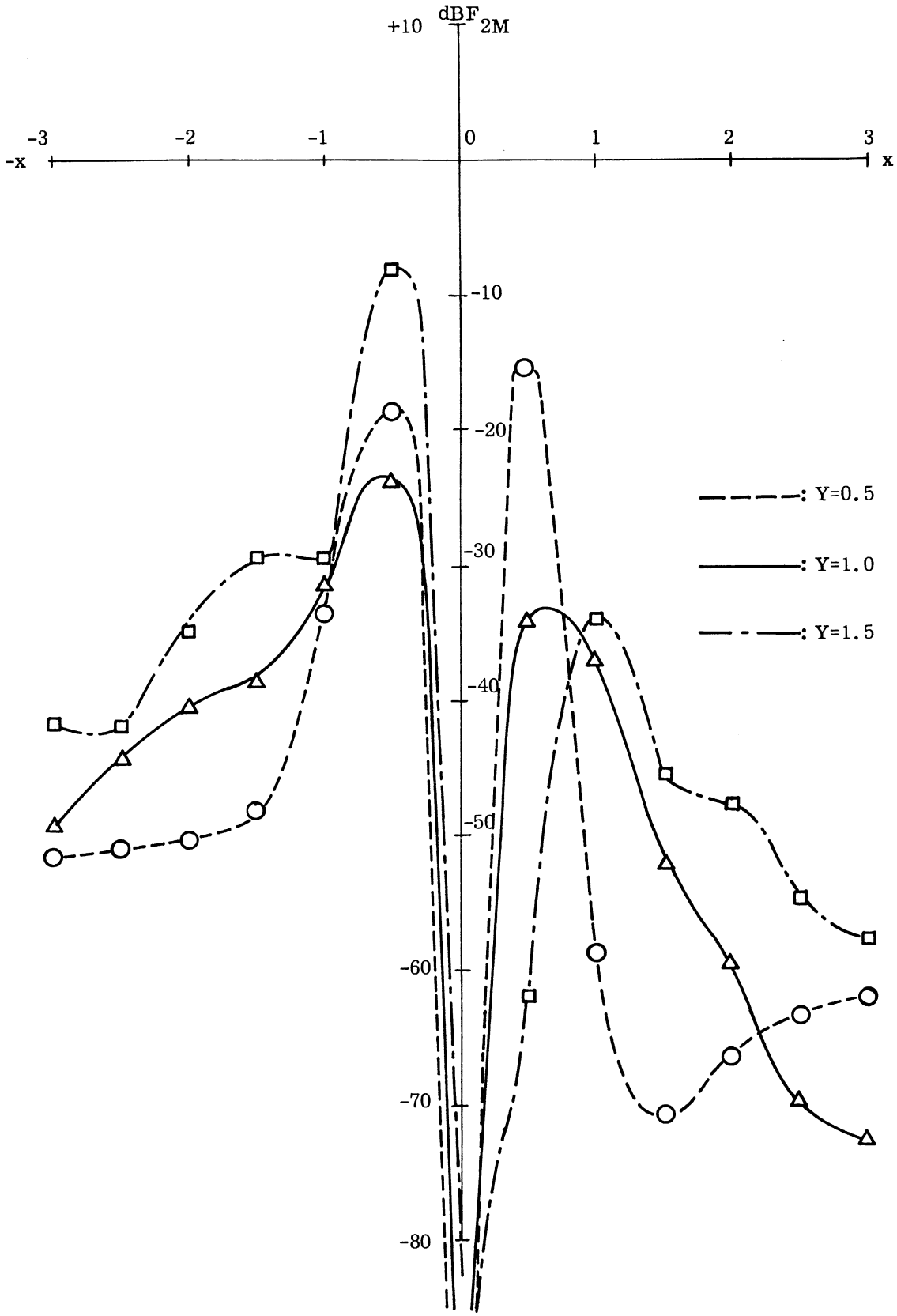

Fig. 3-19a: dBF_{2M} for Down-Wind Speed of 4m/sec at $z_r/z_a = 0.1$.

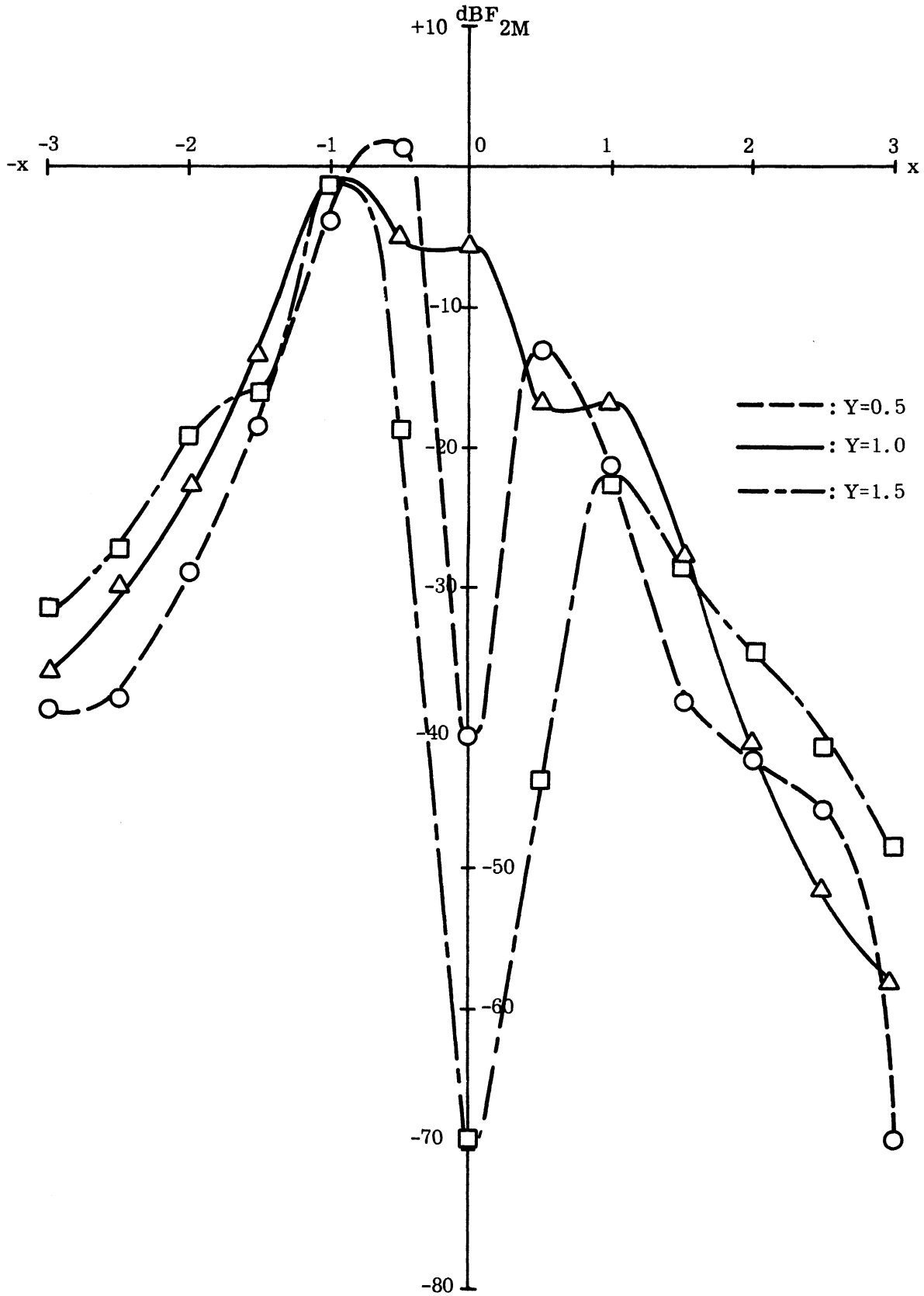

Fig. 3-19b: dBF_{2M} for Down Wind Speed of 4 m/sec at $z_r/z_a = 0.5$.

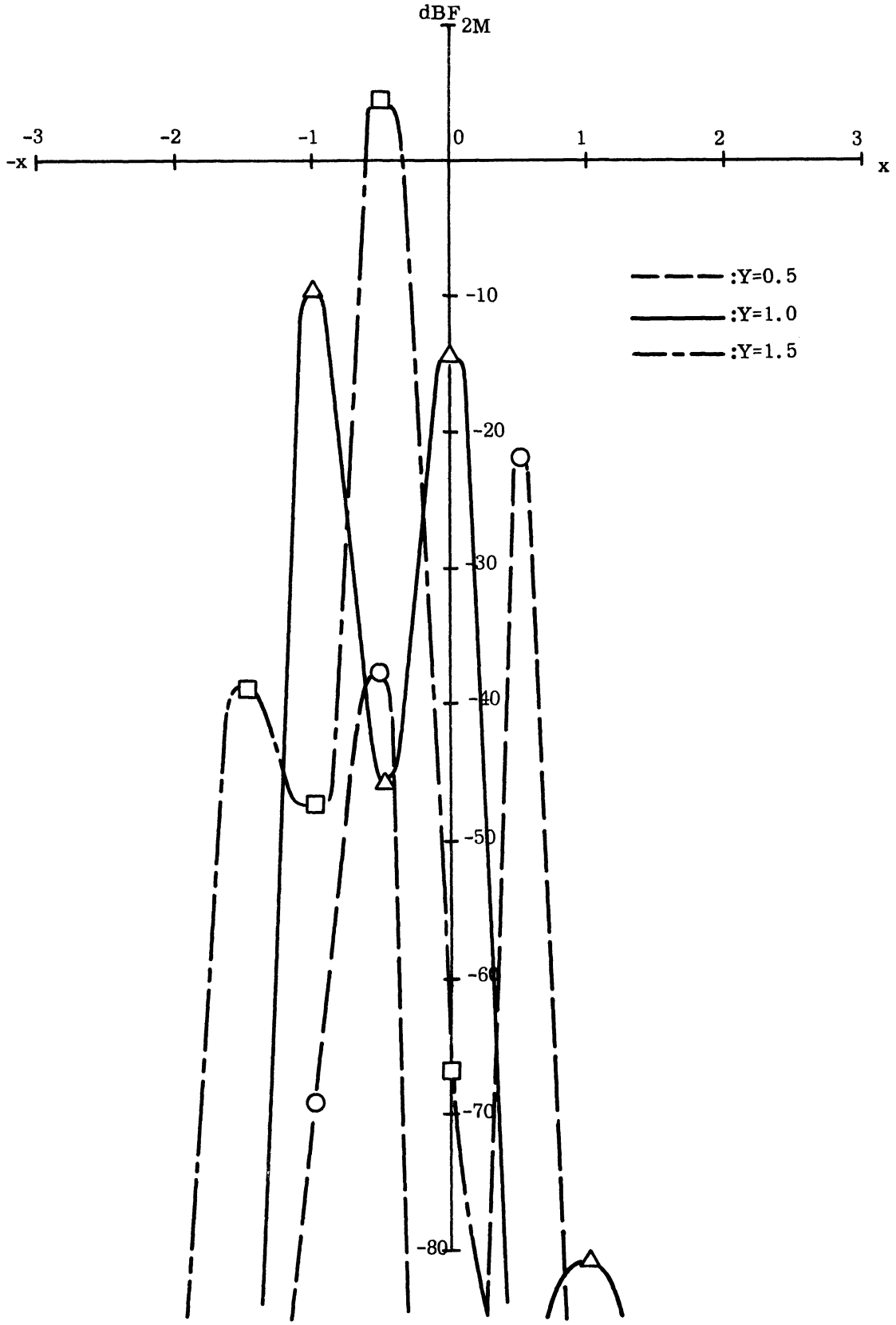

Fig. 3-20a: dBF_{2M} for Cross Wind Speed of 1.5 m/sec at $z_r/z_a = 0.1$.

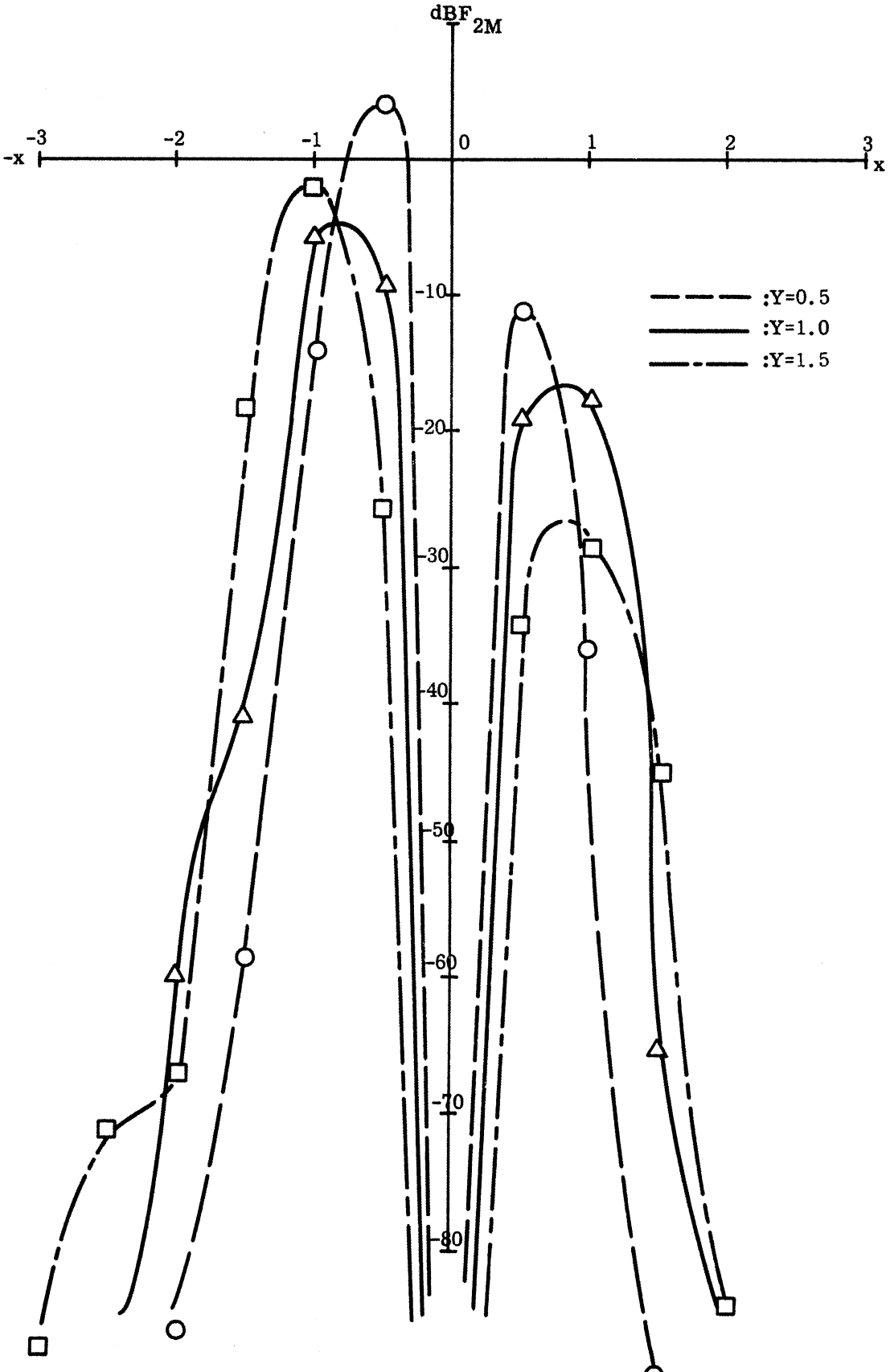

Fig. 3-20b: dBF_{2M} for Cross Wind Speed of 1.5 m/sec at $z_r/z_a = 0.5$.

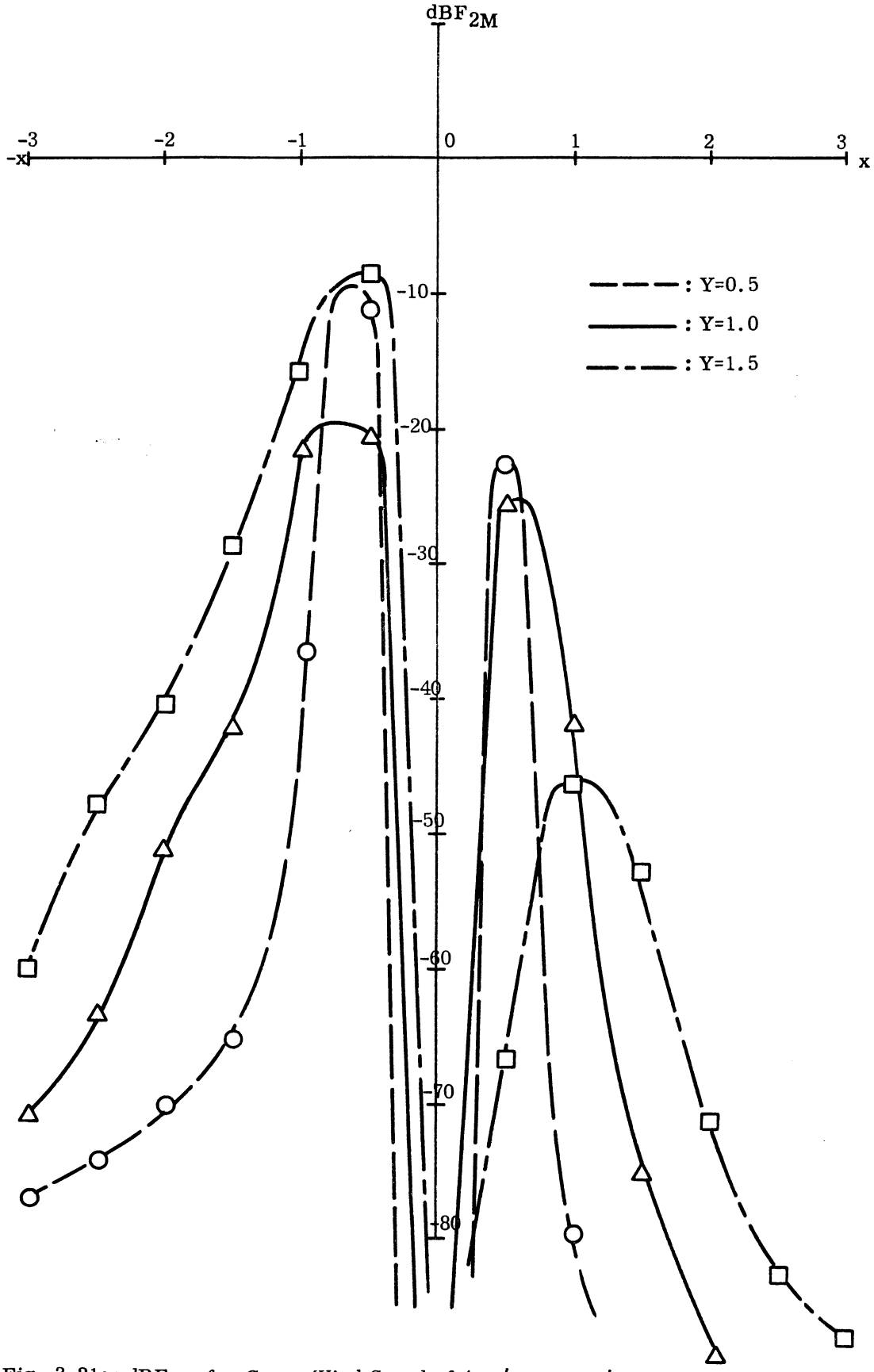

Fig. 3-21a: dBF_{2M} for Cross Wind Speed of 4 m/sec at $z_r/z_a = 0.1$.

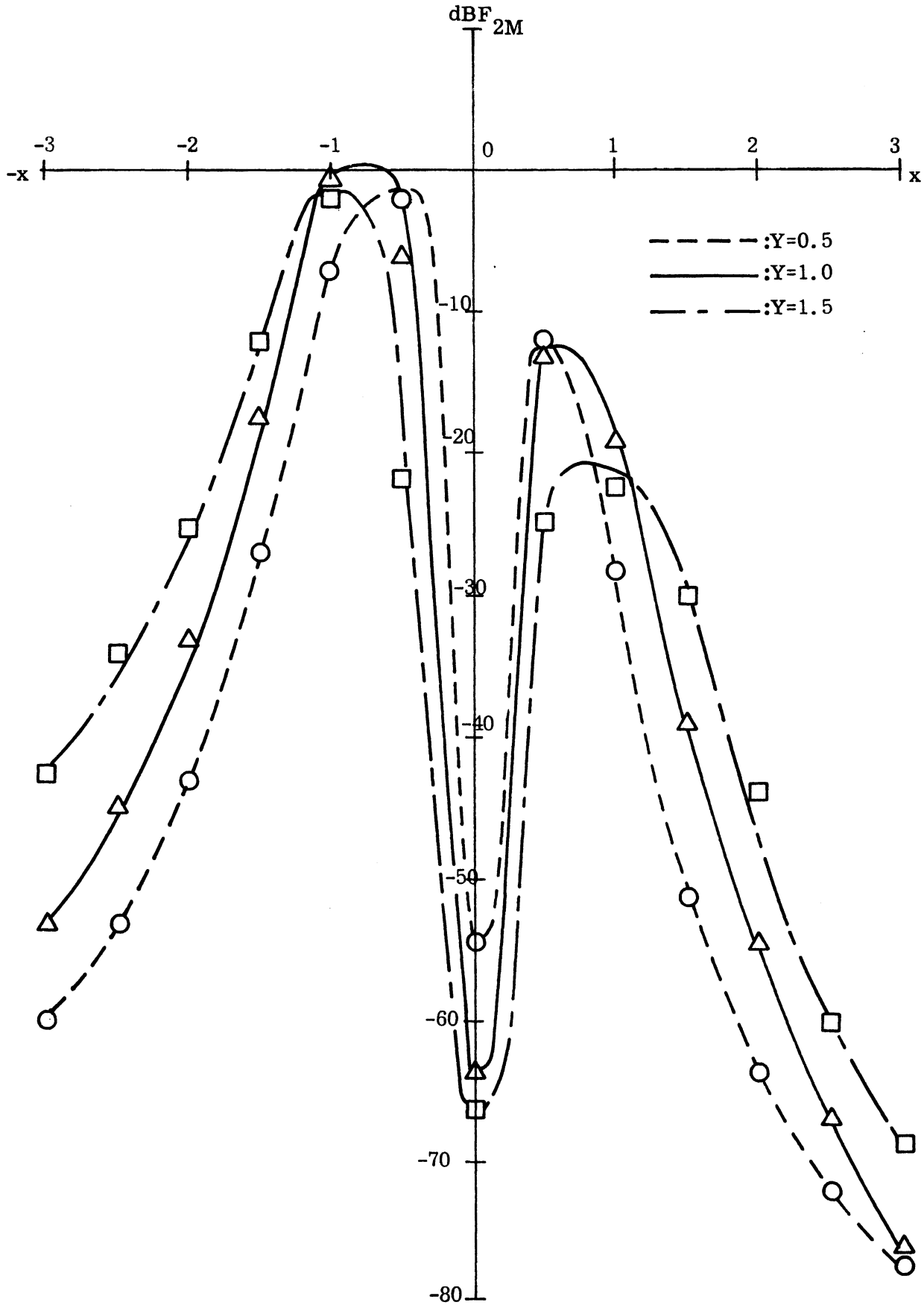

Fig. 3-21b: dBF_{2M} for Cross Wind Speed of 4 m/sec at $z_r/z_a = 0.5$.

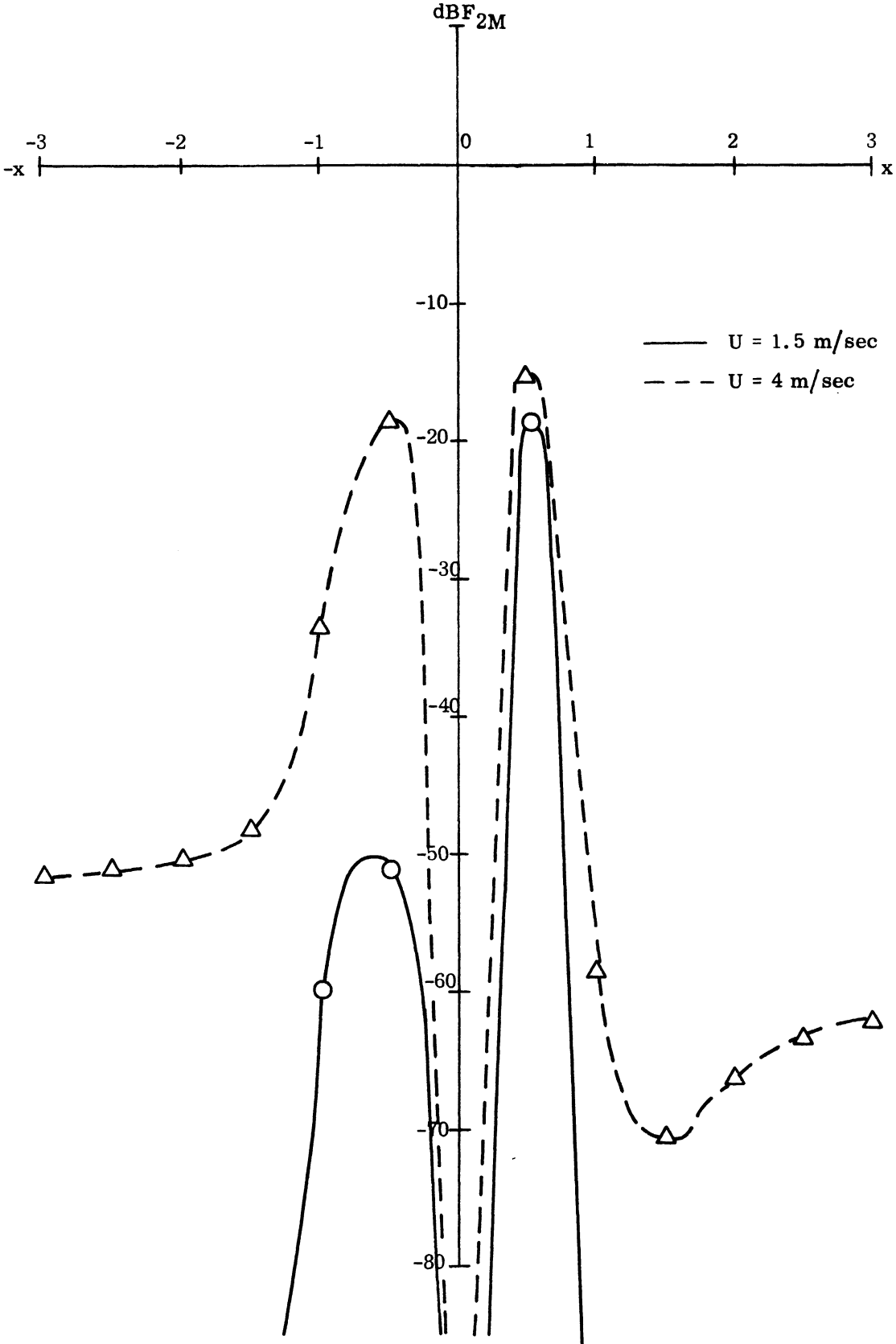

Fig. 3-22a: Effect of the Wind Speed on the Maximum Reflected Radiation Intensity for the Down Wind Case at Y = 0.5, z_r/z_a = 0.1.

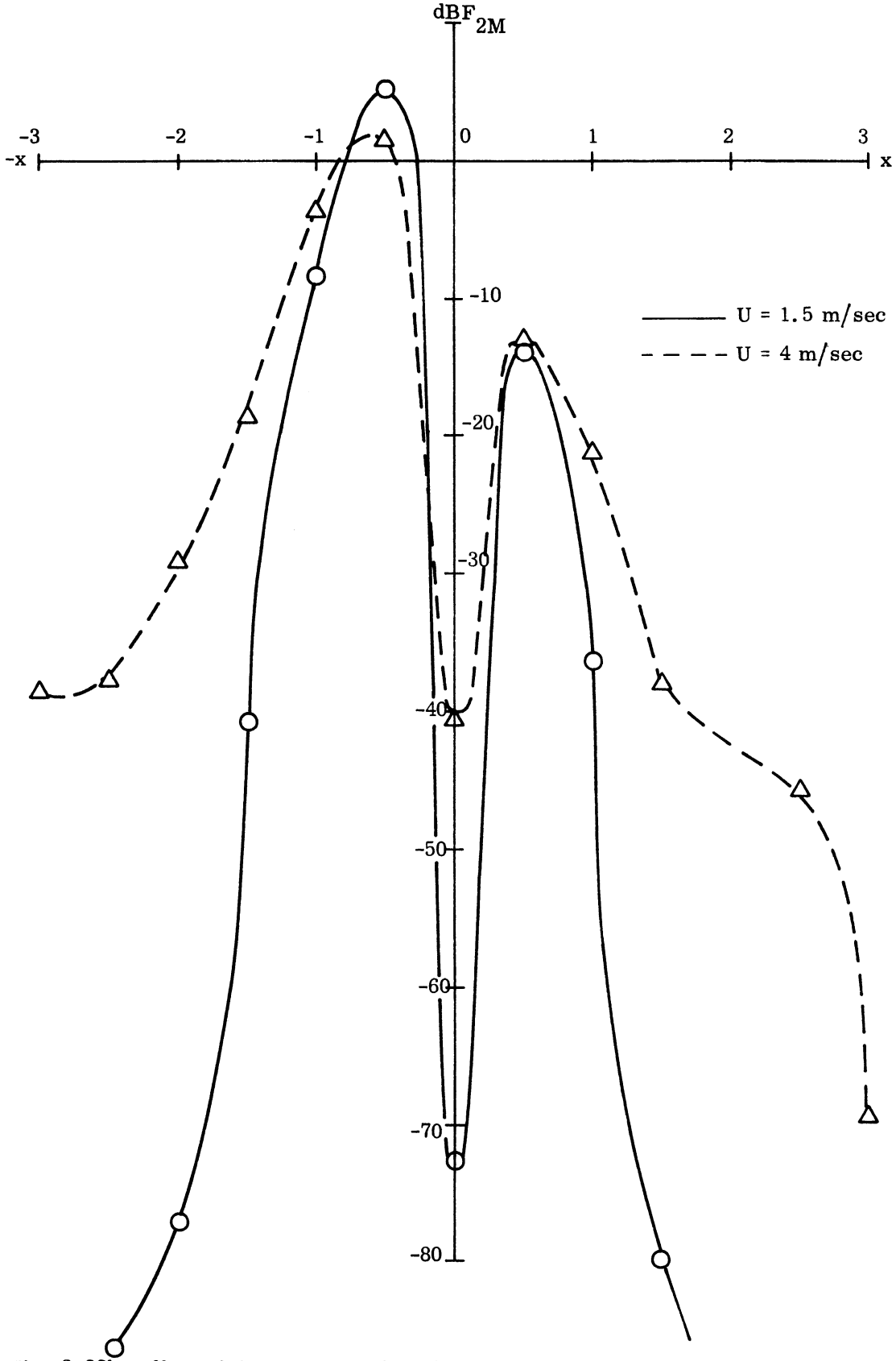

Fig. 3-22b: Effect of the Wind Speed on the Maximum Reflected Radiation Intensity for the Down Wind Case at Y = 0.5, $z_r/za = 0.5$.

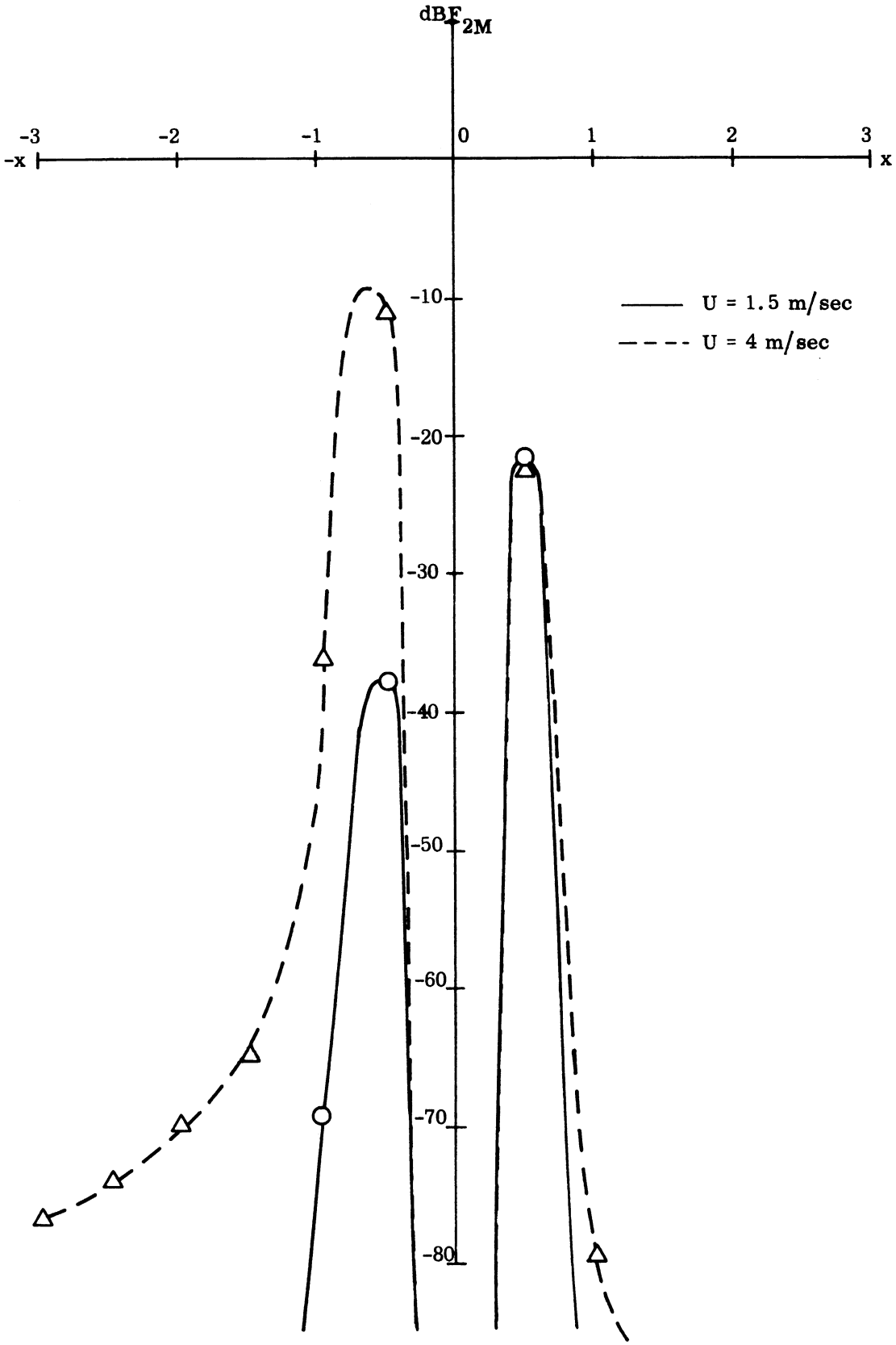

Fig. 3-23a: The Effect of the Wind Speed on the Maximum Reflected Radiation Intensity for the Cross Wind Case at Y = 0.5, z_r/z_a = 0.1.

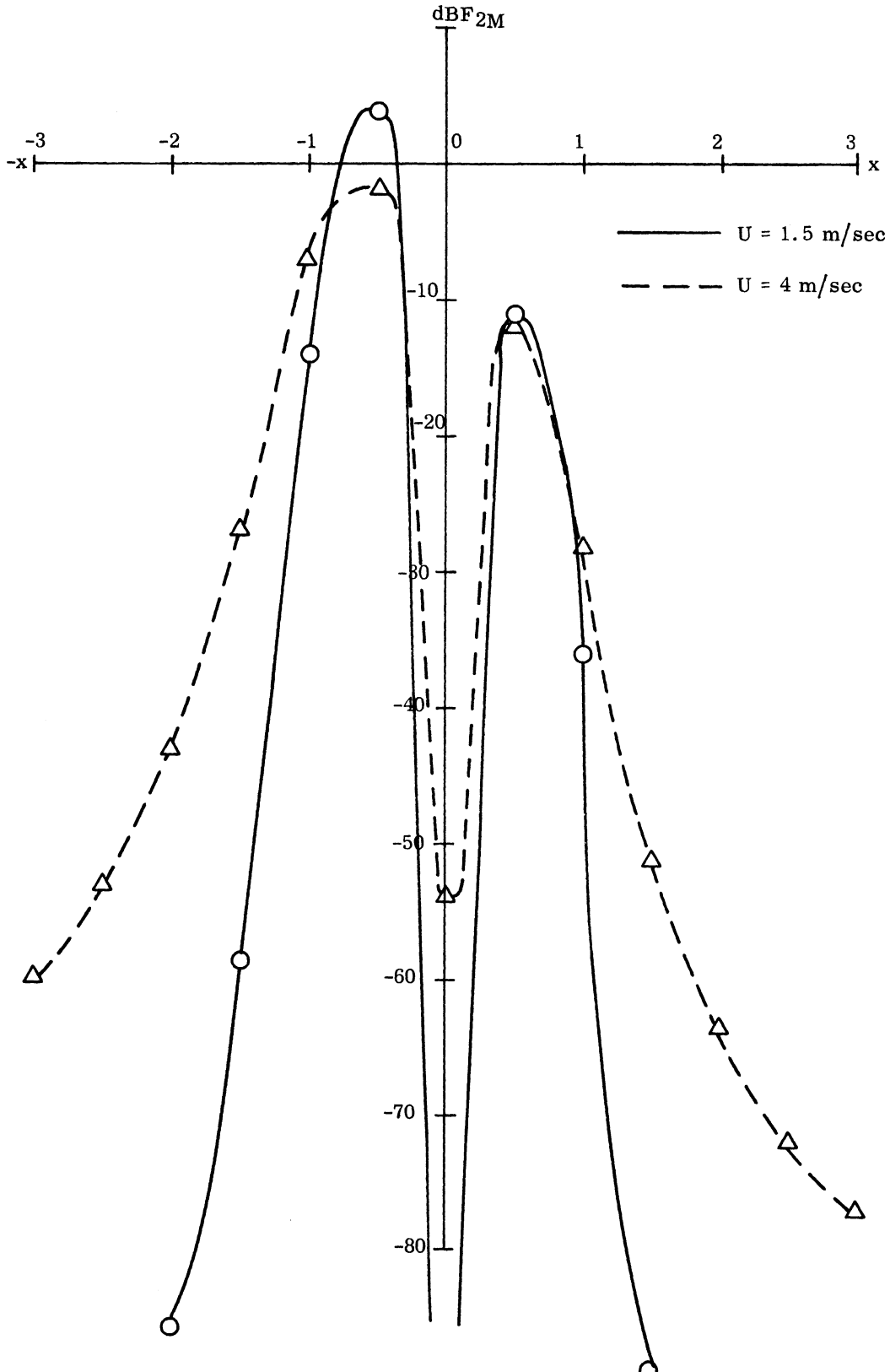

Fig. 3-23b: Effect of the Wind Speed on the Maximum Reflected Radiation Intensity for the Cross Wind Case at Y = 0.5, $z_r/z_a = 0.5$.

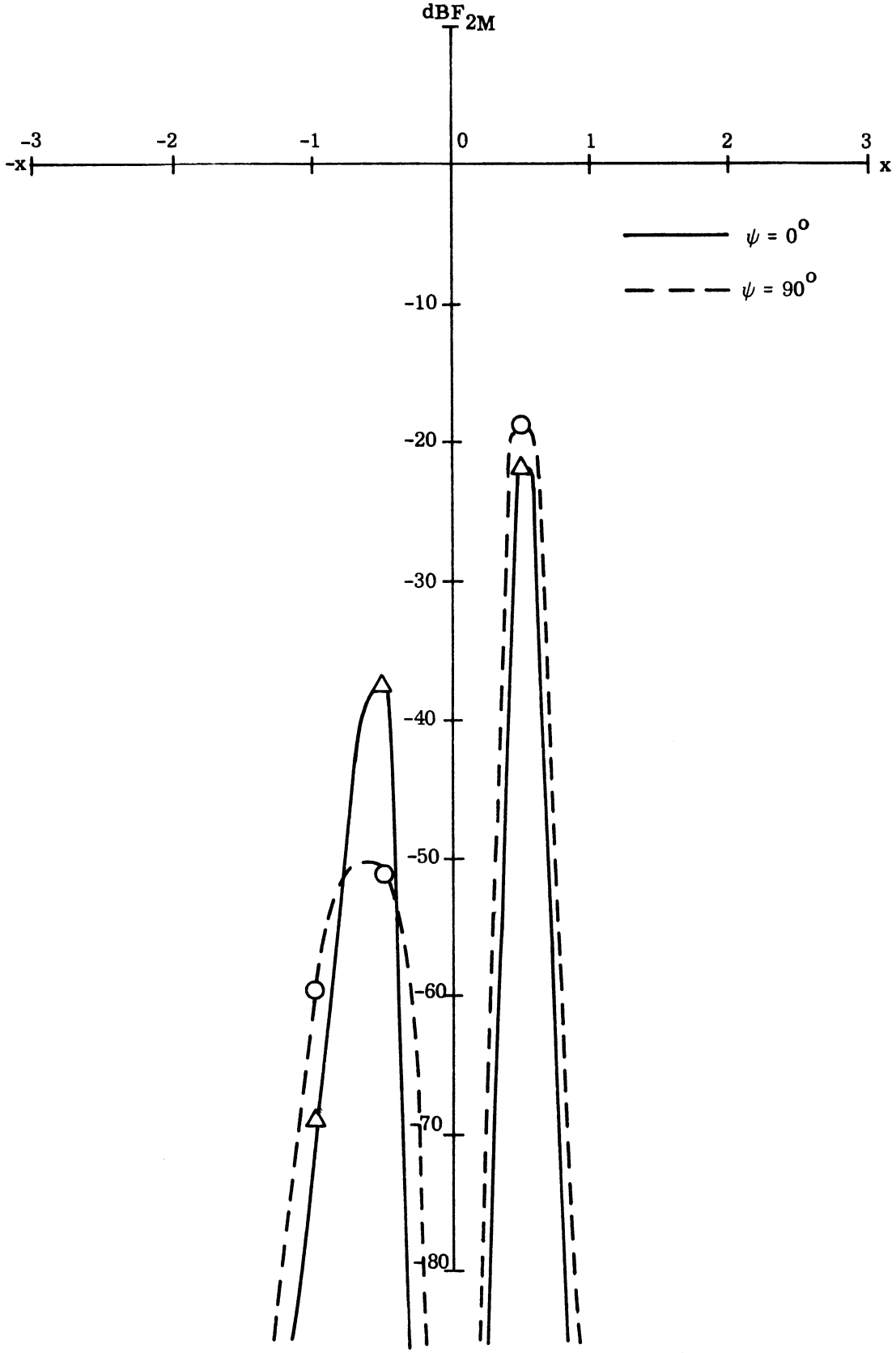

Fig. 3-24a: Effect of the Wind Direction on the Maximum Reflected Radiation Intensity for the Wind Speed of 1.5 m/sec at Y = 0.5, z_r/z_a = 0.1.

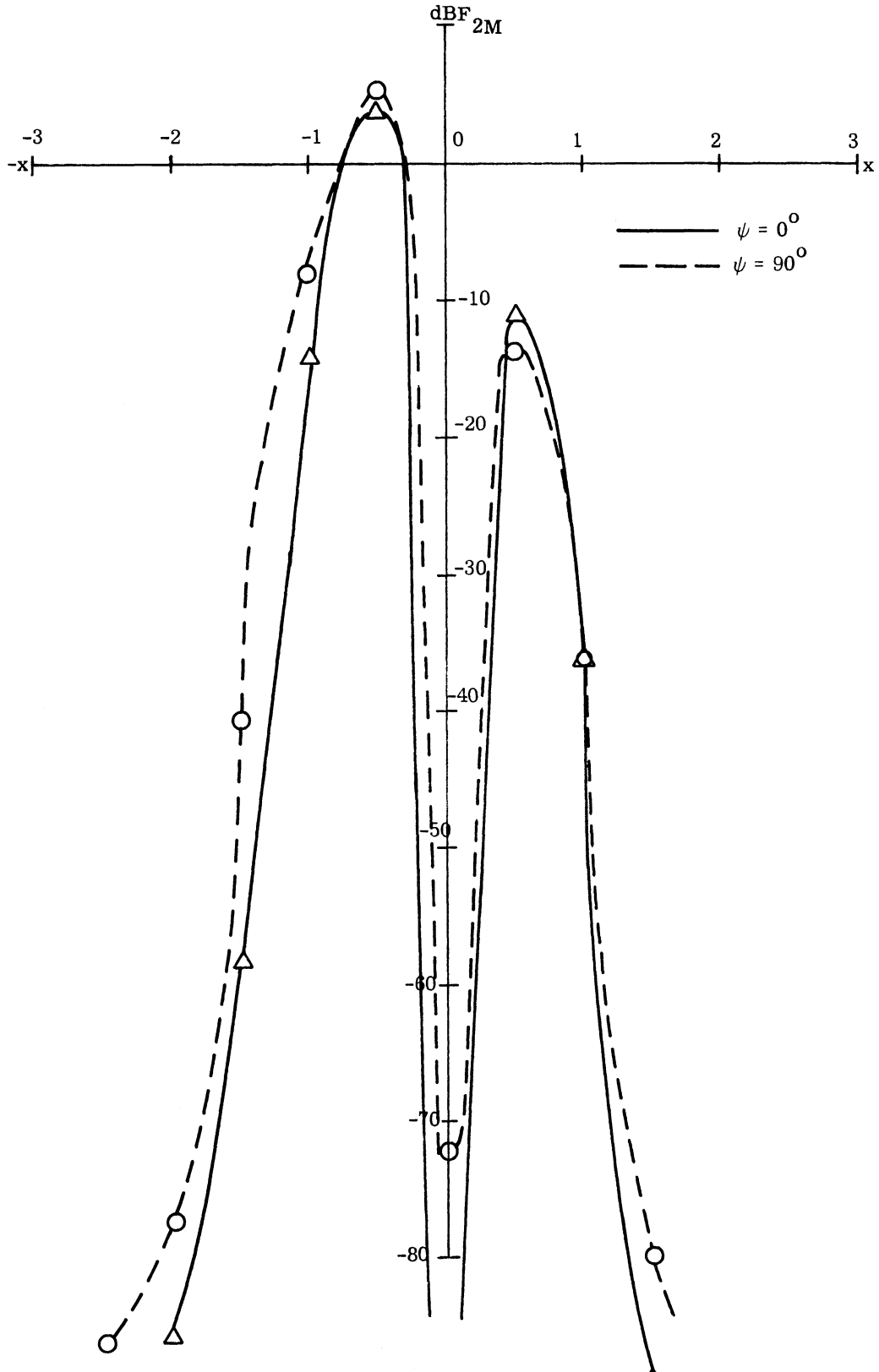

Fig. 3-24b: Effect of the Wind Direction on the Maximum Reflected Radiation Intensity for the Wind Speed of 1.5 m/sec at Y = 0.5, z_r/z_a = 0.5.

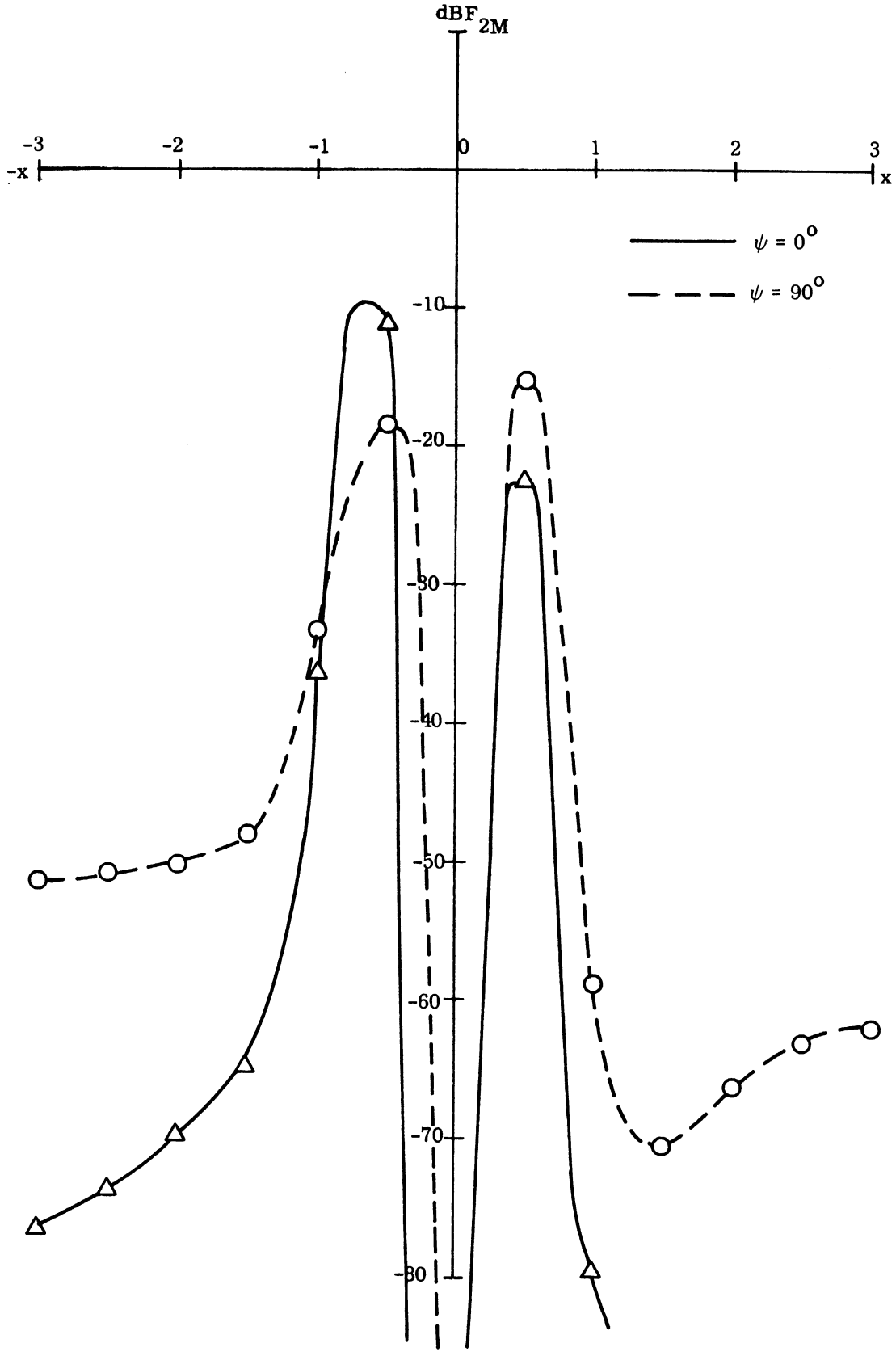

Fig. 3-25a: Effect of the Wind Direction on the Maximum Reflected Radiation Intensity for the Wind Speed of 4 m/sec at Y = 0.5, $z_r/z_a = 0.1$.

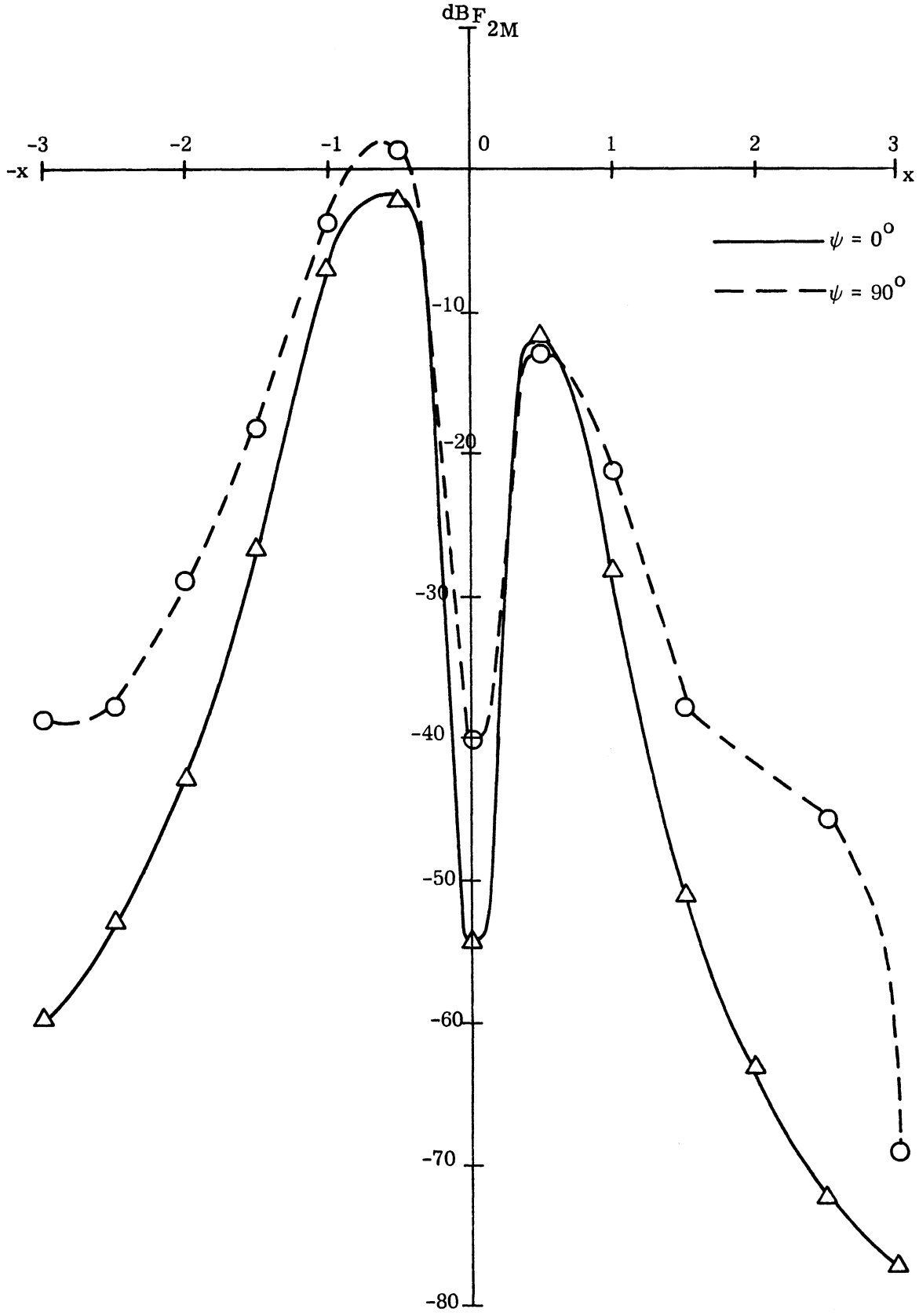

Fig. 3-25b: Effect of the Wind Direction on the Maximum Reflected Radiation Intensity for the Wind Speed of 4 m/sec at Y = 0.5, $z_r/z_a = 0.5$.

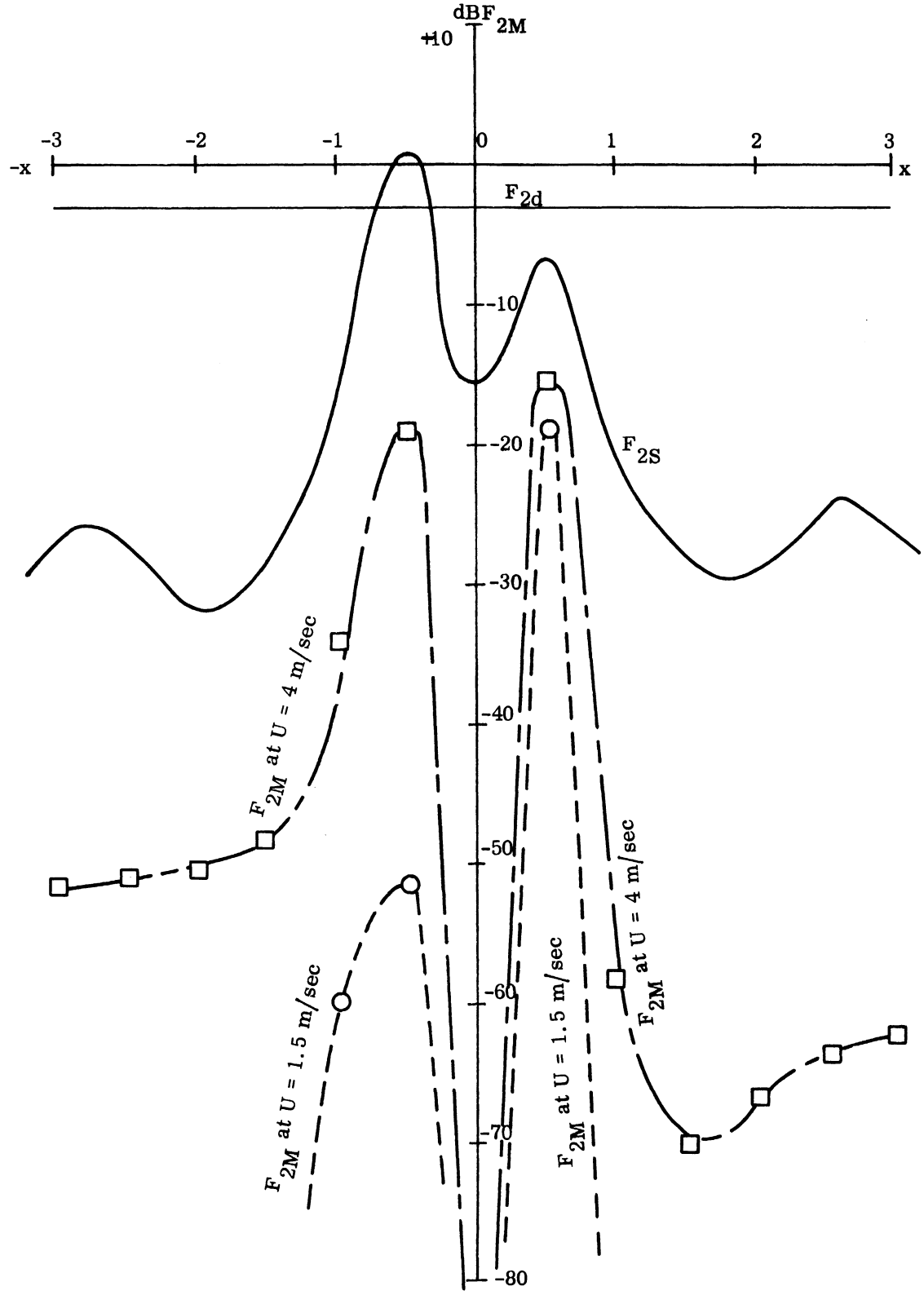

Fig. 3-26a: Comparison of F_{2M} with F_{2S} and F_{2d} at Y = 0.5, $z_r/z_a = 0.1$, $\psi = 0^o$ for U = 1.5, 4 m/sec.

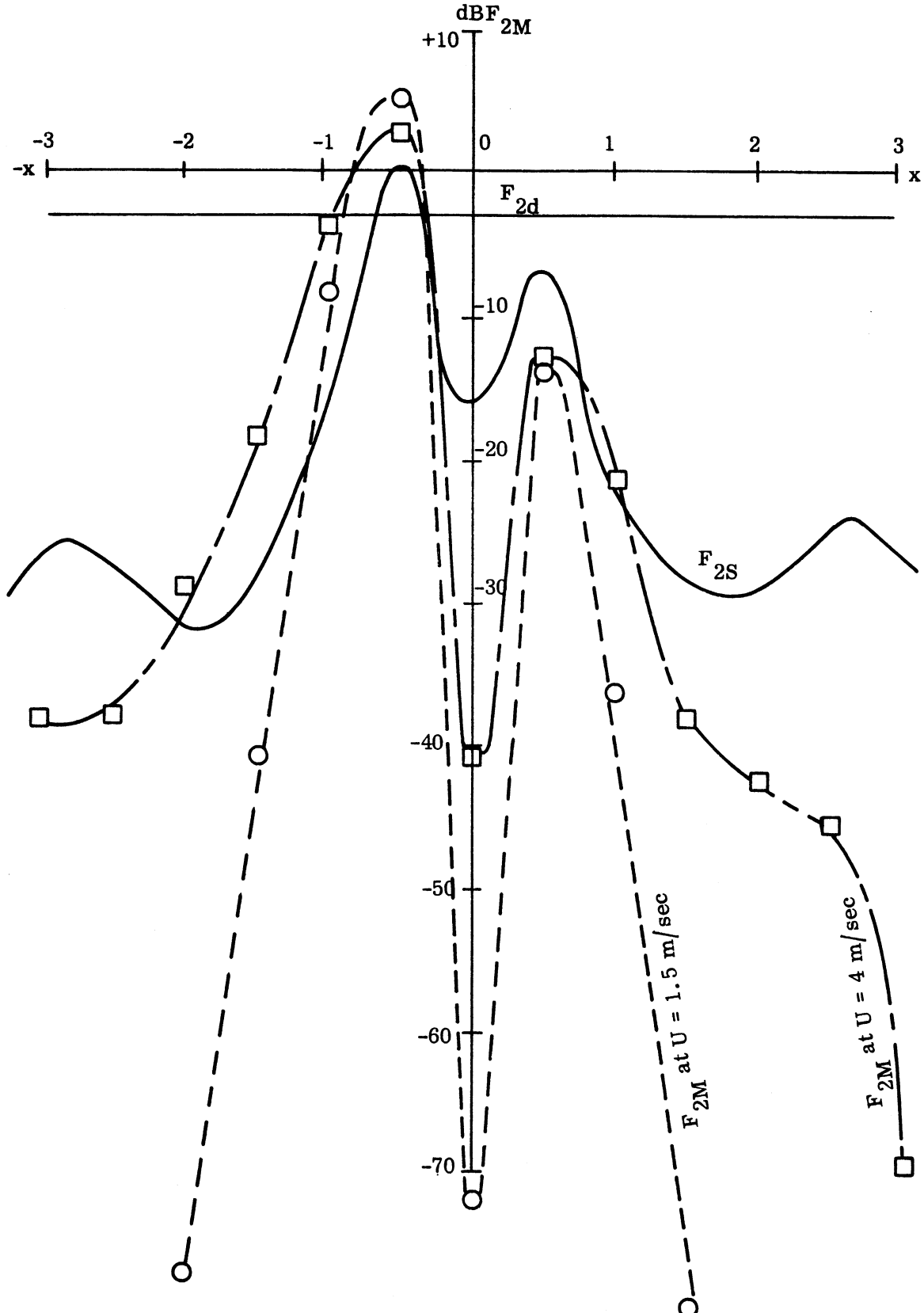

Fig. 3-26b: Comparison of F_{2M} with F_{2S} and F_{2d} at Y = 0.5, z_r/z_a = 0.5, $\psi = 0^o$ for U = 1.5, 4 m/sec.

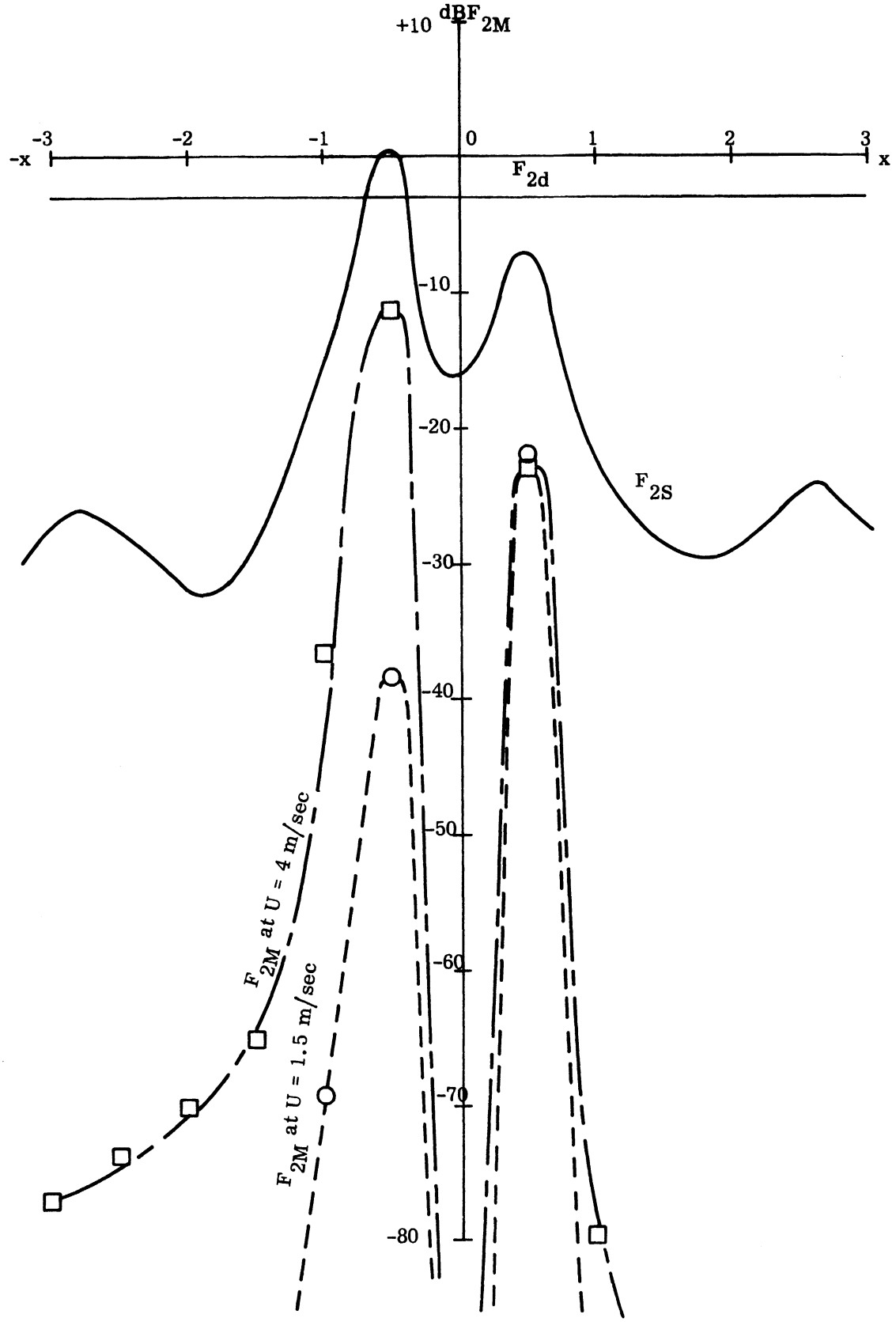

Fig. 3-27a: Comparison of F_{2M} with F_{2S} and F_{2d} at Y = 0.5, z_r/z_a = 0.1, $\psi = 90^o$ for U = 1.5, 4 m/sec.

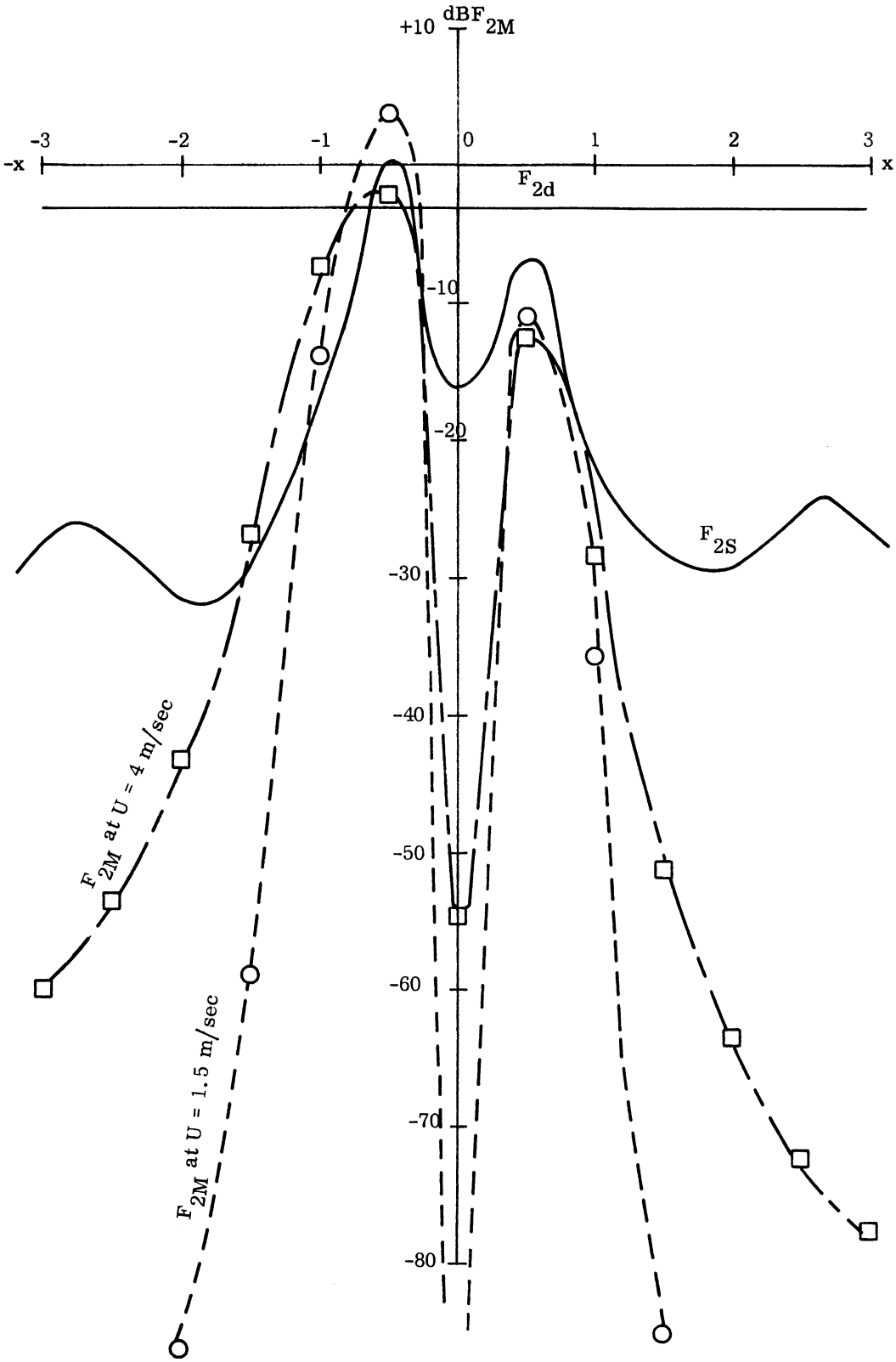

Fig. 3-27b: Comparison of F_{2M} with F_{2S} and F_{2d} at Y = 0.5, z_r/z_a = 0.5, $\psi = 90^{o}$ for U = 1.5, 4 m/sec.

IV

CONCLUSIONS AND RECOMMENDATIONS

A theoretical analysis is performed to investigate the reflection properties of an anisotropic normally distributed rough surface by use of the physical optics method. Approximate formulas are derived for calculation of the reflected radiation from a moderately rough ocean surface which exhibits the Neumann spectrum. A computer program is written for this formulation, and limited numerical computations are carried out for the AN/APN-153 doppler radar antenna. The distribution of the reflected radiation is calculated for several relative geometric configurations of the transmitter and receiver. The numerical calculations are limited only to the down wind case for a few different wind speeds. The computer program, however, is valid for variations of the wind direction within the limit imposed by the Neumann theory, namely, $|\psi| \leq \pi/2$. The cases for different wind directions will be performed in the future program.

The direction of arrival and the intensity of the reflected radiation from a moderately rough ocean surface are presented and compared with those from a specularly reflecting and Lambert Surface. In most of the cases compared, it appears that, in its general trend, the reflected radiation intensity, F_{2M}, from a moderately rough ocean surface resembles that from a specularly reflecting surface, even though the direction does not. The level of the intensity sharply decreases as the receiving point moves away on the X-axis from the origin of the relative coordinate system for a low wind speed, say 1.5 m/sec (or 2.7 knots). As the wind speed increases to 4 m/sec (or 7.4 knots), the drop in the level of the radiation intensity away from X = 0 is less drastic. The direction of arrival, both in azimuth and latitude, tends to approach the same direction each as the receiver moves away from the origin along the X-axis. Within the range $|X| \simeq 1$, however, the variation of the direction of arrival is wide at points, particularly so for the case of a low receiver height. It should be noted that, all in all, the change in the wind direction has only a minor effect both in the magnitude and the direction of the maximum reflected radiation intensity. This is attributed to a small difference in A_o and B_o.

The limitation of the present model and some recommendations on the future works on rough surface scattering (especially ocean surfaces) are given below.

1) The inherent inadequacy of the physical optics method somewhat limits the validity of the present calculation, particularly near the horizon. Further theoretical analysis (exact numerical solutions for some canonical problems) and experimental work (model study of scattering) which may assert the range of the validity and suggest possible refinement on the physical optics method appear to be in need for a more adequate solution to the problem of random surface reflection.

2) An alternative approach, such as the use of the concept of surface waves, in estimating the scattered field near the horizon should be investigated to compliment the results obtained through the physical optics method.

3) The present model is based on the Gaussian correlation for the surface height. It is possible to adapt the analysis to other kinds of statistical models for a rough surface with different correlation. However, in order to extract meaningful numerical results from such efforts, adequate statistical information on the rough surface is necessary. In particular, in the case of the ocean surface, it appears that more experiments are needed which will add a more appropriate statistical description of the ocean surface, incorporating different sea states, in estimating the reflected radiation power.

APPENDIX A:

BISTATIC CROSS SECTION OF A ROUGH SURFACE

A.1 Introduction

It has been recognized that both adequate theoretical formula and experimental data have been scarce in the case of the bistatic scattering cross section for the rough surface and ocean surface. In view of this recognition, the bistatic cross section is investigated both theoretically and experimentally by means of the physical optics approach with special reference to the ocean surface, in an effort to promote a better understanding in this area.

An approximate formula, incorporating the anisotropic nature of a random ocean surface (due to wind effect) is derived for the computation of the reflected radiation from a doppler radar in the main text of this report.

Recognizing the inherent shortcomings in the physical optics method, and the uncertainty in the existing sea surface wave spectra, approximations based primarily on physical grounds are introduced to simplify the result. It is realized that more experimental work and theoretical analyses based on the exact solutions of some canonical problems are necessary for a more complete understanding of the problem. It is our present feeling that the results derived in this appendix are probably inadequate for reflections near the grazing angle, for which the physical optics approach is known to be in error.

A.2 Scattering Cross Section

The conventional description of the scattering properties of a rough surface is given by the bistatic cross section per unit area $\sigma(\hat{\Omega}_2, \hat{\Omega}_1)$. It is an average quantity defined as 4π times the power scattered by a unit solid angle in the direction $\hat{\Omega}_2$, for an incident wave of unit intensity from the direction $\hat{\Omega}_1$. With this definition, for an incident radiation of intensity $p_i(\hat{\Omega}_1)$ impinging on a surface of the area dA, the intensity of the reflected radiation observed at a distance r from the point of reflection in the direction $\hat{\Omega}_2$ is given by

$$dp_r = p_i(\hat{\Omega}_1)\, dA \quad \frac{1}{r^2} \quad \frac{\sigma(\hat{\Omega}_2, \hat{\Omega}_1)}{4\pi} \quad . \tag{A.1}$$

Since the solid angle subtended by dA at the point of observation is

$$d\hat{\Omega}_2 = \frac{dA \cos\theta_2}{r^2} \quad , \tag{A.2}$$

the reflected radiation at a point of observation has the intensity per solid angle as given by

$$\frac{dp_2}{d\hat{\Omega}_2} = \frac{p_i(\hat{\Omega}_1)}{4\pi \cos\theta_2} \sigma(\hat{\Omega}_2, \hat{\Omega}_1) \quad . \tag{A.3}$$

In general, the bistatic cross section $\sigma(\hat{\Omega}_1, \hat{\Omega}_2)$ depends on the polarization of incident and reflected radiation. To fix the direction of polarization, we shall define the direction of the horizontal polarization of the incident radiation by

$$\hat{e}_{h_1} = \frac{\hat{z} \times \hat{\Omega}_1}{|\hat{z} \times \hat{\Omega}_1|} \tag{A.4}$$

and the direction of the vertical polarization by

$$\hat{e}_{v_1} = \hat{\Omega}_1 \times \hat{e}_{h_1} \tag{A.5}$$

Similarly, for the scattered radiation in the direction $\hat{\Omega}_2$, the directions of horizontal and vertical polarization are defined by

$$\hat{e}_{h_2} = \frac{\hat{z} \times \hat{\Omega}_2}{|\hat{z} \times \hat{\Omega}_2|} \tag{A.6}$$

and

$$\hat{e}_{v_2} = \hat{\Omega}_2 \times \hat{e}_{h_2} \quad , \tag{A.7}$$

respectively, These directions are illustrated in Fig. A-1. If $\hat{\Omega}_2$ is the specularly reflecting direction, so that

$$\hat{\Omega}_2 = \hat{\Omega}_1 - 2\hat{z}(\hat{z} \cdot \hat{\Omega}_1) \tag{A.8}$$

then

$$\hat{e}_{h_2} = \hat{e}_{h_1} \tag{A.9}$$

and

$$\hat{e}_{v_2} = \hat{e}_{v_1} - 2(\hat{z} \cdot \hat{\Omega}_1)\, \hat{z} \times \hat{e}_{h_1} \quad . \tag{A.10}$$

On the other hand, if $\hat{\Omega}_2$ is the backscattering direction, so that

$$\hat{\Omega}_2 = -\hat{\Omega}_1 \quad , \tag{A.11}$$

then

$$\hat{e}_{h_2} = -\hat{e}_{h_1} \tag{A.12}$$

and

$$\hat{e}_{v_2} = \hat{e}_{v_1} \quad . \tag{A.13}$$

To stress the polarization dependence of the scattering cross section, we may consider four types of scattering cross section $\sigma_{\ell, m}$, where ℓ and m may stand for h or v. For example, σ_{hv} is the scattering cross section corresponding to horizontally polarized scattered radiation when the incident wave is vertically polarized.

Experimental data concerning the bistatic cross section are very scarce. In the work of Hunter and Senior (1966), Pidgeon (1966) and others, where the bistatic cross section is measured, the incidence angle θ_1 is limited only to nearly 90° and the reflection direction is either nearly specular or nearly in the backscattering direction. The detailed information on the directional distribution of the scattered power from a rough surface in the microwave range has not been so far reported in experimental work.

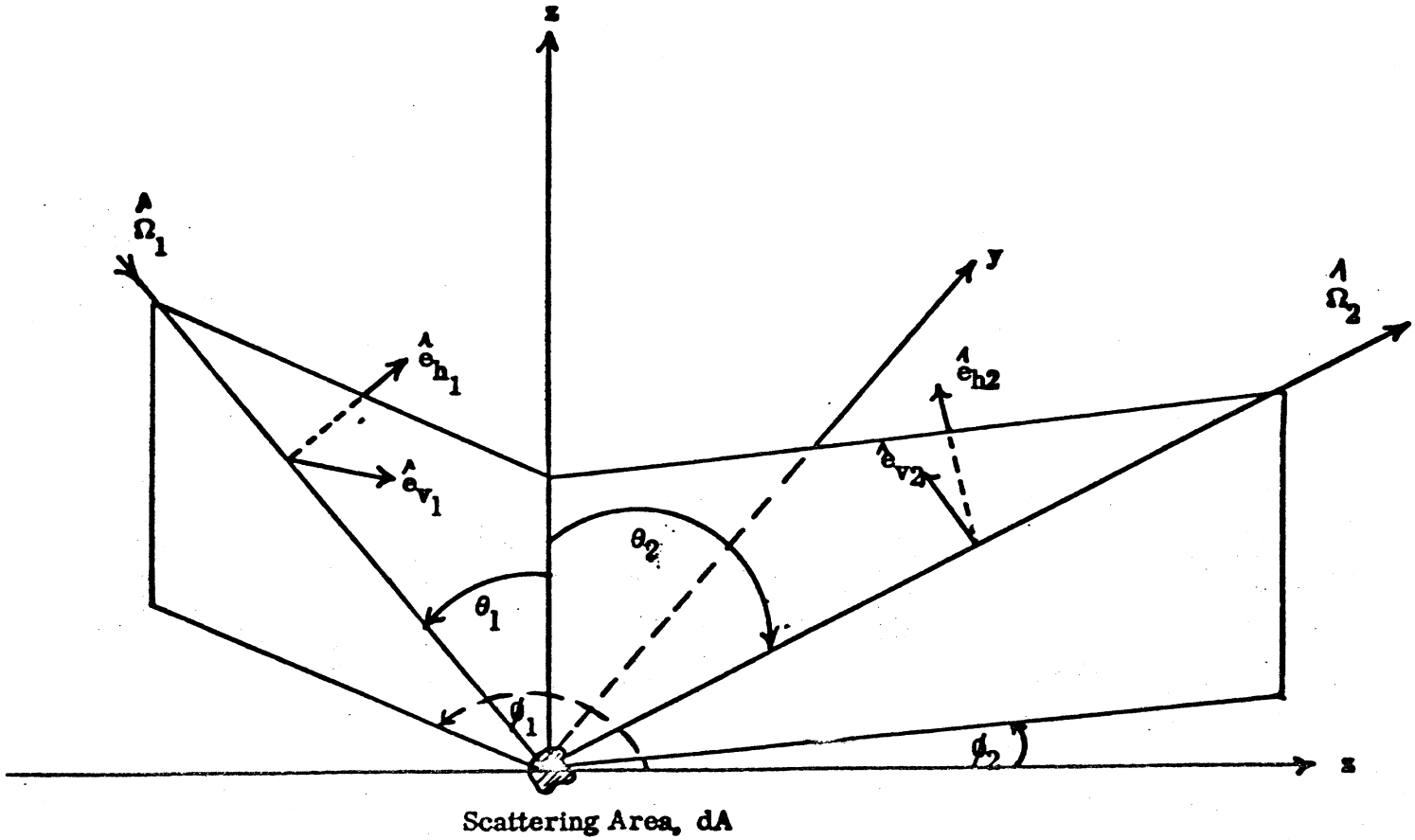

Fig. A-1: Diffraction of Incident and Reflected Waves and the Direction of Polarization.

A theoretical model for rough surface scattering and the derivation of the cross section which is available in the literature may be classified into the following three different approaches.

a) The phenomenological model. By postulation, the surface is taken as an ensemble of distributed spheres, facets and half planes. A review of this model has been given by Beckmann et al (1963).

b) The use of series expansion. In this approach, the incident and scattered fields are expanded in series and boundary conditions are used in determining the coefficients of expansion. Due to the complicated procedure in determining the coefficients, only the first and second order approximate solutions have been reported so far. It is doubtful that any attempt to obtain the more detailed, higher order solutions is feasible.

c) The use of the Kirchhoff approximation. The use of the Kirchhoff integral representation of the scattered field offers a convenient means of finding the approximate expressions for the scattered field from a rough surface. This has been used by various investigators in obtaining theoretical models for rough surface scattering. In the high frequency limit, this offers some basis for the phenomenological models introduced.

Most of the existing investigations, however, are limited to the case of back scattering and for the isotropic random surfaces. In the next few sections, the Kirchhoff approximation shall be used to deduce the bistatic scattering cross section for a sea surface with anisotropic wave spectra.

A.3 Kirchhoff's Integral Formula

A mathematical formulation of electromagnetic scattering, which gives approximate but useful results, is the vector extension of Kirchhoff's integral formula. The Kirchhoff integral formula can be deduced from the physical concept of induced sources as illustrated in Fig. A-2. When an electromagnetic wave is incident on this surface, the scattered radiation may be interpreted as the re-radiation due to the surface electric and magnetic currents.

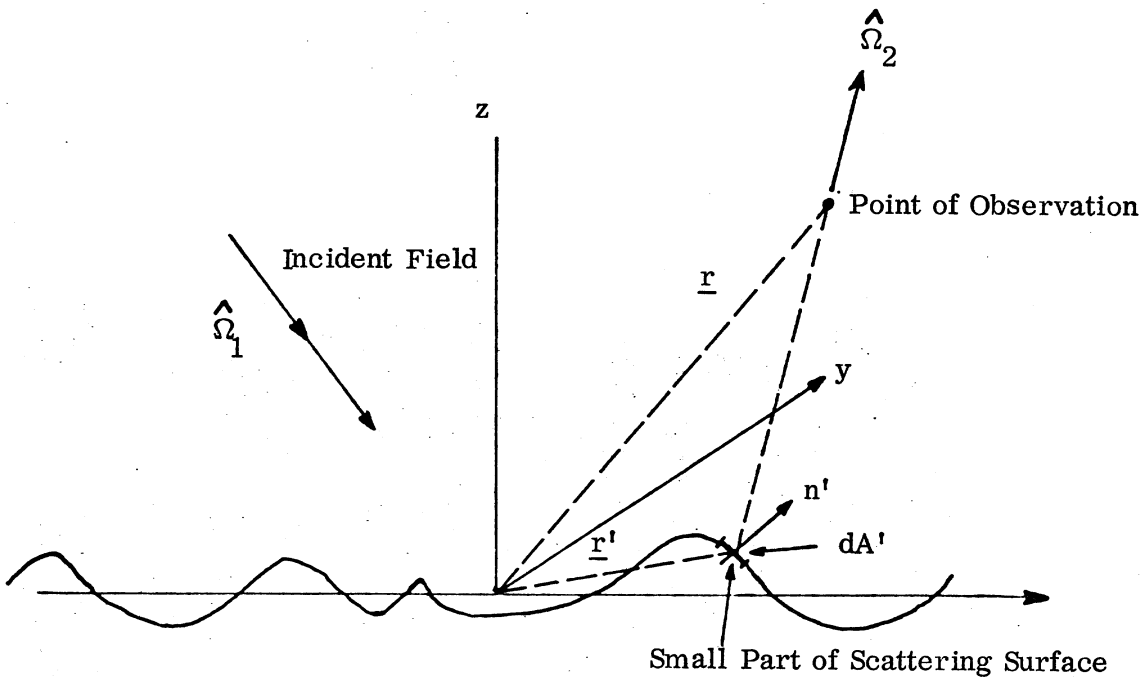

FIG. A-2: Configuration for the Application of Kirchhoff's Integral Formula.

Consider, for example, an elementary area dA', with normal n' , located at r'. If the total (incident and scattered) field at this surface is given by $\underline{E}_s(\underline{r}')$ and $\underline{H}_s(\underline{r}')$, then the surface electric and magnetic currents per unit area at $\underline{r}'$ are given by

$$\underline{J}_e = \hat{n}' \times \underline{H}_s(\underline{r}') \ , \tag{A.14}$$

$$\underline{J}_m = -\hat{n}' \times \underline{E}_s(\underline{r}') \ , \tag{A.15}$$

respectively. The electric field due to these induced sources, observed at any point $\underline{r}$, is given by

$$d\underline{E}(\underline{r}) = \underbrace{(\hat{n}' \times \underline{E}_s(\underline{r}')) \times \nabla' G(\underline{r}, \underline{r}')}_{\text{due to magnetic current}} + i\omega\mu_o \underbrace{(\hat{n}' \times \underline{H}(\underline{r}')) \cdot \left[G(\underline{r}, \underline{r}') + \frac{1}{k^2} \nabla' \nabla' G(\underline{r}, \underline{r}')\right]}_{\text{due to electric current}} , \tag{A.16}$$

where

$$G = \frac{e^{ik\,|\underline{r} - \underline{r}'|}}{4\pi\,|\underline{r} - \underline{r}'|} \tag{A.17}$$

and

$$\nabla' = \hat{x} \frac{\partial}{\partial x'} + \hat{y} \frac{\partial}{\partial y'} + \hat{z} \frac{\partial}{\partial z'} \tag{A.18}$$

Thus, if the tangential field components $\hat{n} \times \underline{E}_s$ and $\hat{n} \times \underline{H}_s$ on the surface are known at all parts of the surface, the scattered fields may be obtained by adding the contributions from each part of the surface, i.e.,

$$\underline{E}_2(\underline{r}) = \int_{\text{Surface}} dA \left\{ (\hat{n}' \times \underline{E}_s(\underline{r}')) \times \nabla' G(\underline{r}, \underline{r}') + i\omega\mu_o (\hat{n} \times \underline{H}(\underline{r}')) \cdot \left[G(\underline{r}, \underline{r}') + \frac{1}{k^2} \nabla' \nabla' G(\underline{r}, \underline{r}')\right] \right\} . \tag{A.19}$$

Similarly the scattered magnetic field is given by

$$\underline{H}_2(\underline{r}) = \int_{\text{Surface}} dA \left\{ (\hat{n}' \times \underline{H}_s(\underline{r}')) \times \nabla' G(\underline{r}, \underline{r}') - i\omega\epsilon_o (n' \times \underline{E}_s(\underline{r}')) \cdot \left[G(\underline{r}, \underline{r}') + \frac{1}{k^2} \nabla' \nabla' G(\underline{r}, \underline{r}') \right] \right\} . \tag{A.20}$$

Equations (A.17) and (A.20) are exact, provided that the exact surface fields are used in the integration.

In most practical cases, the point of observation is high above the ground, so that the far zone approximation may be introduced. Referring to Fig. A-2, any point of observation may be represented by

$$\underline{r} = \hat{\Omega}_2 r \quad , \tag{A.21}$$

and the approximation

$$|\underline{r} - \underline{r}'| \cong (\underline{r} - \underline{r}') \cdot \hat{\Omega}_2 \qquad (r >> r') \quad , \tag{A.22}$$

is adequate. Then,

$$\underline{E}_2(\underline{r}) = ik \frac{e^{ikr}}{4\pi r} \int_{\text{Surface}} dA \left\{ \hat{\Omega}_2 \times (\hat{n}' \times \underline{E}_s(\underline{r}')) - \eta \Omega_2 \times \left[\Omega_2 \times (\hat{n}' \times \underline{H}_s(\underline{r}')) \right] \right\} e^{-ik\hat{\Omega}_2 \cdot \underline{r}'} \tag{A.23}$$

and

$$\underline{H}_2(\underline{r}) = ik \frac{e^{ikr}}{4\pi r} \int_{\text{Surface}} dA \left\{ \frac{1}{\eta} \hat{\Omega}_2 \times \left[\hat{\Omega}_2 \times (\hat{n}' \times \underline{E}_s(\underline{r}')) \right] + \hat{\Omega}_2 \times (\hat{n}' \times \underline{H}_s(\underline{r}')) \right\} e^{-ik\hat{\Omega}_2 \cdot \underline{r}'} , \tag{A.24}$$

where $$\eta \triangleq \mu_o / \epsilon_o \quad . \tag{A.25}$$

Equations (A.23) and (A.24) are the fundamental relations used in the approximate calculations of the scattered field (e.g., Hoffman (1955); Aksenov (1958)).

For plane wave incidence, the incident fields are given by:

$$\underline{E}_1(\underline{r}') = \underline{E}_1(0)\, e^{ik\hat{\Omega}_1 \cdot \underline{r}'} \quad . \tag{A.26}$$

$$\underline{H}_1(\underline{r}') = \frac{1}{\eta}\, \hat{\Omega}_1 \times \underline{E}_1(0)\, e^{ik\hat{\Omega}_1 \cdot \underline{r}'} \quad . \tag{A.27}$$

Then, if $\underline{E}_s$ and $\underline{H}_s$ are interpreted as the surface fields due to an incident field with the electric and magnetic field respectively given by $\underline{E}_1(0)$ and $\frac{1}{\eta}\hat{\Omega}_1 \times \underline{E}_1(0)$ at each part of the surface, we may have

$$\underline{E}_2(\underline{r}) = ik\, \frac{e^{ikr}}{4\pi r} \int_{\text{Surface}} dA \left\{ \hat{\Omega}_2 \times (\hat{n}' \times \underline{E}_s(\underline{r}')) - \eta \hat{\Omega}_2 \times \left[\hat{\Omega}_2 \times (\hat{n}' \times \underline{H}_s(\underline{r}')) \right] \right\} e^{ik(\hat{\Omega}_1 - \hat{\Omega}_2) \cdot \underline{r}'} \quad . \tag{A.28}$$

Similar equations can be obtained for $\underline{H}_2(\underline{r})$.

In practice, the integral (A.28) cannot be carried out exactly, even if we know the shape of the surface, due to the difficulties in obtaining $\underline{E}_s$ and $\underline{H}_s$. A commonly used approximation is the so-called local tangent plane approximation. Assume that the local radius of curvature of the scattering surface is much larger than the wave length, so that locally, the reflected fields at any point may be considered the same as those reflected by a plane tangent to the reflecting surface at that point. With this approximation, it may be easily shown that, (Aksenov, 1958)

$$\hat{n}' \times \underline{E}_s = (1 + R_\perp)(\underline{E}_1(0) \cdot \hat{t})\, \hat{n}' \times \hat{t} + (1 - R_{||})(\underline{E}_1(0) \cdot \hat{t}')\, \hat{n}' \times \hat{t}' \tag{A.29}$$

$$\eta \hat{n}' \times \underline{H}_s = (1 - R_\perp)(\underline{E}_1(0) \cdot \hat{t})\, \hat{n}' \times \hat{t}' - (1 + R_{||})(\underline{E}_1(0) \cdot \hat{t}')\, \hat{n}' \times \hat{t} \quad , \tag{A.30}$$

where

$$\hat{t} = \frac{\hat{\Omega}_1 \times \hat{n}'}{|\hat{\Omega}_1 \times \hat{n}'|} \quad , \tag{A.31}$$

and $$\hat{t}' = \hat{\Omega}_1 \times \hat{t} \quad . \tag{A.32}$$

Also

$$R_{\perp} = \frac{\cos\gamma - \sqrt{N^2 - \sin^2\gamma}}{\cos\gamma + \sqrt{N^2 - \sin^2\gamma}} \quad , \tag{A.33}$$

$$R_{\parallel} = \frac{N^2\cos\gamma - \sqrt{N^2 - \sin^2\gamma}}{N^2\cos\gamma + \sqrt{N^2 - \sin^2\gamma}} \quad , \tag{A.34}$$

where

$$\cos\gamma = -\hat{\Omega}_1 \cdot \hat{n} \tag{A.35}$$

and

N = index of refraction of the surface.

In particular, if the reflecting surface is perfectly conducting, then,

$$R_{\perp} = -1 \tag{A.36}$$

and

$$R_{\parallel} = +1 \quad . \tag{A.37}$$

For this case, we have,

$$\hat{n}' \times \underline{E}_s = 0 \tag{A.38}$$

and

$$\hat{n}' \times \underline{H}_s = 2\,\hat{n}' \times \underline{H}_1(0) \quad , \tag{A.39}$$

which are the approximate relations used by most investigators to simplify computations.

By introducing Eqs. (A.29) and (A.30) into (A.28), an approximate relation results between the incident electric field $\underline{E}_1$ and the scattered electric field $\underline{E}_2$. This result is given by

$$\underline{E}_2 = (r, \hat{\Omega}_2) = ik \frac{e^{ikr}}{4\pi r}$$

$$\hat{\Omega}_2 \times \int dA' \left[(1+R_\perp)(\hat{n}' \times \hat{t})(\hat{E}_1 \cdot \hat{t}) + (1 - R_\parallel)(\hat{n}' \times \hat{t}')(\underline{E}_1 \cdot \hat{t}') \right] e^{ik(\hat{\Omega}_1 - \hat{\Omega}_2) \cdot r'}$$

$$-\hat{\Omega}_2 \times \hat{\Omega}_2 \times \int dA' \left[(1 - R_\perp)(\hat{n}' \times \hat{t}')(\underline{E}_1 \cdot \hat{t}) - (1+R_\parallel)(\hat{n}' \times \hat{t})(\underline{E}_1 \cdot \hat{t}') \right] e^{ik(\hat{\Omega}_1 - \hat{\Omega}_2) \cdot r'} . \quad \text{(A.40)}$$

In order to clarify the polarization effect on the scattered field, let us, by using the directions of polarization defined by Equations (A.4) through (A.5), resolve the incident and scattered fields into the vertically and horizontally polarized components as indicated below:

$$\underline{E}_1 = \left[\hat{e}_{h1} + \hat{e}_{v1} E_{v1} \right] e^{ik\hat{\Omega}_1 \cdot \underline{r}} \quad \text{(A.41)}$$

and

$$\underline{E}_2 = \left[\hat{e}_{h2} E_{h2} + \hat{e}_{v2} E_{v2} \right] \frac{e^{ikr}}{r} . \quad \text{(A.42)}$$

From (A.40), it is seen that the components of the incident field and the scattered field may be related by a matrix:

$$\begin{bmatrix} E_{h2} \\ E_{v2} \end{bmatrix} = \begin{bmatrix} S_{hh} & S_{hv} \\ S_{vh} & S_{vv} \end{bmatrix} \begin{bmatrix} E_{h1} \\ E_{v1} \end{bmatrix} \quad \text{(A.43)}$$

where each component of the scattering matrix $S_{\ell m}$ may be expressed by:

$$S_{\ell m} = \frac{ik}{4\pi} \int dA' e^{ik(\hat{\Omega}_1 - \hat{\Omega}_2)\cdot \underline{r}'} \left\{ \begin{array}{lll} -(1+R_\perp) & (\hat{e}_{m1}\cdot\hat{t}) & (\hat{\Omega}_2 x \hat{e}_{\ell 2})\cdot(\hat{n}' x \hat{t}) \\ -(1-R_{||}) & (\hat{e}_{m1}\cdot\hat{t}') & (\hat{\Omega}_2 x \hat{e}_{\ell 2})\cdot(\hat{n}' x \hat{t}') \\ +(1-R_\perp) & (\hat{e}_{m1}\cdot\hat{t}) & \hat{e}_{\ell 2}\cdot(\hat{n}' x \hat{t}') \\ -(1+R_{||}) & (\hat{e}_{m1}\cdot\hat{t}') & \hat{e}_{\ell 2}\cdot(\hat{n}' x \hat{t}) \end{array} \right\} . \qquad (A.44)$$

The relations between the elements of the scattering matrix and the scattering cross section may be easily deduced from the definition of the scattering cross section. For example, for an incident wave with polarization direction m (h or v), the power scattered by a surface area A, in the direction Ω_2, with polarization ℓ is given by

$$dp_r = \frac{p_i A}{r^2} \left| S_{\ell m} \right|^2 . \qquad (A.45)$$

Therefore, if a rough surface A is relatively homogeneous, the average scattering cross section from an incident wave of polarization m to a scattered wave of polarization ℓ is given by

$$\sigma_{\ell m} = \frac{4\pi \left\langle \left| S_{\ell m} \right|^2 \right\rangle}{A} \qquad (A.46)$$

where $\langle\ \rangle$ enclosing any quantity indicates the statistical average.

In order to carry out the average such as given in (A.46), it is necessary to express $S_{\ell m}$ in terms of the configuration of the surface.

To be explicit, let us assume that the surface is given by

$$z = z(x, y) \tag{A.47}$$

so that

$$\hat{n} = \frac{-\hat{x}\, z_x - \hat{y}\, z_y + \hat{z}}{\sqrt{1+z_x^2 + z_y^2}} \tag{A.48}$$

where

$$z_x \triangleq \frac{\partial z}{\partial x} \quad , \qquad z_y \triangleq \frac{\partial z}{\partial y} \quad . \tag{A.49}$$

Moreover, we let

$$\hat{\Omega}_1 = -\left[\hat{x}\sin\theta_1\cos\phi_1 + \hat{y}\sin\theta_1\sin\phi_1 + \hat{z}\cos\theta_1\right] \tag{A.50}$$

and

$$\hat{\Omega}_2 = \left[\hat{x}\sin\theta_2\cos\phi_2 + \hat{y}\sin\theta_2\sin\phi_2 + \hat{z}\cos\theta_2\right] \quad . \tag{A.51}$$

Then, in terms of z, θ_1, ϕ_1, θ_2 and ϕ_2, we may, after tedious algebraic manipulation, express $S_{\ell m}$ in the form

$$S_{\ell m} = \frac{ik}{4\pi} \int dx \int dy\, g_{\ell m} e^{-ik(q_x x + q_y y + q_z z)} \quad , \tag{A.52}$$

where

$$q_x = \sin\theta_1 \cos\phi_1 + \sin\theta_2 \cos\phi_2 \tag{A.53}$$

$$q_y = \sin\theta_1 \sin\phi_1 + \sin\theta_2 \sin\phi_2 \tag{A.54}$$

and

$$q_z = \cos\theta_1 + \cos\theta_2 \quad . \tag{A.55}$$

The function $g_{\ell m}$, in the case of finite index of refraction N, are complicated functions involving $\theta_1, \theta_2, \phi_1$ and ϕ_2 and the reflection coefficients $R_\perp$ and $R_{||}$,

which in turn depend on the angle of incidence γ where

$$\cos\gamma = \hat{\Omega}_1 \cdot \hat{n} = \frac{+\sin\theta_1\cos\phi_1 z_x + \sin\theta_1\sin\phi_1 z_y - \cos\theta_1}{\sqrt{\left[1 + z_x^2 + z_y^2\right]}} \qquad (A.56)$$

Anticipating that, for most cases, when $N \longrightarrow \infty$, $R_\perp \cong -1$, and $R_{||} \cong +1$, one may arrange $g_{\ell m}$ in the following form:

$$g_{\ell m} = -(1+R_\perp)P_{\ell m} - (1-R_{||})Q_{\ell m} + 2\,G_{\ell m} \quad .$$

The function P, Q and G depend on the direction of incidence, reflection and the slope of the surface. For highly conducting surfaces, the dominant contribution to the scattering matrix comes from the factors $G_{\ell m}$, and the other terms may be treated as a perturbation. By straightforward algebraic manipulation, the explicit expressions of the dominant coefficients $G_{\ell m}$, in terms of $\theta_1, \phi_1, \theta_2, \phi_2$ and the slope at the surface $z_z = \partial z/\partial x$ and $z_y = \partial z/\partial y$ are given below:

$$\begin{aligned} G_{hh} = & -\cos\theta_1\cos(\phi_2-\phi_1) \\ & +z_x \sin\theta_1\cos\phi_2 \\ & +z_y \sin\theta_1\sin\phi_2 \quad , \end{aligned} \qquad (A.57)$$

$$G_{hv} = \sin(\phi_2-\phi_1) \qquad (A.58)$$

$$\begin{aligned} G_{vh} = & \cos\theta_1\cos\theta_2\sin(\phi_2-\phi_1) \cdot \\ & +z_x(\cos\theta_1\sin\theta_2\sin\phi_1 - \cos\theta_2\sin\theta_1\sin\phi_2) \\ & +z_y(\sin\theta_1\cos\theta_2\cos\phi_2 - \sin\theta_2\cos\theta_1\cos\phi_1) \end{aligned} \qquad (A.59)$$

and

$$\begin{aligned} G_{vv} = & \cos\theta_2\cos(\phi_2-\phi_1) \\ & -z_x\cos\phi_1\sin\theta_2 \\ & -z_y\sin\phi_1\sin\theta_2 \quad . \end{aligned} \qquad (A.60)$$

The coefficients $P_{\ell m}$ and $Q_{\ell m}$, which have less effect on the scattering matrix for surfaces of large index of refraction, may be expressed as

$$\left.\begin{aligned} P_{hh} &= -Q_{vv} = \frac{AC}{\Delta} \\ P_{hv} &= Q_{vh} = \frac{AD}{\Delta} \\ P_{vh} &= Q_{hv} = \frac{BC}{\Delta} \\ P_{vv} &= -Q_{hh} = \frac{BD}{\Delta} \end{aligned}\right\} , \qquad (A.61)$$

where

$$\begin{aligned} A = z_x^2 & \left[\sin\theta_1\cos\theta_2\sin\phi_1\sin\phi_2 - \cos\theta_1\sin\theta_2 - \sin\theta_1\cos\theta_1\cos\phi_1\cos\phi_2\right] \\ & + z_y^2 \left[\sin\theta_1\cos\theta_2\cos\phi_1\cos\phi_2 - \cos\theta_1\sin\theta_2 - \sin\theta_1\cos\theta_1\sin\phi_1\sin\phi_2\right] \\ & - z_x z_y \left[\sin\theta_1\cos\theta_2\sin(\phi_2+\phi_1) + \sin\theta_1\cos\theta_1\sin(\phi_2+\phi_1)\right] \\ & - z_x \left[\sin\theta_1\sin\theta_2\cos\phi_1 - \cos\theta_1\cos\theta_2\cos\phi_2 - \cos^2\theta_1\cos\phi_2 + \sin^2\theta_1\cos\phi_1\cos(\phi_2-\phi_1)\right] \\ & - z_y \left[\sin\theta_1\sin\theta_2\sin\phi_1 - \cos\theta_1\cos\theta_2\sin\phi_2 - \cos^2\theta_1\sin\phi_2 + \sin^2\theta_1\sin\phi_1\cos(\phi_2-\phi_1)\right] \\ & + \sin\theta_1\cos(\phi_2-\phi_1)\left[\cos\theta_1 + \cos\theta_2\right] . \end{aligned} \qquad (A.62)$$

$$\begin{aligned} B = z_x^2 & \sin\theta_1 \left[\sin\phi_1\cos\phi_2 + \cos\phi_1(\cos\theta_1\cos\theta_2\sin\phi_2 + \sin\theta_1\sin\theta_2\sin\phi_1)\right] \\ & - z_y^2 \sin\theta_1 \left[\cos\phi_1\sin\phi_2 + \sin\phi_1(\cos\theta_1\cos\theta_2\cos\phi_2 + \sin\theta_1\sin\theta_2\cos\phi_1)\right] \\ & - z_x z_y \sin\theta_1 \left[\cos(\phi_2+\phi_1) + \cos\theta_1\cos\theta_2\cos(\phi_2+\phi_1) + \sin\theta_1\sin\theta_2\cos 2\phi_1\right. \\ & \qquad \left. - \sin\theta_1(1+\cos\theta_1\cos\theta_2)\sin(\phi_2-\phi_1)\right] \\ & + z_x \left[\sin^2\theta_1\cos\theta_2\cos\phi_1\sin(\phi_2-\phi_1) - \cos\theta_1(\sin\phi_2 + \cos\theta_1\cos\theta_2\sin\phi_2 + \sin\theta_1\sin\theta_2\sin\phi_1)\right] \\ & + z_y \left[\sin^2\theta_1\cos\theta_2\sin\phi_1\sin(\phi_2-\phi_1) + \cos\theta_1(\cos\phi_2 + \cos\theta_1\cos\theta_2\cos\phi_2 + \sin\theta_1\sin\theta_2\cos\phi_1)\right] \end{aligned} \qquad (A.63)$$

$$C = -z_x \cos\theta_1 \cos\phi_1 - z_y \cos\theta_1 \sin\phi_1 - \sin\theta_1 \tag{A.64}$$

$$D = -z_x \sin\phi_1 + z_y \cos\phi_1 \tag{A.65}$$

$$\Delta = \left[1+z_x^2+z_y^2\right]^{3/2} \left[z_x^2(1-\sin^2\theta_1\cos^2\phi_1)+z_y^2(1-\sin^2\theta_1\sin^2\phi_1) - 2z_x z_y \sin^2\theta_1 \sin\phi_1\cos\phi_1 + 2z_x \sin\theta_1\cos\theta_1\cos\phi_1 + 2z_y \sin\theta_1\cos\theta_1\sin\phi_1 + \sin^2\theta_1\right] . \tag{A.66}$$

The above expressions involved in $S_{\ell m}$ are too complicated to be of practical use. For the case of slightly rough surfaces, however, we may neglect powers involving z_x and z_y, and retaining only terms up to the linear terms. Within this approximation, we have;

$$g_{\ell m} = a_{\ell m} + b_{\ell m} z_x + c_{\ell m} z_y \ , \tag{A.67}$$

where

$$a_{hh} = -2\cos\theta_1\cos(\phi_2-\phi_1)+(1+R_\perp)(\cos\theta_1+\cos\theta_2)\cos(\phi_2-\phi_1) \tag{A.68}$$

$$b_{hh} = 2\sin\theta_1\cos\phi_2 - \frac{(1+R_\perp)}{\sin\theta_1}\left[(1+\cos\theta_1\cos\theta_2)\cos\phi_1\cos(\phi_2-\phi_1) + \cos\phi_1\sin\theta_1\sin\theta_2 - \cos\theta_1(\cos\theta_1+\cos\theta_2)\cos\phi_2\right] + \frac{(1-R_{||})}{\sin\theta_1}\left[(1+\cos\theta_1\cos\theta_2)\sin\phi_1\sin(\phi_2-\phi_1)\right] \tag{A.69}$$

$$c_{hh} = 2\sin\theta_1\sin\phi_2 - \frac{(1+R_\perp)}{\sin\theta_1}\left[(1+\cos\theta_1\cos\theta_2)\sin\phi_1\cos(\phi_2-\phi_1) + \sin\phi_1\sin\theta_1\sin\theta_2 - \sin\phi_2\cos\theta_1(\cos\theta_1+\cos\theta_2)\right] - \frac{(1-R_{||})}{\sin\theta_1}(1+\cos\theta_1\cos\theta_2)\cos\phi_1\sin(\phi_2-\phi_1) \tag{A.70}$$

$$a_{hv} = 2\sin(\phi_2-\phi_1)-(1-R_{||})(1+\cos\theta_1\cos\theta_2)\sin(\phi_2-\phi_1) \quad \text{(A.71)}$$

$$b_{hv} = \frac{(1+R_\perp)}{\sin\theta_1}(\cos\theta_1+\cos\theta_2)\sin\phi_1\cos(\phi_2-\phi_1) + \frac{(1-R_{||})}{\sin\theta_1}\left[(\cos\theta_1+\cos\theta_2)\cos\phi_1\sin(\phi_2-\phi_1)\right.$$
$$\left.-\cos\theta_1(1+\cos\theta_1\cos\theta_2)\sin\phi_2-\sin\theta_1\cos\theta_1\sin\theta_2\sin\phi_2\right] \quad \text{(A.72)}$$

$$c_{hv} = -\frac{(1+R_\perp)}{\sin\theta_1}(\cos\theta_1+\cos\theta_2)\cos\phi_1\cos(\phi_2-\phi_1)+\frac{(1-R_{||})}{\sin\theta_1}\left[(\cos\theta_1+\cos\theta_2)\sin\phi_1\sin(\phi_2-\phi_1)\right.$$
$$\left.+\cos\theta_1(1+\cos\theta_1\cos\theta_2)\cos\phi_2+\sin\theta_1\cos\theta_1\sin\theta_2\cos\phi_1\right] \quad \text{(A.73)}$$

$$a_{vh} = 2\cos\theta_1\cos\theta_2\sin(\phi_2-\phi_1)-(1+R_\perp)(1+\cos\theta_1\cos\theta_2)\sin(\phi_2-\phi_1) \quad \text{(A.74)}$$

$$b_{vh} = 2\left[\cos\theta_1\sin\theta_2\sin\phi_1-\sin\theta_1\cos\theta_2\sin\phi_2\right]+\frac{(1+R_\perp)}{\sin\theta_1}\left[(\cos\theta_1+\cos\theta_2)\cos\phi_1\sin(\phi_2-\phi_1)\right.$$
$$\left.-\cos\theta_1(1+\cos\theta_1\cos\theta_2)\sin\phi_2-\sin\theta_1\cos\theta_1\sin\theta_2\sin\phi_1\right]$$
$$+\frac{(1-R_{||})}{\sin\theta_1}(\cos\theta_1+\cos\theta_2)\sin\phi_1\cos(\phi_2-\phi_2) \quad \text{(A.75)}$$

$$c_{vh} = 2\left[\sin\theta_1\cos\theta_2\cos\phi_2-\cos\theta_1\sin\theta_2\cos\phi_1\right]+\frac{(1+R_\perp)}{\sin\theta_1}\left[(\cos\theta_1+\cos\theta_2)\sin\phi_1\sin(\phi_2-\phi_1)\right.$$
$$\left.+\cos\theta_1(1+\cos\theta_1\cos\theta_2)\cos\phi_2+\sin\theta_1\cos\theta_1\sin\theta_2\cos\phi_1\right]$$
$$-\frac{(1-R_{||})}{\sin\theta_1}(\cos\theta_1+\cos\theta_2)\cos\phi_1\cos(\phi_2-\phi_1) \quad \text{(A.76)}$$

$$a_{vv} = 2\cos\theta_2\cos(\phi_2-\phi_1)-(1-R_{||})(\cos\theta_1+\cos\theta_2)\cos(\phi_2-\phi_1) \quad \text{(A.77)}$$

$$b_{vv} = -2\sin\theta_2\cos\phi_1-\frac{(1+R_\perp)}{\sin\theta_1}(1+\cos\theta_1\cos\theta_2)\sin\phi_1\sin(\phi_2-\phi_1)+\frac{(1-R_{||})}{\sin\theta_1}\left[(1+\cos\theta_1\cos\theta_2)\right.$$
$$\left.\cdot\cos\phi_1\cos(\phi_2-\phi_1)+\sin\theta_1\sin\theta_2\cos\phi_2-\cos\theta_1(\cos\theta_1+\cos\theta_2)\cos\phi_2\right]$$
$$\text{(A.78)}$$

$$c_{vv} = -2\sin\theta_2\sin\phi_1 + \frac{(1+R_\perp)}{\sin\theta_1}(1+\cos\theta_1\cos\theta_2)\cos\phi_1\sin(\phi_2-\phi_1)$$
$$+\frac{(1-R_{||})}{\sin\theta_1}\left[(1+\cos\theta_1\cos\theta_2)\sin\phi_1\cos(\phi_2-\phi_1)+\sin\theta_1\sin\theta_2\sin\phi_1\right.$$
$$\left.-\cos\theta_1(\cos\theta_1+\cos\theta_2)\sin\phi_2\right] . \qquad (A.79)$$

Here the approximate $R_\perp$ and $R_{||}$ are evaluated through $\cos\gamma = \cos\theta_1$. Thus, for the case where the surface is highly conducting, which allows the approximation

$$R_\perp \cong -1, \quad R_{||} \cong +1 ,$$

it is reasonable to retain only the first terms in Eqs. (A.68) through (A.79) for the calculation. This approximation is introduced in the calculation of the scattering cross section, σ, in this report.

A.4 Average Scattering Cross Section of Random Surface

In carrying out the statistical average of the bistatic cross section for a rough surface, we assume that the surface is spatially homogeneous and temporally stationary. That is, the surface described by $z=z(x,y,t)$ is a homogeneous, stationary random variable. In order to specify the statistical properties of this surface, we shall further assume that the random variable is normally distributed and has the correlation function given by:

$$\langle z(x,y),\ z(x',y') \rangle = H(\tau_x,\tau_y) \quad , \qquad (A.80)$$

where

$$\tau_x \triangleq x' - x \qquad (A.81)$$
$$\tau_y \triangleq y' - y .$$

Based on this homogeneous approximation, it is possible to carry out the computation of the bistatic cross section.

From Eqs. (A.46) and (A.52) through (A.55), the formal expressions for the cross section may be given by

$$\sigma_{\ell m} = \frac{k^2}{4\pi}\int dx \int dy \int dx' \int dy'\, e^{-ik(q_x\tau_x + iq_y\tau_y)}$$
$$\left\langle g_{\ell m}(x,y)\, g_{\ell m}(x+\tau_x, y+\tau_y)\, e^{iq_z(z'-z)} \right\rangle \qquad (A.82)$$

where, for simplicity, we denoted

$$z' \triangleq z(x', y') \quad . \tag{A.83}$$

For a spatially stationary random surface, we infer that

$$\left\langle g_{\ell m}(x,y) g_{\ell m}(x+\tau_x, y+\tau_y) e^{iq_z(z'-z)} \right\rangle \triangleq K_{\ell m}(\tau_x, \tau_y) , \tag{A.84}$$

which is independent of x, y . Thus, we have

$$\sigma_{\ell m}(\hat{\Omega}_2, \hat{\Omega}_1) = \frac{k^2}{4\pi \cos\theta_1} \int d\tau_x \int d\tau_y \, e^{-ikq_x\tau_x} \, e^{-ikq_y\tau_y} K_{\ell m}(\tau_x, \tau_y) \tag{A.85}$$

In order to estimate the statistical average $K_{\ell m}$, we use the approximate linearized form of $g_{\ell m}$ given by (A.67), so that

$$K_{\ell m}(\tau_x, \tau_y) = \left\langle (a_{\ell m} + b_{\ell m} z_x + c_{\ell m} z_y)(a_{\ell m} + b_{\ell m} z'_x + c_{\ell m} z'_y) e^{ikq_z(z'-z)} \right\rangle \tag{A.86}$$

For normally distributed surfaces whose slopes are also normally distributed, the joint probability of the five random variables

$$\left.\begin{aligned} u_1 &\triangleq z'-z \\ u_2 &\triangleq z_x \\ u_3 &\triangleq z_y \\ u_4 &\triangleq z_{x'} \\ u_5 &\triangleq z_{y'} \end{aligned}\right\} \tag{A.87}$$

can easily be written down and the statistical averages taken.

For a simple way of evaluating $K_{\ell m}$, we note that, for normally distributed variables

$$\left\langle \exp\left(i \sum_j q_j u_j\right)\right\rangle = \exp\left[-\frac{1}{2}\sum_i \sum_j \rho_{ij}\, q_i q_j\right], \tag{A.88}$$

where

$$\rho_{ij} = \langle u_i u_j \rangle \quad . \tag{A.89}$$

Explicitly, we have

$$\left.\begin{aligned}
\rho_{11} &= 2\left[H(0,0) - H(\tau_x, \tau_y)\right] \\
\rho_{22} &= \rho_{44} = H_{xx}(0,0) \\
\rho_{33} &= \rho_{55} = H_{yy}(0,0) \\
\rho_{12} &= \rho_{14} = \rho_{21} = \rho_{41} = -H_x(\tau_x, \tau_y) \\
\rho_{13} &= \rho_{15} = \rho_{31} = \rho_{51} = -H_y(\tau_x, \tau_y) \\
\rho_{23} &= \rho_{32} = H_{xy}(0,0) \\
\rho_{24} &= \rho_{42} = -H_{xx}(\tau_x, \tau_y) \\
\rho_{25} &= \rho_{52} = \rho_{34} = \rho_{43} = -H_{xy}(\tau_x, \tau_y) \\
\rho_{35} &= \rho_{53} = -H_{yy}(\tau_x, \tau_y) \\
\rho_{45} &= \rho_{54} = H_{yy}(0,0)
\end{aligned}\right\}, \tag{A.90}$$

where, for simplicity, we denoted

$$H_x \triangleq \frac{\partial H}{\partial \tau_x} \quad , \text{ etc.} \tag{A.91}$$

It follows, therefore, that

$$\left\langle (a+b\,u_2+c\,u_3)(a+b\,u_4+c\,u_5)\left[\exp -i\sum_j q_j u_j\right]\right\rangle$$
$$=\left(a+ib\frac{\partial}{\partial q_2}+ic\frac{\partial}{\partial q_3}\right)\left(a+ib\frac{\partial}{\partial q_4}+ic\frac{\partial}{\partial q_5}\right)\exp\left[-\frac{1}{2}\sum_i\sum_j \rho_{ij}u_i u_j\right] . \tag{A.92}$$

Using the above and noting that

$$q_1 = kq_2 \quad ,$$

$$q_2 = q_3 = q_4 = q_5 = 0 \quad ,$$

one finds that

$$K_{\ell m}(\tau_x,\tau_y) = \exp\left\{-k^2 q_z^2\left[H(0,0) - H(\tau_x,\tau_y)\right]\right\}$$
$$\cdot\left\{a_{\ell m}^2 + 2a_{\ell m}b_{\ell m}\left[ikq_z H_x\right] + 2a_{\ell m}c_{\ell m}\left[ikq_z H_y\right] - b_{\ell m}^2\left[H_{xx}+k^2q_z^2 H_x^2\right]\right.$$
$$\left. -c_{\ell m}^2\left[H_{yy}+k^2q_z^2 H_y^2\right] - 2b_{\ell m}c_{\ell m}\left[H_{xy}+k^2q_z^2 H_x H_y\right]\right\} \quad . \tag{A.93}$$

Now, it is easily recognized that

$$\int d\tau_x \int d\tau_y \exp\left\{-k^2q_z^2\left[H(0,0)-H(\tau_x,\tau_y)\right] - ikq_x\tau_x - ikq_y\tau_y\right\}$$
$$\cdot\begin{Bmatrix} H_x \\ H_y \\ H_{xx}+k^2q_z^2 H^2 \\ H_{xy}+k^2q_z^2 H_x H_y \\ H_{yy}+k^2q_z^2 H_y^2 \end{Bmatrix} = \frac{1}{k^2q_z^2}\begin{Bmatrix} ikq_x \\ ikq_y \\ -k^2q_x^2 \\ -k^2q_xq_y \\ -k^2q_y^2 \end{Bmatrix}$$
$$\cdot\int d\tau_x \int d\tau_y \exp\left\{-k^2q_z^2\left[H(0,0)-H(\tau_x,\tau_y)\right] - ikq_x\tau_x - ikq_y\tau_y\right\} \tag{A.94}$$

Therefore, from (A.93) we may have the relatively simple result:

$$\sigma_{\ell m} = \frac{k^2}{4\pi q_z^2} \left[a_{\ell m} q_z - b_{\ell m} q_x - c_{\ell m} q_y \right]^2$$

$$\cdot \int d\tau_x \int d\tau_y \exp\left\{ -k^2 q_z^2 \left[H(0,0) - H(\tau_x, \tau_y) \right] - ikq_x \tau_x - ikq_y \tau_y \right\} . \tag{A.95}$$

Thus, based on the assumptions that

i) the surface is slightly rough (neglecting the higher order terms of z_x, z_y)

and

ii) the surface height is normally distributed,

the scattering cross section may be evaluated if the surface height correlation is known. The result so obtained is probably adequate for slightly perturbed ocean surfaces. The application of the results of this section to an ocean surface is given next.

A.5 The Ocean Surface Wave Spectrum and the Scattering Cross Section

In order to apply the result of the last section to a rough surface such as the sea surface, it is necessary to find the correlation of the surface height. Searching through the available literature, it has been found that such information is not readily available. However, directional spectra of ocean surface waves, based on the empirical data, have been reported (Kinsman, 1965). We, therefore, shall start from the directional spectra of the ocean surface and deduce approximately the correlation of the surface height.

For small perturbations of the ocean surface, including the effect of gravity and surface tension, each component of ocean wave may be represented by the form

$$z \sim a \exp\left[-i\sigma t + \kappa_1 + x + \kappa_2 y \right] . \tag{A.96}$$

For deep water, the frequency σ and the wave number

$$\kappa = \sqrt{\kappa_1^2 + \kappa^2} \tag{A.97}$$

satisfy the dispersion relation

$$\sigma^2 = g\kappa + \Gamma\kappa^3 , \qquad (A.98)$$

where

$$g = 980 \text{ cm/sec}^2 = 9.8 \text{ m/sec}^2$$

and

Γ = coefficient of surface tension/density

$= 74 \text{ dyn-cm}^2/\text{gm} = 74 \times 10^{-6} \text{ Nt-m}^2/\text{kg}.$

In Fig. A-3, the relation between σ and κ are sketched. For waves of small perturbations, one generally divides the ocean surface-wave spectrum into gravity waves and capillary waves. It is easy to see that the phase velocity of the wave is minimum at

$$\kappa_m = \sqrt{\frac{g}{\Gamma}} = 364 \text{ Ra/m} \qquad (A.99)$$

corresponding to a wavelength of

$$L_m = \frac{2\pi}{\kappa_m} = 1.73 \times 10\text{-}2 \text{ meters}. \qquad (A.100)$$

Waves for which

$$\kappa > \kappa_m , \ (L < L_m)$$

are dominated by capillary effect of the sea water (surface tension) and hence are called capillary waves, while waves for which

$$\kappa < \kappa_m \ (L > L_m)$$

are dominated by gravity effect and hence are called gravity waves.*

---

* For the doppler frequency under current investigation, the wavelength is about $\lambda \cong 3.5 \times 10^{-2}$ meters, so that, roughly, components of ocean surface waves of dominant importance in the scattering process is in the upper ultra-gravity wave range.

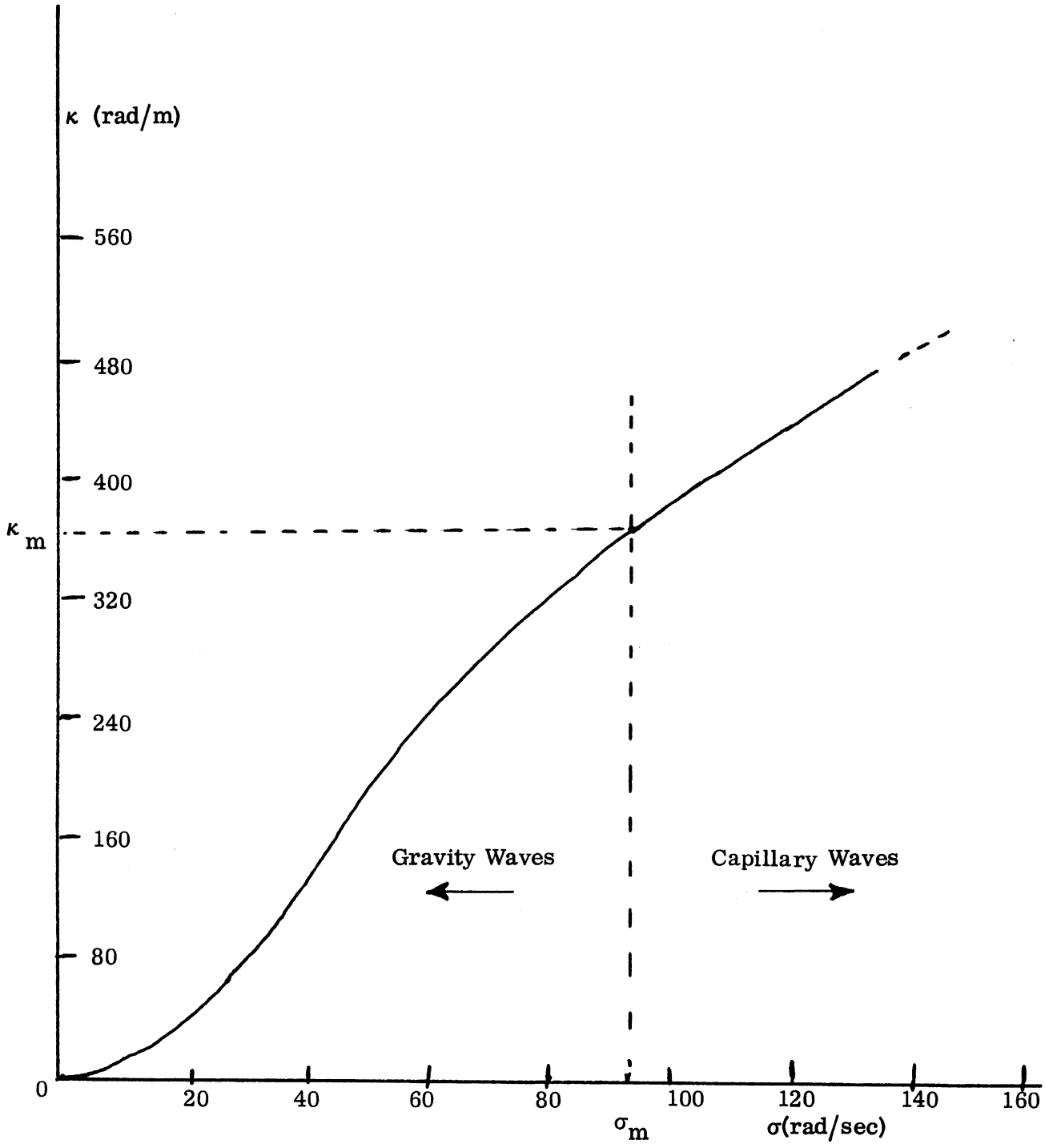

FIG. A-3: The Wave Number vs Frequency for the Sea Surface.

In an open, developed sea, especially with wind blowing, the wind energy is coupled to the particular component of wave with velocity the same as that of the wind. This energy then spreads into all other wave components by the viscosity and nonlinear effects which are not accounted for by the linear perturbation theory. Due to the complicated mechanism of the coupling of energy between the wind excitation and various components of waves for an open, developed sea, we represent the sea surface as

$$z(x, y, t) = \int_{-\infty}^{\infty} d\sigma \int_{-\infty}^{\infty} d\kappa_x \int_{-\infty}^{\infty} d\kappa_y \; a(\kappa_x, \kappa_y, \sigma) \exp\left\{ -i\left[\sigma t + \kappa_x x + \kappa_y y\right] \right\} , \tag{A.101}$$

where a is treated as a stochastic variable. Thus, in general, we have a three dimensional correlation function

$$H(\tau_x, \tau_y, \tau_t) = \left\langle z(x, y, t) z(x+\tau_x, y+\tau_y, t+\tau_t) \right\rangle = \int d\sigma \int d\tau_x \int d\tau_y \, \bar{\Phi}(\kappa_x, \kappa_y, \sigma) \cdot \exp\left\{ -i\left(\sigma\tau_t - \kappa_x \tau_x - \kappa_y \tau_y\right) \right\} . \tag{A.102}$$

The function

$$\bar{\Phi}(\kappa_x, \kappa_y, \sigma) \triangleq \bar{\Phi}(\kappa, \alpha, \sigma) \quad , \tag{A.103}$$

where

$$\left.\begin{aligned} \kappa_x &= \kappa \cos\alpha \\ \kappa_y &= \kappa \sin\alpha \end{aligned}\right\} , \tag{A.104}$$

is known as the three-dimensional spectrum of ocean surface waves.

Actually, the measurement of the three-dimensional spectrum is not necessary, since by the dispersion relation

$$\sigma^2 = g\kappa + \Gamma\kappa^3 \quad ,$$

a relation such as

$$\sigma(\kappa) \quad \text{or} \quad \kappa(\sigma)$$

exists. Therefore, we may express $\Phi(\kappa,\alpha,\sigma)$ either as functions of (κ,α) or, alternatively as a function of (σ,α). Mathematically, therefore, we may have

$$d\kappa_x d\kappa_y d\sigma\, \Phi(\kappa_x,\kappa_y,\sigma) = \kappa\, d\kappa\, d\alpha\, d\sigma\, \Phi(\kappa,\alpha,\sigma)$$

$$\triangleq \kappa\, d\kappa\, d\alpha\, d\sigma\, \Phi_\kappa(\kappa,\alpha)\delta[\sigma-\sigma(\kappa)] \triangleq d\kappa\, d\alpha\, d\sigma\, \Phi_\sigma(\sigma,\alpha)\delta[\kappa-\kappa(\sigma)] \quad . \tag{A.106}$$

Substituting the above in Eq. (A.102) and carrying out the integration over the δ-functions, we have

$$H(\tau_x,\tau_y,\tau_t) = \int \kappa\, d\kappa \int d\alpha\, \Phi_\kappa(\kappa,\alpha)\exp\left\{-i\left[\sigma(\kappa)\tau_t-\kappa(\tau_x\cos\alpha+\tau_y\sin\alpha)\right]\right\}$$

$$= \int d\sigma \int d\alpha\, \Phi_\sigma(\sigma,\alpha)\exp\left\{-i\left[\sigma\tau_t-\kappa(\sigma)(\tau_x\cos\alpha+\tau_y\sin\alpha)\right]\right\} . \tag{A.107}$$

A comparison of the two integrals above yields

$$\Phi_\kappa(\kappa,\alpha) = \Phi_\sigma(\sigma,\alpha)\,\frac{1}{k}\,\frac{d\sigma(k)}{dk} \quad . \tag{A.108}$$

This relation may be used in obtaining $H(\tau_x,\tau_y)$ to the measured directional spectra.

According to Kinsman (1965), the directional spectra deduced from SWOP measurements is estimated to be

$$\Phi_\sigma(\sigma,\alpha) = C\,\frac{\pi}{2}\,\sigma^{-6}\exp\left\{-2g^2\sigma^{-2}U^{-2}\right\}\cdot\frac{1}{\pi}\left\{1+\left[0.50+0.82\exp\left(-\frac{1}{2}g^{-4}\sigma^4U^2\right)\right]\cos 2\alpha\right.$$

$$\left.+\left[0.32\exp\left(-\frac{1}{2}g^{-4}\sigma^4U^2\right)\right]\cos 4\alpha\right\} \tag{A.109}$$

for

$$\frac{\pi}{2} \leq \alpha \leq \frac{\pi}{2} \quad ,$$

where

U is the wind velocity

α is the direction measured from U

and $C = (2.05)\ m^2/sec^5$

On the other hand, in the calculation of the scattering cross section, we like to have the correlation function

$$H(\tau_x, \tau_y) = H(\tau_x, \tau_y, 0) = \int_0^\infty \kappa\, d\kappa \int \Phi_\kappa(\kappa, \alpha) \exp\left[i\kappa(\tau_x \cos\alpha + \tau_y \sin\alpha)\right] . \tag{A.110}$$

Thus, the information on $\Phi_\sigma(\sigma, \alpha)$ and the relation of (A.108), in principle, enables one to calculate $H(\tau_x, \tau_y)$.

Due to the uncertainty involved in the measurement of ocean surface spectra, it is felt that a complicated numerical procedure of computing $H(\tau_x, \tau_y)$ seems to be unjustified. For a simple approximation, we shall, by taking the x-axis parallel to the wind velocity, approximate $H(\tau_x, \tau_y)$ by

$$H(\tau_x, \tau_y) \cong H(0, 0)\left[1 - \frac{\tau_x^2}{\ell_x^2} - \frac{\tau_y^2}{\ell_y^2}\right] \tag{A.111}$$

and neglect all the higher order terms which , in general, contribute only to the second order effect at best.

With this approximation, we find that

$$H(0, 0) = \int_0^\infty \kappa\, d\kappa \int_{-\pi/2}^{\pi/2} d\alpha\, \Phi_\kappa(\kappa, \alpha) \quad , \tag{A.112}$$

$$\frac{H(0, 0)}{\ell_x^2} = \frac{1}{2} \int_0^\infty \kappa\, d\kappa \int_{-\pi/2}^{\pi/2} d\alpha\, \Phi_\kappa(\kappa, \alpha) \cos^2\alpha \quad , \tag{A.113}$$

$$\frac{H(0, 0)}{\ell_y^2} = \frac{1}{2} \int_0^\infty \kappa\, d\kappa \int_{-\pi/2}^{\pi/2} d\alpha\, \Phi_\kappa(\kappa, \alpha) \sin^2\alpha \quad . \tag{A.114}$$

By using (A.109) and (A.110), one finds, by direct integration,

$$H(0,0) = 3C\left(\frac{\pi}{2}\right)^{3/2}\left(\frac{U}{2g}\right)^{5} \quad .$$

Since, however, the "correlation distances" ℓ_x and ℓ_y cannot be evaluated analytically, one has to resort to the numerical integration. The results are presented in Figs. A-4 and A-5. In Fig. A-4, the mean square surface height is plotted against wind speed, while in Fig. A-5, ℓ_x and ℓ_y are plotted against U. In this formulation, therefore, we relate approximately the effect of the wind speed to the ocean surface scattering.*

To include the effect of the direction of the wind, we shall now assume that the wind is blowing in a direction making an angle ψ with the x-axis. Then by simple rotation of coordinates, we may write

$$H(\tau_x,\tau_y) = H(0,0)\left[1 - \frac{(\tau_x\cos\psi+\tau_y\sin\psi)^2}{\ell_x^2} - \frac{(\tau_y\cos\psi-\tau_x\sin\psi)^2}{\ell_y^2}\right] \quad (A.115)$$

By introducing this approximate correlation function into (A.95), we obtain the following expression for the bistatic scattering cross section:

$$\sigma_{\ell m} = \frac{\ell_x\ell_z}{4q_z^4 H(0,0)}\left[a_{\ell m}q_z - b_{\ell m}q_x - c_{\ell m}q_y\right]^2 \cdot \exp\left[\frac{(q_x\cos\psi+q_y\sin\psi)^2\ell_x^2}{4q_z^2 H(0,0)}\right] \cdot$$

$$\exp\left[-\frac{(q_y\cos\psi-q_x\sin\psi)^2\ell_y^2}{4q_z^2 H(0,0)}\right] . \quad (A.116)$$

*It should be noted that the correlation distances ℓ_x, ℓ_y are calculated by a linearization approximation (cf eq. A-111). The values of ℓ_x, ℓ_y, presented in the Fig. A-5, are within the limitation, where the linearization approximation is considered valid. For wind speeds higher than, say, 5m/sec , the nonlinear effects should be taken into account, and, as a consequence, a direct extrapolation of ℓ_x, ℓ_y for higher wind speeds is probably tenuous.

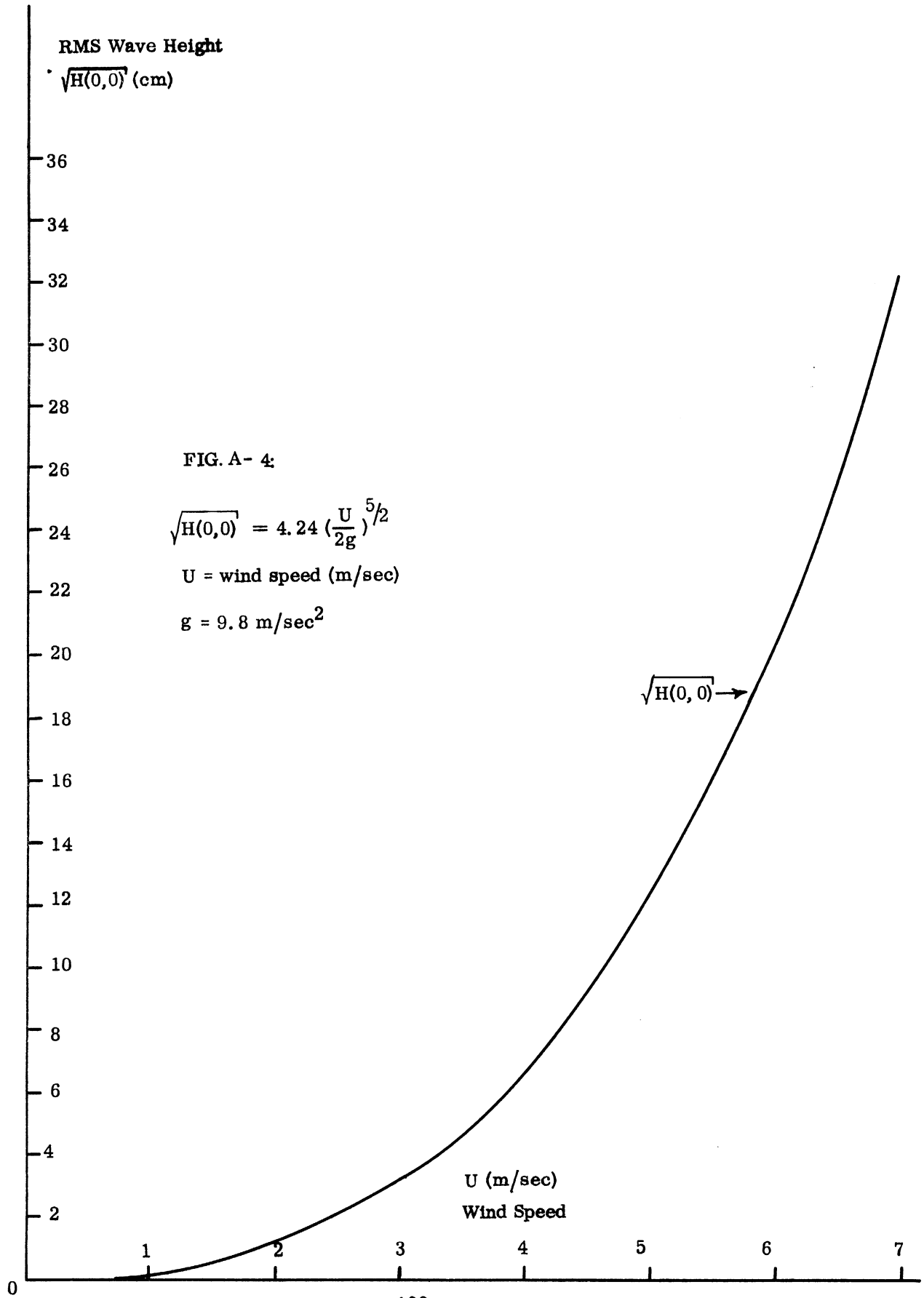

FIG. A- 4:

$$\sqrt{H(0,0)} = 4.24 \left(\frac{U}{2g}\right)^{5/2}$$

U = wind speed (m/sec)

g = 9.8 m/sec^2

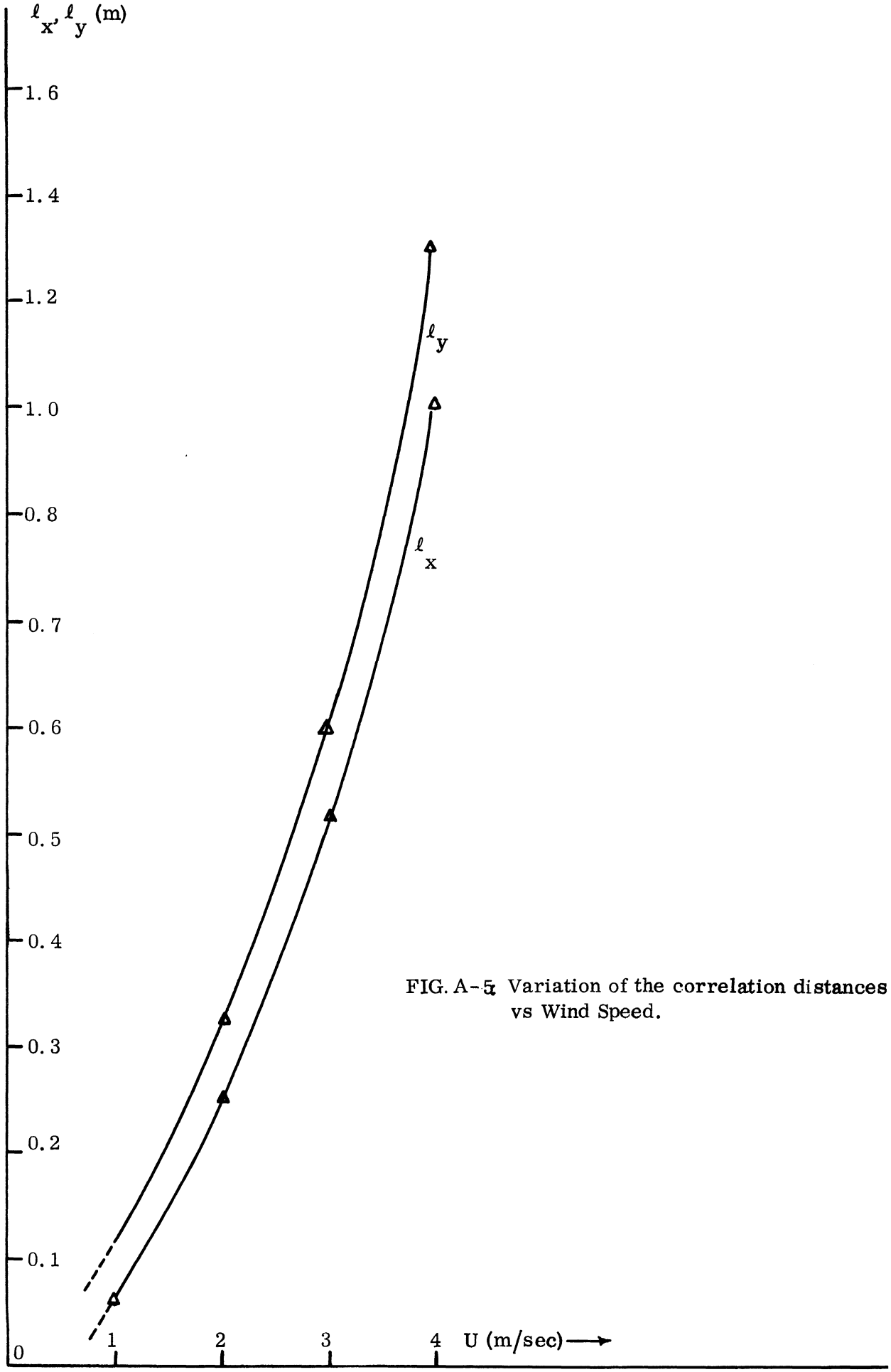

FIG. A-5 Variation of the correlation distances vs Wind Speed.

For the purpose of carrying out the computations involved in this work, we only consider the scattering cross section under the following conditions:

i) the incident radiation is horizontally polarized,

ii) the conductivity of the ocean surface is assumed to be very large, so that $R_{\perp} \cong -1$, $R_{\parallel} \cong +1$,

iii) the observer for the detection of the reflected radiation may receive both components (vertically and horizontally polarized) of radiation, so that $\sigma = \sigma_{hh} + \sigma_{vh}$.

Based on these approximations and using Eqs. (A.68) through (A.70) and (A.74) through (A.76), we find

$$\sigma(\hat{\Omega}_2, \hat{\Omega}_1) = \frac{\ell_x \ell_y}{q_z^4 H(0,0)} \left[1 - \hat{\Omega}_1 \cdot \hat{\Omega}_2\right]^2$$

$$\cdot \exp\left[-\frac{(q_x \cos\psi + q_y \sin\psi)^2 \ell_x^2 + (q_y \cos\psi - q_x \sin\psi)^2 \ell_y^2}{4q_z^2 H(0,0)}\right] \cdot \quad \text{(A.117)}$$

This is the approximate relation, Eq. (2.23), used in the present investigation. It is recognized that a more accurage result could have been obtained by including higher order terms of $(\partial z/\partial x)$ and $(\partial z/\partial y)$ and also by incorporating a finite index of refraction for the sea surface. The resulting computation would be enormously cumbersome, even though such an extension is stratightforward. However, due to uncertainty involved in the sea surface spectra and also the inherent shortcomings of the physical optics approach, it is felt that Eq. (A.117) is adequate as a first order approximation for a surface which is intermediate between a specularly reflecting surface and a surface that gives rise to a completely diffused scattering.

APPENDIX B

COMPUTER PROGRAMS

Rough Surface Program

This program was used to calculate the directions of the maximum radiation received and the power level received at various points above the sea surface. The input to the program consists of the radiation pattern of the antenna, X, Y, and z_r/z_a for the location of the receiving point, the wind speed and the direction. The output consists of the power levels received at various locations, coming from different directions from both the major and minor lobes of the antenna.

This program took 9.5 seconds to compile and 21 seconds of CPU time to run for 13 points of the coordinate points and one case of ZRA, PSI and U .

The Flow Chart and the input data for the Rough Surface Program are included for reference, along with some comments on the antenna pattern.

The radiation pattern of the doppler antenna AN/APN-153 employed in our present work was experimentally obtained for 360 x 90 = 32400 coordinate points covering the entire hemisphere with one degree steps in each coordinate. That is, the azimuth coordinate ranges from 1^o to 360^o and the latitude coordinate from 91^o to 180^o . The peak intensity of the AN/APN-153 antenna pattern is 37 dB.

The radiation intensity at each coordinate point was expressed in dB, multiplied by 10 and then converted into its binary form. The entire antenna pattern, then, is filed in a 360 x 90 matrix form as shown below.

$\longrightarrow \theta_o$

$\downarrow \phi_o$

$$
\begin{array}{llll}
A_{1,1} & A_{1,2} & A_{1,3} \cdots & A_{1,90} \\
A_{2,1} & A_{2,2} & A_{2,3} \cdots & A_{2,90} \\
A_{3,1} & A_{3,2} & A_{3,3} \cdots & A_{3,90} \\
\vdots & \vdots & \vdots & \\
A_{360,1} & A_{360,2} & A_{360,3} & A_{360,90}
\end{array}
$$

The element $A_{1,1}$ represents the antenna radiation intensity at $\phi_o = 1^o$, $\theta_o = 91^o$; $A_{152,50}$ at $\phi_o = 152^o$, $\theta_o = 50^o + 90^o = 140^o$ (cf. Program List No. 43).

The antenna pattern is usually expressed in such a way that it is unity at its peak point, when expressed in the linear form, by normalizing the pattern intensity by its peak value (in our present case, $10^{3.7}$). The FORTRAN statement of the List No. 12 yields the desired antenna pattern in the linear form. It can be seen from the following.

In the expression

$$FF(I) = e^{2.302585\left\{0.1\left[FF'(I)-37\right]\right\}}, \qquad (B.1)$$

let

$$FF'(I) \triangleq 10 \log_{10} F_1(I)$$

$$37 \triangleq 10 \log_{10} F_2,$$

so that

$$FF'(I)-37 = 10 \log_{10} \frac{F_1(I)}{F_2} \quad ,$$

or

$$\log_{10} \frac{F_1(I)}{F_2} = 0.1 \left[FF'(I)-37\right] \quad . \tag{B.2}$$

Since

$$\text{Ln } x = \text{Ln}_{10} \log_{10} x \equiv 2.302585 \log_{10} x,$$

$$e^{\text{Ln } 10 \log_{10} \frac{F_1(I)}{F_2}} = e^{\text{Ln } \frac{F_1(I)}{F_2}}$$

$$= \frac{F_1(I)}{F_2} \quad .$$

Let

$$\frac{F_1(I)}{F_2} \triangleq F_0(I) \quad . \tag{B.3}$$

The equation (B. 3) is the desired pattern expression .

The List No. 6 is the UNFORMATED FORTRAN READ Statement. The procedure for activating this statement depends on the particular computing terminal facility through which the program is run.

For convenience, the input data for;

a) the selected coordinate points of (ϕ_o, θ_o)

b) the relative receiving coordinate points, and

c) the wind speeds and their directions

used in carrying out the numerical calculation are presented, along with the AN/APN-153 antenna radiation pattern $F_o(\theta_o, \phi_o)$ for the 57 points selected in calculating F_2M.

```
FORTRAN IV G COMPILER        MAIN          12-11-69        10:48.35

                C      ......THIS PROGRAM COMPUTES SCATTERED
                C             RADIATION INTENSITY FROM OCEAN SURFACE ....
                C
0001                   DIMENSION CCNAB(2),ZRAA(100),PSIA(100),UA(100)
0002                   DIMENSION PO(200),TC(200),XO(200),YO(200)
0003                   DIMENSION F(360,90),FI(32400),FF(32400)
0004                   INTEGER*2 IF(32400)
0005                   EQUIVALENCE (F,FF),(IF(1),FI(16201))
                C
                C      .....READ INPUT DATA OF RADIATION PATTERN......
0006                   READ(2) IF
0007                   PI=3.1415927
0008                   ADJ=37.
0009                   DO 45 I=1,32400
0010                   FI(I)=IF(I)
0011                   FF(I)=0.1*FI(I)
0012                45 FF(I)=EXP(2.302585*0.1*(FF(I)-ADJ))
                C
                C      ......READ INPUT DATA......
                C      N......NO. OF THE ANGLES(THETAO,PHIO)
                C      M......NO. OF RECEIVER POINTS(X,Y)
                C      L......NO. OF THE VARIATIONS FOR ZRA,PSI AND U
                C      TC.....THETAO
                C      PC.....PHIO
                C      XC.....RELATIVE X COORDINATE OF RECEIVER
                C      YC.....RELATIVE Y COORDINATE OF RECEIVER
                C      ZRAA...RATIO OF HEIGHT BETWEEN THE RECEIVER
                C             AND THE TRANSMITTER
                C      PSIA...WIND DIRECTION
                C      UA.....WIND SPEED
0013                   READ(5,101)N
0014                   READ(5,101)M
0015                   READ(5,101) L
0016             101 FORMAT(I5)
0017                   READ(5,102)((TC(I),PC(I)),I=1,N)
0018                   READ(5,102)((XC(I),YC(I)),I=1,M)
0019             102 FORMAT(2F10.5)
0020                   READ(5,100) ((ZRAA(I),PSIA(I),UA(I)),I=1,L)
0021             100 FORMAT(3F10.5)
0022                   DO 999 KK=1,L
0023                   ZRA=ZRAA(KK)
0024                   PSI=PSIA(KK)
0025                   U=UA(KK)
                C
                C      .......CALL SUBPROGRAM TO COMPUTE AO&BO.......
0026                   CALL DELINT(U,CCNAB)
0027                   AC=1./4./CCNAB(1)
0028                   BC=1./4./CCNAB(2)
0029                   Y3=SQRT(AC*PC)
0030                   DO 999 JJ=1,M
0031                   X=XO(JJ)
0032                   Y=YO(JJ)
0033                   WRITE(6,1000) PSI,U,AC,BC
0034                   WRITE(6,1001) ZRA,X,Y
0035                   WRITE(6,1002)
```

```
0036          1000 FORMAT(1H1,2X,4HPSI=F10.5,2X,2HU=F10.5,2X,
                  1                  3HAO=E12.5,2X,3HBO=E12.5)
0037          1001 FORMAT(2X,6HZR/ZA=F10.5,2X,2HX=F10.5,
                  1                          2X,2HY=F10.5//)
0038          1002 FORMAT(4X,4HPHIC,2X,6HTHETAC,4X,4HPHI1,2X,
                  1       6HTHETA1,4X,4HPHI2,2X,6HTHETA2,
                  2       11X,2HFO,11X,2HF2,11X,2HDK,9X,
                  3       4HDKF2,6X,5HDBKF2,6X,4HDBF2//)
0039                DO 99 II=1,N
                C
                C     .......COMPUTE FO(RADIATION PATTERN)......
0040                APHIC=PC(II)
0041                ATHC=TC(II)
0042                IPHIO=APHIC+0.51-1.0
0043                ITHO=ATHC+0.51-90.
0044                FO=F(IPHIO,ITHO)
0045                THETAO=ATHO*PI/180.
0046                PHIO=APHIC*PI/180.
                C
                C     .......COMPUTE THETA1,PHI1.......
0047                ATH1=180.-ATHC
0048                THETA1=ATH1*PI/180.
0049                APHI1=APHIC+180.
0050                IF(APHI1 .LE. 360.) GO TO 60
0051                APHI1=APHI1-360.
0052             60 PHI1=APHI1*PI/180.
                C
                C     .......COMPUTE THETA2,PHI2.......
0053                ARG1=X+TAN(THETA1)*COS(PHI1)
0054                ARG2=Y+TAN(THETA1)*SIN(PHI1)
0055                IF(ABS(ARG1).LT.1.E-20.AND.ABS(ARG2)
                  1.LT.1.E-20) GO TO 99
0056                IF(ABS(ARG1).LT.1.E-20) GO TO 23
0057                IF(ABS(ARG2).LT.1.0E-20) GO TO 26
0058                PHI2=ATAN(ARG2/ARG1)
0059                IF(ARG1.GT.0..AND.ARG2.GT.0.) GO TO 20
0060                IF(ARG1.LT.0..AND.ARG2.GT.0.) GO TO 21
0061                IF(ARG1.LT.0..AND.ARG2.LT.0.) GO TO 21
0062                IF(ARG1.GT.0..AND.ARG2.LT.0.) GO TO 22
0063             26 PHI2=0.
0064                GO TO 20
0065             21 PHI2=PHI2+PI
0066                GO TO 20
0067             22 PHI2=PHI2+2.*PI
0068                GO TO 20
0069             23 PHI2=PI/2.
0070             20 THETA2=ATAN(ARG1/COS(PHI2)/ZRA)
0071                ATH2=THETA2*180./PI
0072                APHI2=PHI2*180./PI
                C
                C     .......COMPUTE QX,QY,QZ.......
0073                QX=SIN(THETA1)*COS(PHI1)+SIN(THETA2)*COS(PHI2)
0074                QY=SIN(THETA1)*SIN(PHI1)+SIN(THETA2)*SIN(PHI2)
0075                QZ=COS(THETA1)+COS(THETA2)
                C
```

```
C      ..... COMPUTE THE FUNCTIONS DK,F2,
C            DKF2,DBKF2 AND DBF2.....
C      F2.....THE REFLECTED RADIATION INTENSITY
C      DK.....THE FUNCTION INVOLVED IN ESTIMATING
C            THE REFLECTED RADIATION INTENSITY
C            FROM AN ANISOTROPIC OCEAN SURFACE
C      DKF2...THE APPROXIMATE INTEGRATION TO ESTIMATE
C            THE LEVEL OF THE REFLECTED RADIATION
C            INTENSITY FROM AN OCEAN SURFACE
C      DBKF2..DKF2 IN DB
C      DBF2...F2 IN DB
0076         IF(ABS(QZ).LE.1.E-20) GO TO 99
0077         ALPHA=QX/QZ
0078         BETA=QY/QZ
0079         ALPHA2=ALPHA**2
0080         BETA2=BETA**2
0081         GAMMA1=ALPHA*COS(PSI)+BETA*SIN(PSI)
0082         GAMMA2=BETA*COS(PSI)-ALPHA*SIN(PSI)
0083         BG1=GAMMA1**2
0084         BG2=GAMMA2**2
0085         DELTA=1.+ALPHA2+BETA2
0086         DELTA2=DELTA**2
0087         EPSI1=AC*BG1
0088         EPSI2=BC*BG2
0089         TAU=EPSI1+EPSI2
0090         IF(ABS(TAU) .GE. 174.) GO TO 50
0091         F3=1./EXP(TAU)
0092         F1=DELTA2*F3
0093         GO TO 52
0094      50 F3=0.0
0095      52 CONTINUE
0096         W=COS(THETA1)*COS(THETA1)/COS(THETA2)
0097         F2=ABS(Y3*W*FC*F1/4./PI)
0098         IF(ABS(F2).LT.1.E-70) GO TO 81
0099         FM2=ALOG(F2)/2.302585
0100         DBF2=10.*FM2
0101         GO TO 80
0102      81 DBF2=0.
0103      80 DK1=COS(THETA1)+COS(THETA2)
0104         DK2=COS(THETA1)*COS(THETA2)
0105         DK3=1.+SIN(THETA1)*SIN(THETA2)*COS(PHI1-PHI2)+DK2
0106         IF(ABS(COS(THETA2)).LT.1.E-20) GO TO 99
0107         DK4=COS(THETA1)/COS(THETA2)
0108         DK5=ZRA*DK1*DK4/COS(THETA2)
0109         DK6=ZRA*ZRA*DK4**2
0110         DK7=1.+DK5+DK6
0111         IF(ABS(DK7) .LT. 1.E-20) GO TO 99
0112         DK=ABS(PI*DK1**3*DK3/DK7/Y3)
0113         DKF2=ABS(DK*F2)
0114         IF(ABS(DKF2).LT.1.E-70) GO TO 82
0115         ADKF2=ALOG(DKF2)/2.302585
0116         DBKF2=10.*ADKF2
0117         GO TO 83
0118      82 DBKF2=0.
0119      83 CONTINUE
```

```
                C
                C      .......PRINT OUT APHIC,ATHO,APHI1,ATH1,APHI2,
                C              ATH2,FO,F2,DK,DKF2,DBKF2 & DBF2
0120                   WRITE(6,1003)APHIC,ATHO,APHI1,ATH1,APHI2,
                     1              ATH2,FO,F2,DK,DKF2,DBKF2,DBF2
0121            1003 FORMAT(6F8.1,4E13.3,F11.3,F10.3)
0122              99 CONTINUE
0123             999 CONTINUE
0124                   CALL SYSTEM
0125                   END

 TOTAL MEMORY REQUIREMENTS 041714 BYTES
```

```
FORTRAN IV G COMPILER        DBLINT          12-11-69        10:48.55

0001                 SUBROUTINE DBLINT(U,CONAB)
                C
                C    .......THIS PROGRAM COMPUTES CONAB(1)&CONAB(2)
                C            IN THE FUNCTION REPRESENTING THE
                C            SCATTERING CROSS SECTION FOR AN
                C            ANISOTROPIC OCEAN SURFACE.......
0002                 DIMENSION AF1(600),AF2(600),CONAB(2)
0003                 REAL K
0004                 PIO2=1.570796
                C
                C    .......THE INTEGRATION INTERVAL IS DIVIDED
                C            INTO THE TWO REGIONS.......
                C    Q......THE CUMULATIVE STEPS IN THE EVALUATION
                C            OF THE INTEGRATION BY SIMPSON FORMULA
                C    H......THE STEP-SIZE IN THE SIMPSON FORMULA
                C    M......NO. OF THE STEPS IN THE INTEGRATION
0005                 Q=0.1
0006                 H=0.1
0007                 M=301
0008               101 CONTINUE
0009                 DO 200 I=1,M
0010                 K=Q
0011                 K2=K*K
0012                 K3=K2*K
0013                 U2=U*U
0014                 U4=U2*U2
0015                 C1=7.5+0.00017*K2
0016                 C2=9.8*K+0.000074*K3
0017                 C3=SQRT(C2)
0018                 C4=192./U2/C2
0019                 IF(C4 .GE. 174.) GO TO 20
0020                 C5=1./EXP(C4)
0021                 C6=C2**2
0022                 C7=0.000054*U4*C6
0023                 IF( C7 .GE. 174. ) GO TO 30
0024                 C8=1./EXP(C7)
0025                 GO TO 21
0026              30 C8=0.
0027              21 C9=C3**7
0028                 X10=K2*C1*C5/C9
0029                 X20=0.41*C8
0030                 F1=X10*(1.25+X20)
0031                 F2=X10*(0.75-X20)
0032                 GO TO 22
0033              20 F1=0.
0034                 F2=0.
0035              22 AF1(I)=F1
0036                 AF2(I)=F2
0037                 Q=Q+H
0038              200 CONTINUE
0039                 Q=Q-H
                C
                C    .......COMPUTE FUNCTION SIMP(H,AF,M).....
0040                 BBF1=SIMP(H,AF1,M)
0041                 BBF2=SIMP(H,AF2,M)
```

```
0042                IF(H.EQ.2.C) GC TC 103
0043                H=2.0
0044                M=201
0045                BF1=BBF1
0046                BF2=BBF2
0047                GC TC 101
0048           103  BF1=BF1+BBF1
0049                BF2=BF2+BBF2
0050                CCNAB(1)=PIC2*BF1
0051                CCNAB(2)=PIC2*BF2
0052                RETURN
0053                END

 TOTAL MEMORY REQUIREMENTS 001F18 BYTES
```

```
FORTRAN IV G COMPILER        SIMP          12-11-69        10:49.00

0001                  FUNCTION SIMP(H,SP,M)
                      C
                      C     .......COMPUTE FUNCTION SIMP(H,SP,M)......
0002                  DIMENSION SP(600)
0003                  S=SP(1)+SP(M)+4.*SP(2)
0004                  MM1=M-1
0005                  DO 10 I=4,MM1,2
0006                10 S=S+2.*SP(I-1)+4.*SP(I)
0007                  SIMP=S*H/3.
0008                  RETURN
0009                  END

   TOTAL MEMORY REQUIREMENTS 000166 BYTES
EXECUTION TERMINATED
```

The Coordinates of the Selected Locations in the Antenna Pattern.

		(ϕ_o)	(θ_o)
#SLIS DATAAA			
>	1	151.0	140.0
>	2	150.0	142.0
>	3	155.00	152.0
>	4	153.00	139.0
>	5	145.00	134.0
>	6	148.00	146.0
>	7	155.00	164.0
>	8	158.00	172.0
>	9	159.00	158.0
>	10	154.00	137.0
>	11	144.00	123.0
>	12	138.00	120.0
>	13	132.00	121.0
>	14	140.00	137.0
>	15	147.00	150.0
>	16	152.00	168.0
>	17	155.00	188.0
>	18	162.00	178.0
>	19	162.00	156.0
>	20	156.00	134.0
>	21	146.00	120.0
>	22	135.00	114.0
>	23	110.00	111.0
>	24	128.00	126.0
>	25	138.00	134.0
>	26	142.00	153.0
>	27	148.00	172.0
>	28	153.00	190.0
>	29	156.00	199.0
>	30	165.00	174.0
>	31	165.00	150.0
>	32	153.00	128.0
>	33	149.00	114.0
>	34	130.00	110.0
>	35	125.00	109.0
>	36	114.00	106.0
>	37	98.00	106.0
>	38	117.00	118.0
>	39	118.00	122.0
>	40	130.00	134.0
>	41	148.00	230.0
>	42	149.00	234.0
>	43	155.00	216.0
>	44	146.00	225.0
>	45	138.00	236.0
>	46	150.0	237.0
>	47	158.0	225.0
>	48	162.0	203.0
>	49	153.0	209.0
>	50	144.0	218.0
>	51	136.0	225.0
>	52	130.0	240.0
>	53	117.0	242.0
>	54	106.0	250.0
>	55	119.0	250.0
>	56	133.00	245.0
>	57	118.00	247.0

The (X, Y) Coordinates of the Receiving Points

	(X)	(Y)
58	-3.0	-1.5
59	-2.5	-1.5
60	-2.0	-1.5
61	-1.5	-1.5
62	-1.0	-1.5
63	-0.5	-1.5
64	0.0	-1.5
65	0.5	-1.5
66	1.0	-1.5
67	1.5	-1.5
68	2.0	-1.5
69	2.5	-1.5
70	3.0	-1.5
71	-3.0	-1.0
72	-2.5	-1.0
73	-2.0	-1.0
74	-1.5	-1.0
75	-1.0	-1.0
76	-0.5	-1.0
77	0.0	-1.0
78	0.5	-1.0
79	1.0	-1.0
80	1.5	-1.0
81	2.0	-1.0
82	2.5	-1.0
83	3.0	-1.0
84	-3.0	-0.5
85	-2.5	-0.5
86	-2.0	-0.5
87	-1.5	-0.5
88	-1.0	-0.5
89	-0.5	-0.5
90	0.0	-0.5
91	0.5	-0.5
92	1.0	-0.5
93	1.5	-0.5
94	2.0	-0.5
95	2.5	-0.5
96	3.0	-0.5
97	-3.0	0.0
98	-2.5	0.0
99	-2.0	0.0
100	-1.5	0.0
101	-1.0	0.0
102	-0.5	0.0
103	0.0	0.0
104	0.5	0.0
105	1.0	0.0
106	1.5	0.0
107	2.0	0.0
108	2.5	0.0
109	3.0	0.0
110	-3.0	0.5
111	-2.5	0.5
112	-2.0	0.5
113	-1.5	0.5
114	-1.0	0.5
115	-0.5	0.5
116	0.0	0.5
117	0.5	0.5
118	1.0	0.5
119	1.5	0.5
120	2.0	0.5
121	2.5	0.5
122	3.0	0.5
123	-3.0	1.0
124	-2.5	1.0
125	-2.0	1.0
126	-1.5	1.0
127	-1.0	1.0
128	-0.5	1.0
129	0.0	1.0
130	0.5	1.0
131	1.0	1.0
132	1.5	1.0
133	2.0	1.0
134	2.5	1.0
135	3.0	1.0
136	-3.0	1.5
137	-2.5	1.5
138	-2.0	1.5
139	-1.5	1.5
140	-1.0	1.5
141	-0.5	1.5
142	0.0	1.5
143	0.5	1.5
144	1.0	1.5
145	1.5	1.5
146	2.0	1.5
147	2.5	1.5
148	3.0	1.5

The Relative Receiver Height, Wind Direction and Speed.

		(z_r/z_a)	(ψ)	(U)
>	149	0.1	0.0	1.5
>	150	0.1	0.0	2.0
>	151	0.1	0.0	3.0
>	152	0.1	0.0	4.0
>	153	0.1	45.0	1.5
>	154	0.1	45.0	2.0
>	155	0.1	45.0	3.0
>	156	0.1	45.0	4.0
>	157	0.1	90.0	1.5
>	158	0.1	90.0	2.0
>	159	0.1	90.0	3.0
>	160	0.1	90.0	4.0
>	161	0.5	0.0	1.5
>	162	0.5	0.0	2.0
>	163	0.5	0.0	3.0
>	164	0.5	0.0	4.0
>	165	0.5	45.0	1.5
>	166	0.5	45.0	2.0
>	167	0.5	45.0	3.0
>	168	0.5	45.0	4.0
>	169	0.5	90.0	1.5
>	170	0.5	90.0	2.0
>	171	0.5	90.0	3.0
>	172	0.5	90.0	4.0

#END OF FILE

The Radiation Pattern of AN/APN-153.

PHIO	THETAO	FO
140.0	151.0	0.851E 00
142.0	150.0	0.832E 00
152.0	155.0	0.776E 00
139.0	153.0	0.603E 00
134.0	145.0	0.724E 00
146.0	148.0	0.257E 00
164.0	155.0	0.372E 00
172.0	158.0	0.309E 00
158.0	159.0	0.363E 00
137.0	154.0	0.309E 00
123.0	144.0	0.186E 00
120.0	138.0	0.200E 00
121.0	132.0	0.316E 00
137.0	140.0	0.257E-01
150.0	147.0	0.209E-01
168.0	152.0	0.245E-01
188.0	155.0	0.372E-01
178.0	162.0	0.447E-01
156.0	162.0	0.263E-01
134.0	156.0	0.316E-01
120.0	146.0	0.120E-01
114.0	135.0	0.891E-02
111.0	110.0	0.240E-01
126.0	128.0	0.123E-01
134.0	138.0	0.331E-01
153.0	142.0	0.513E-02
172.0	148.0	0.269E-02
190.0	153.0	0.339E-02
199.0	156.0	0.631E-02
174.0	165.0	0.141E-02
150.0	165.0	0.182E-02
128.0	158.0	0.437E-02
114.0	149.0	0.550E-02
110.0	130.0	0.219E-02
109.0	125.0	0.977E-02
106.0	114.0	0.214E-02
106.0	98.0	0.316E-02
118.0	117.0	0.479E-01
122.0	118.0	0.178E-02
134.0	130.0	0.741E-02
230.0	148.0	0.490E-01
234.0	149.0	0.525E-01
216.0	155.0	0.263E-01
225.0	146.0	0.269E-01
236.0	138.0	0.708E-02
237.0	150.0	0.182E-01
225.0	158.0	0.589E-02
203.0	162.0	0.245E-02
209.0	153.0	0.513E-03
218.0	144.0	0.275E-02
225.0	136.0	0.229E-02
240.0	130.0	0.107E-02
242.0	117.0	0.282E-03
250.0	106.0	0.251E-02
250.0	119.0	0.138E-01
245.0	133.0	0.794E-02
247.0	118.0	0.832E-02

FLOW CHART FOR ROUGH SURFACE PROGRAM

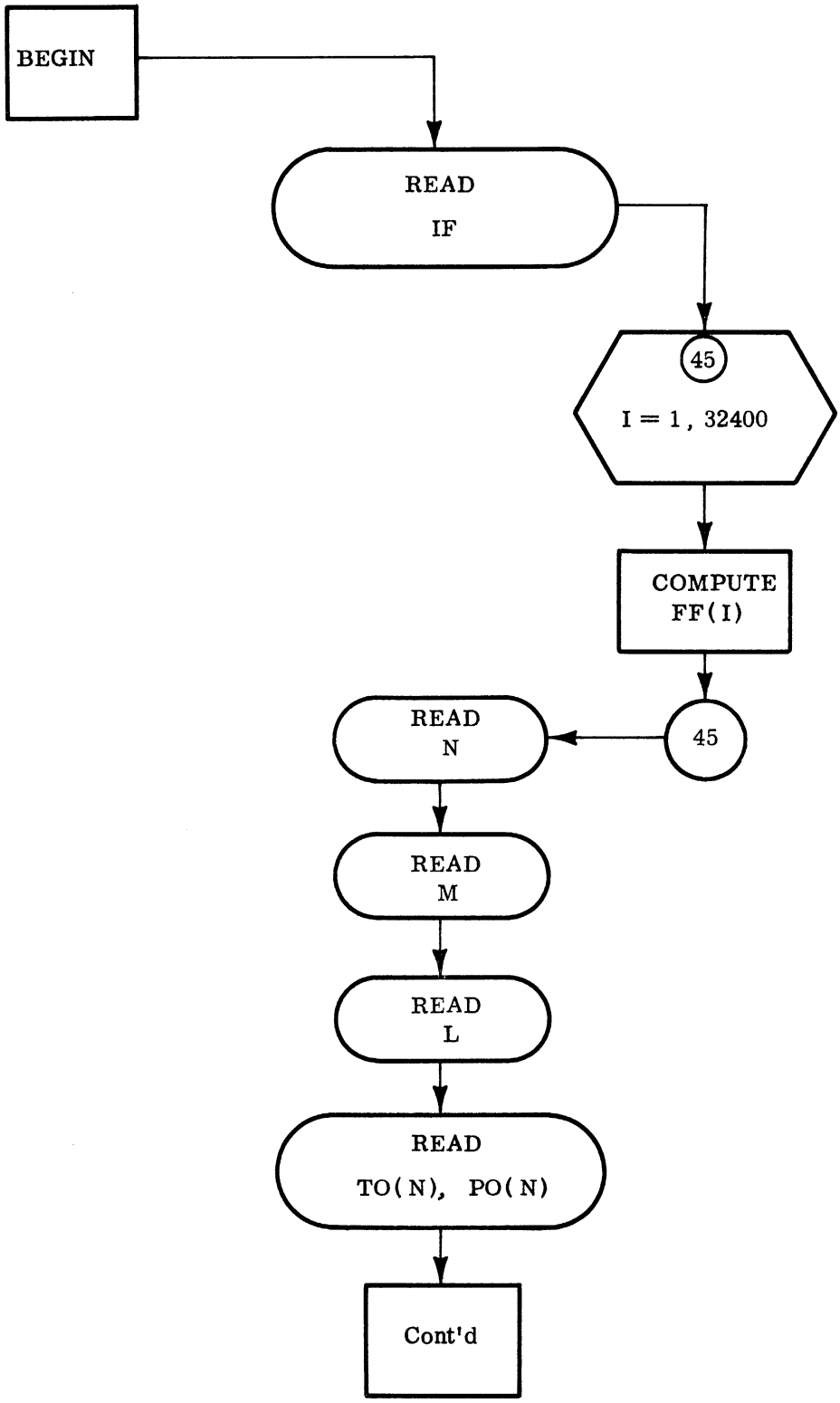

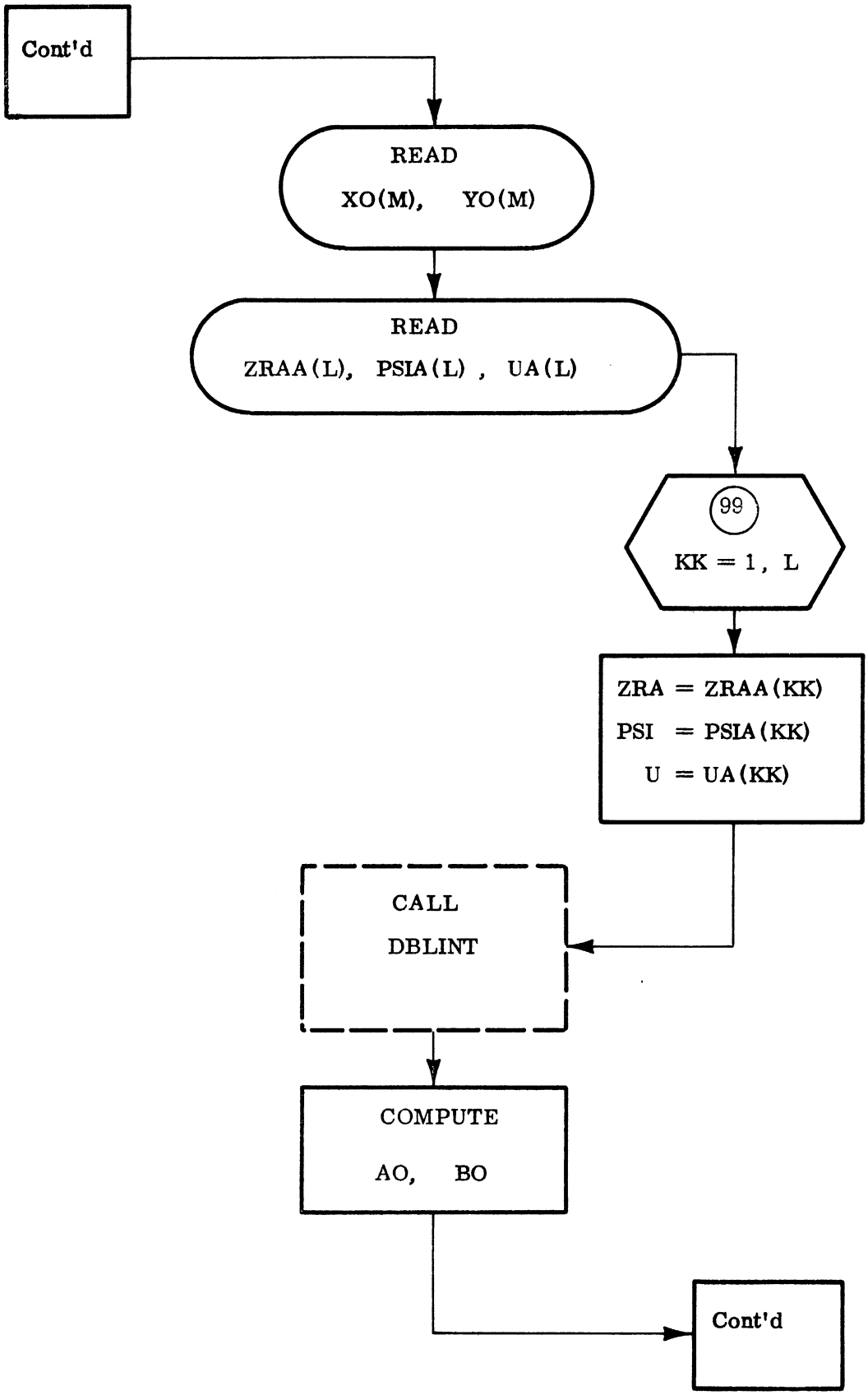
Cont'd
READ
XO(M), YO(M)
READ
ZRAA(L), PSIA(L) , UA(L)
99
KK = 1, L
ZRA = ZRAA(KK)
PSI = PSIA(KK)
U = UA(KK)
CALL
DBLINT
COMPUTE
AO, BO
Cont'd

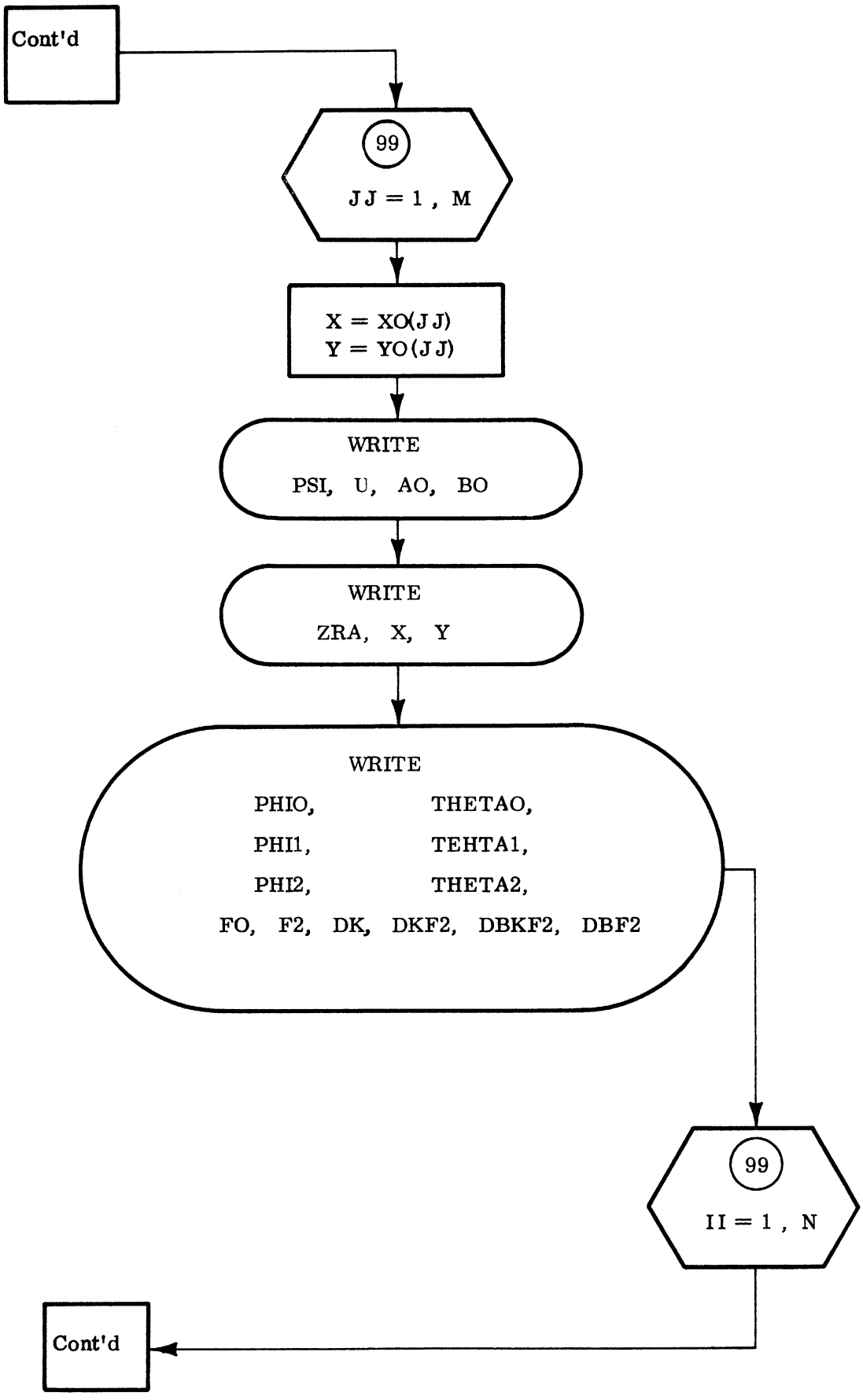
Cont'd
99
JJ = 1 , M
X = XO(JJ)
Y = YO(JJ)
WRITE
PSI, U, AO, BO
WRITE
ZRA, X, Y
WRITE
PHIO, THETAO,
PHI1, TEHTA1,
PHI2, THETA2,
FO, F2, DK, DKF2, DBKF2, DBF2
99
II = 1 , N
Cont'd

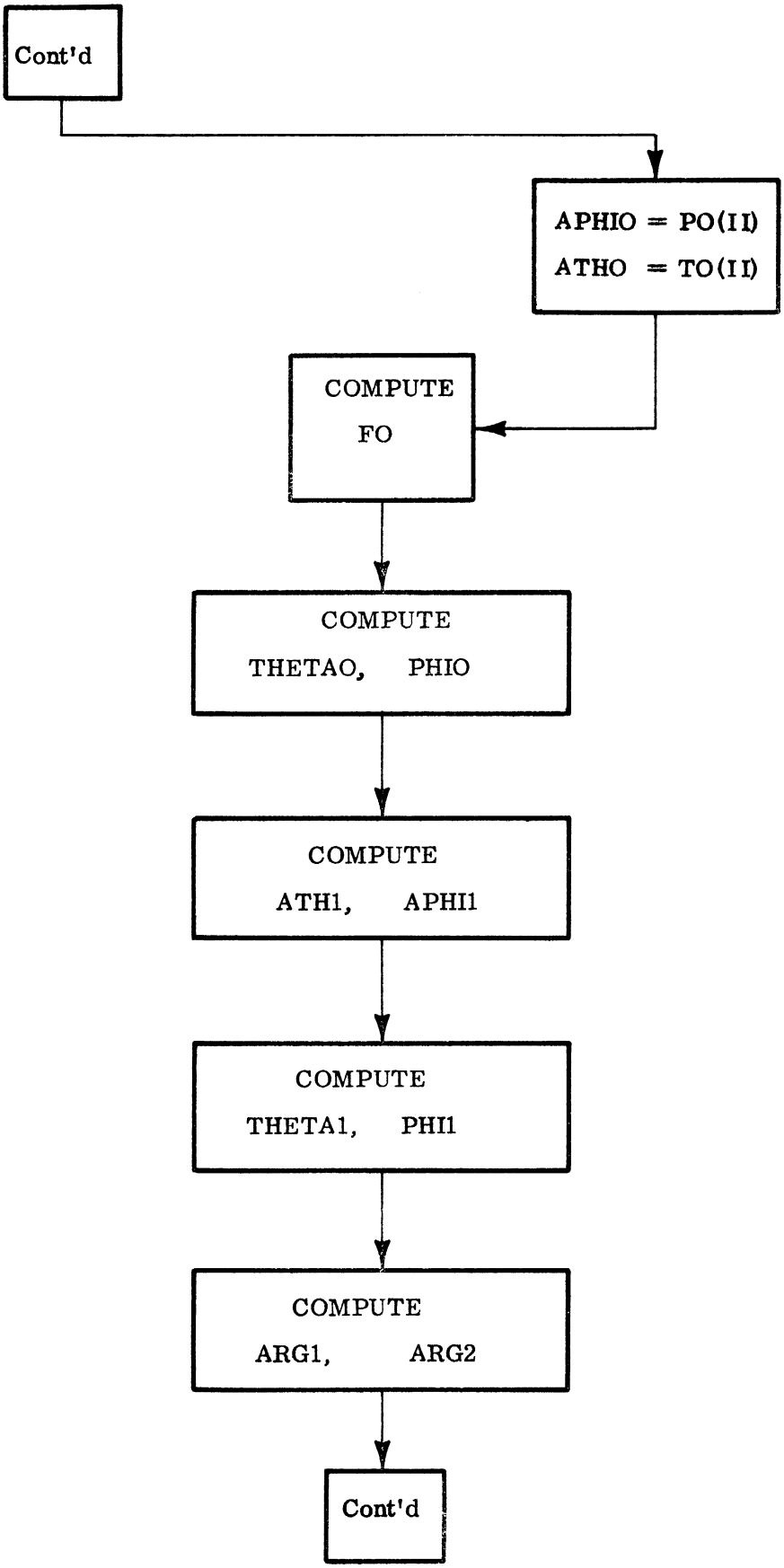
Cont'd
APHIO = PO(II)
ATHO = TO(II)
COMPUTE
FO
COMPUTE
THETAO, PHIO
COMPUTE
ATH1, APHI1
COMPUTE
THETA1, PHI1
COMPUTE
ARG1, ARG2
Cont'd

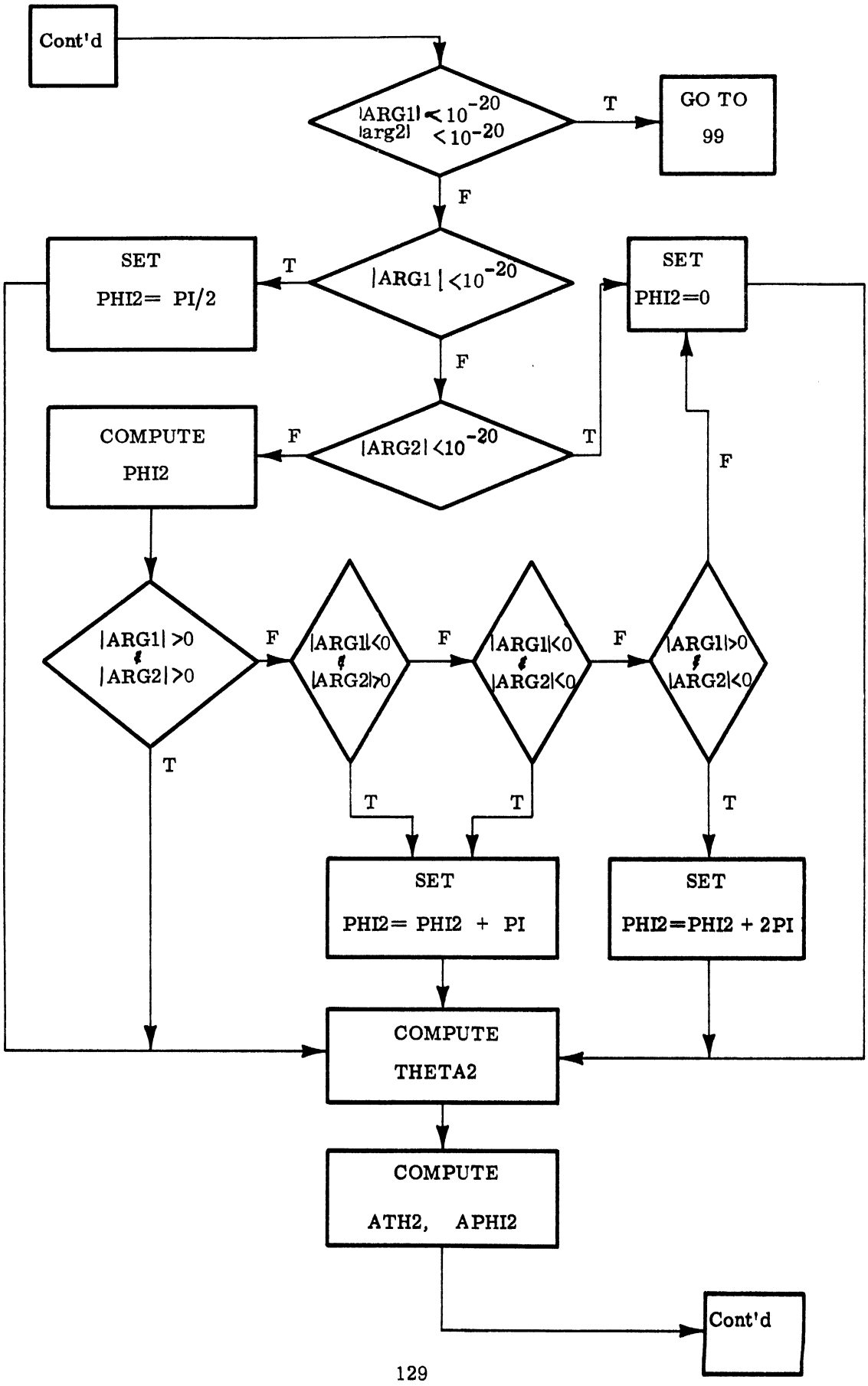
Cont'd
|ARG1| < 10^-20
|arg2| < 10^-20
T
GO TO
99
F
SET
PHI2= PI/2
T
|ARG1 | <10^-20
SET
PHI2=0
F
COMPUTE
PHI2
F
|ARG2| <10^-20
T
F
|ARG1| >0
|ARG2| >0
F
|ARG1|<0
|ARG2|>0
F
|ARG1|<0
|ARG2|<0
F
|ARG1|>0
|ARG2|<0
T
T
T
T
SET
PHI2= PHI2 + PI
SET
PHI2=PHI2 + 2PI
COMPUTE
THETA2
COMPUTE
ATH2, APHI2
Cont'd

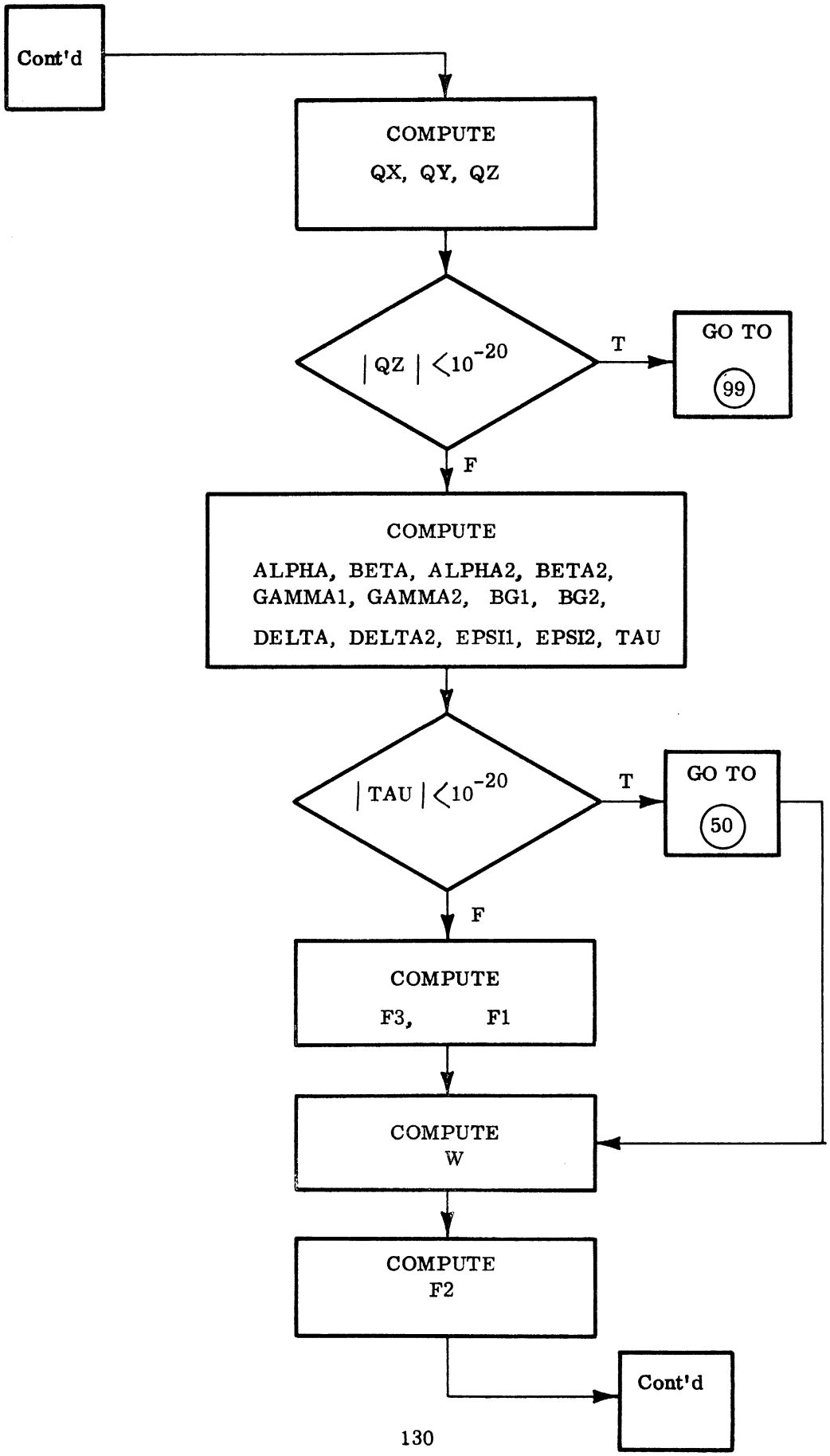
Cont'd
COMPUTE
QX, QY, QZ
| QZ | <10^-20
T
GO TO
99
F
COMPUTE
ALPHA, BETA, ALPHA2, BETA2,
GAMMA1, GAMMA2, BG1, BG2,
DELTA, DELTA2, EPSI1, EPSI2, TAU
| TAU | <10^-20
T
GO TO
50
F
COMPUTE
F3, F1
COMPUTE
W
COMPUTE
F2
Cont'd

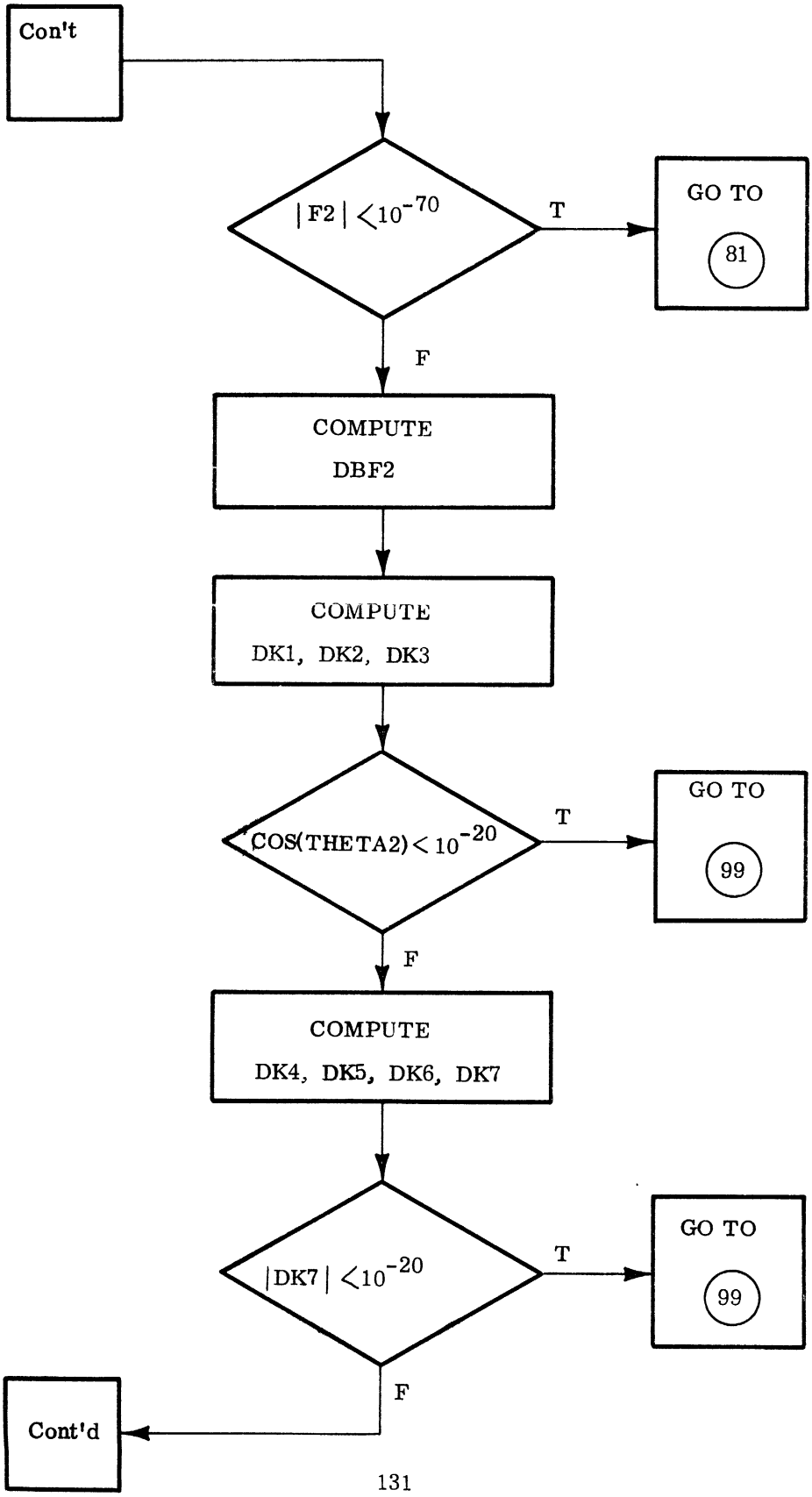
Con't
|F2| <10^-70
T
GO TO
81
F
COMPUTE
DBF2
COMPUTE
DK1, DK2, DK3
COS(THETA2) < 10^-20
T
GO TO
99
F
COMPUTE
DK4, DK5, DK6, DK7
|DK7| <10^-20
T
GO TO
99
F
Cont'd

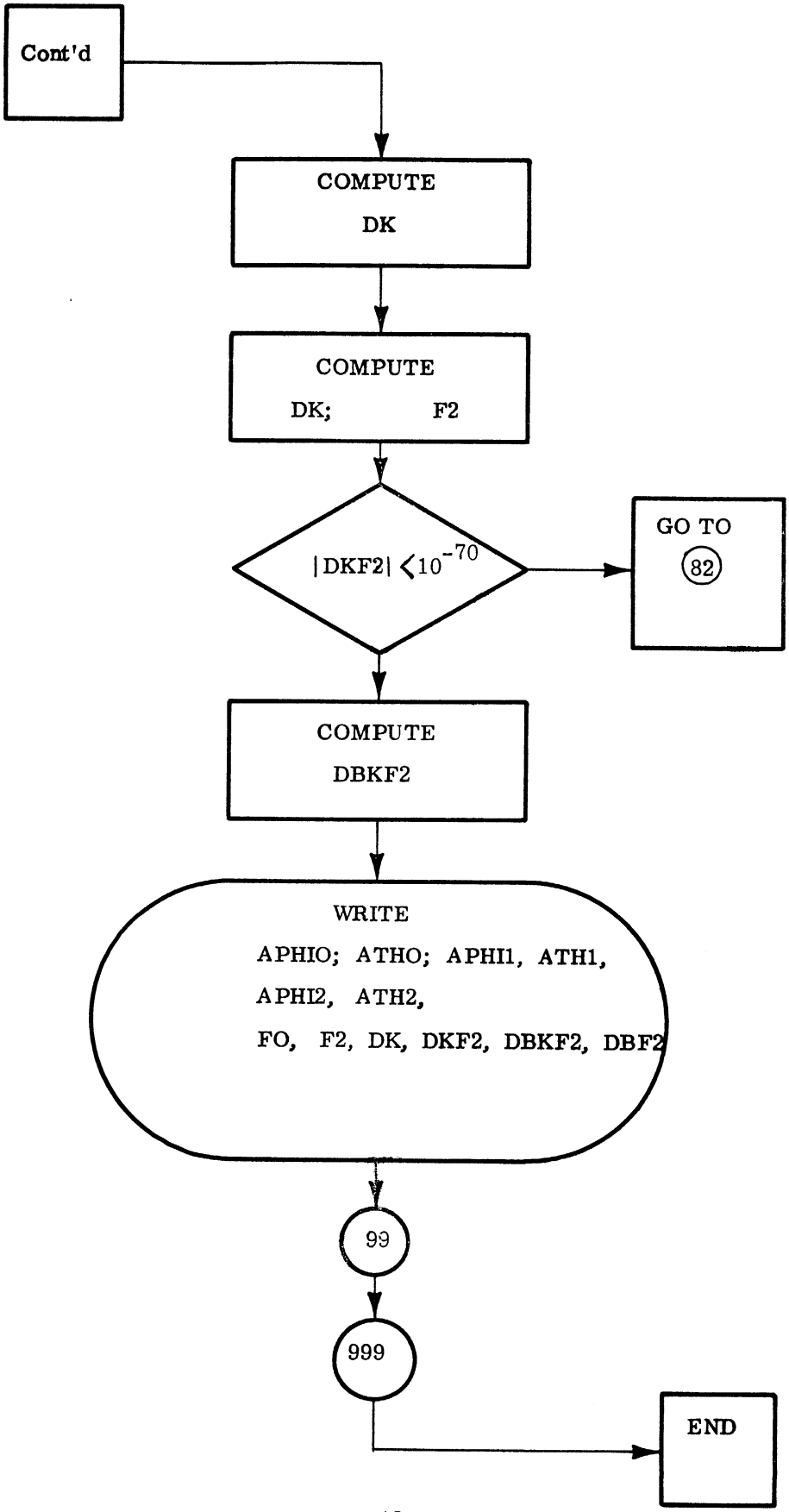
Cont'd
COMPUTE
DK
COMPUTE
DK; F2
|DKF2| < 10^-70
GO TO
82
COMPUTE
DBKF2
WRITE
APHIO; ATHO; APHI1, ATH1,
APHI2, ATH2,
FO, F2, DK, DKF2, DBKF2, DBF2
99
999
END

REFERENCES

Aksenov, V.I. (1958), "The Scattering of Electromagnetic Waves by Sinusoidal and Trochoidal Surfaces with Finite Conductivity," Radioteknika i Elektronika, 4, 459-466.

Beckmann, P. and A. Spizzichino (1963), "The Scattering of Electromagnetic Waves from Rough Surfaces," The MacMillan Co., New York.

Chu, C.M. et al (1968), "Doppler Radiation Study,"The University of Michigan Radiation Laboratory Report 1082-1-F, SECRET. 140 pp.

Hoffman, W.C. (1955), "Scattering of Electromagnetic Waves from a Random Surface," J. Appl. Math. XIII, 3, 291-304.

Kinsman, B. (1965), Wind Waves, Prentice-Hall, New York.

Pidgeon, V.W. (1966) "Bistatic Cross Section of the Sea," IEEE Trans., AP-14, 3, 405.

Senior, T.B.A. and Hunter, I.M. (1966), "Experimental Studies of Sea-Surface Effects on Low-Angle Radar," Proc. IEE, 113, 11, November, 1966.

UNCLASSIFIED

Security Classification

DOCUMENT CONTROL DATA - R & D

(Security classification of title, body of abstract and indexing annotation must be entered when the overall report is classified)

1. ORIGINATING ACTIVITY (Corporate author)	2a. REPORT SECURITY CLASSIFICATION
The University of Michigan Radiation Laboratory, Dept. of Electrical Engineering, 201 Catherine Street, Ann Arbor, Michigan 48108	UNCLASSIFIED
	2b. GROUP

3. REPORT TITLE

Doppler Radiation Study : Phase 1 Report of Contract N62269-68-C-0715

Volume I.

4. DESCRIPTIVE NOTES (Type of report and inclusive dates)

Interim Report July 1968 - July 1969

5. AUTHOR(S) (First name, middle initial, last name)

Chiao-Min Chu, Soon K. Cho and Joseph E. Ferris

6. REPORT DATE	7a. TOTAL NO. OF PAGES	7b. NO. OF REFS
December 1969	133	7

8a. CONTRACT OR GRANT NO.	9a. ORIGINATOR'S REPORT NUMBER(S)
N62269-68-C-0715	1969-1-F, Volume I
b. PROJECT NO.	
c.	9b. OTHER REPORT NO(S) (Any other numbers that may be assigned this report)
d.	

10. DISTRIBUTION STATEMENT Transmittal outside agencies of U. S. Government must have prior approval of NAVAIRDEVCEN or NAVAIRSYSCOM

11. SUPPLEMENTARY NOTES	12. SPONSORING MILITARY ACTIVITY
	Naval Air Development Center Johnsville, Warminster, PA. 18974

13. ABSTRACT

The radiation characteristics of a doppler velocity sensor radar have been studied. A theoretical investigation has been made of the reflection of the electromagnetic radiation from an anisotropic Gaussian surface. In particular, from the known angular spectrum of ocean surfaces, the bistatic scattering cross section is derived for an open developed sea. The results thus obtained are then applied to the study of the reflected radiation from the doppler sensor equipment on an airplane. Computer programs are set up to calculate the directional distribution of the reflected radiation for a transmitting antenna of given radiation pattern. Computed results for the AN/APN-153 antenna, showing the spatial and temporal variations of the reflected radiation, are given for a wide range of relative positions of the transmitter and receiver for a few different wind speeds. Finally, the reflected radiation from an anisotropic ocean surface of Gaussian distribution is compared with models of specularly and diffusely reflecting surfaces.

DD FORM 1 NOV 65 1473

UNCLASSIFIED

Security Classification

14. KEY WORDS	LINK A		LINK B		LINK C	
	ROLE	WT	ROLE	WT	ROLE	WT
Doppler Radar						
Velocity Radar						
Detectability						
Radiation Characteristics						
Specular Scatter						
Diffuse Scatter						

DISTRIBUTION LIST: Air Task No. A3605337/202B/F08-232-602
Work Unit A53373A-3

NAVAIRSYSCOM, AIR-604
(2 for retention)
(1 for AIR-533)
(1 for AIR-5337)
(1 for AIR-360E) 5 cys

DDC 20 cys

NAVAIRDEVCEN, Johnsville, Warminster, Pa
(3 for ADL)
(6 for AMD)
(3 for AMX)
(1 for AMXI)
(2 for AMXA) 15 cys